1976-03

Satellite-tuned fleet numerical weather central radiation model applied to the 1973-1974 data year over oceanic gridpoints

Woods, Robert Deane

Monterey, California. Naval Postgraduate School

SATELLITE-TUNED FLEET NUMERICAL WEATHER CENTRAL RADIATIONAL MODEL APPLIED TO THE 1973-1974 DATA YEAR OVER OCEANIC GRIDPOINTS

Robert Deane Woods

NAVAL POSTGRADUATE SCHOOL

Monterey, California

THESIS

SATELLITE-TUNED FLEET NUMERICAL WEATHER CENTRAL
RADIATIONAL MODEL APPLIED TO THE 1973-1974
DATA YEAR OVER OCEANIC GRIDPOINTS

by

Robert Deane Woods

March 1976

Thesis Advisor: F. L. Martin

Approved for public release; distribution unlimited.

SECURITY CLASSIFICATION OF THIS PAGE (When Data Entered)

REPORT DOCUMENTATION PAGE		READ INSTRUCTIONS BEFORE COMPLETING FORM
1. REPORT NUMBER	2. GOVT ACCESSION NO.	3. RECIPIENT'S CATALOG NUMBER
4. TITLE (and Subtitle) Satellite-tuned Fleet Numerical Weather Central Radiational Model Applied to the 1973-1974 Data Year over Oceanic Gridpoints		5. TYPE OF REPORT & PERIOD COVERED Master's Thesis March 1976
		6. PERFORMING ORG. REPORT NUMBER
7. AUTHOR(s) Robert Deane Woods		8. CONTRACT OR GRANT NUMBER(s)
9. PERFORMING ORGANIZATION NAME AND ADDRESS Naval Postgraduate School Monterey, CA 93940		10. PROGRAM ELEMENT, PROJECT, TASK AREA & WORK UNIT NUMBERS
11. CONTROLLING OFFICE NAME AND ADDRESS Naval Postgraduate School Monterey, CA 93940		12. REPORT DATE March 1976
		13. NUMBER OF PAGES 127
14. MONITORING AGENCY NAME & ADDRESS(if different from Controlling Office) Naval Postgraduate School Monterey, CA 93940		15. SECURITY CLASS. (of this report) Unclassified
		15a. DECLASSIFICATION/DOWNGRADING SCHEDULE

16. DISTRIBUTION STATEMENT (of this Report)

Approved for public release; distribution unlimited.

17. DISTRIBUTION STATEMENT (of the abstract entered in Block 20, if different from Report)

18. SUPPLEMENTARY NOTES

19. KEY WORDS (Continue on reverse side if necessary and identify by block number)

20. ABSTRACT (Continue on reverse side if necessary and identify by block number)

This is a final study of a radiational model for use in the FNWC prediction system. This model utilizes original FNWC data over oceanic gridpoints which were adapted to the FNWC five-layer initial data analysis in four mid-seasonal studies for the data year 16 January 1974, 16 April 1974, 16 July 1974 and 16 October 1973.

The radiational model parameterizes the large-scale cloud amounts in two layers. The primary objective was to tune model albedo values

DD FORM 1 JAN 73 1473 EDITION OF 1 NOV 65 IS OBSOLETE
(Page 1) S/N 0102-014-6601 |

SECURITY CLASSIFICATION OF THIS PAGE (When Data Entered)

to those taken from satellite climatology by changing the cloud-reflectance coefficients used in previous studies. The albedo values were tuned for least squares deviation relative to satellite climatology albedos. The present model using tuned albedos better verified the radiational balance at the top of the atmosphere against satellite climatology than did pre-existing untuned models, both on a seasonal and annual basis.

Satellite-tuned Fleet Numerical Weather Central
Radiational Model Applied to the 1973-1974
Data Year over Oceanic Gridpoints

by

Robert Deane Woods
Commander, United States Navy
B.S., University of Kansas, 1965

Submitted in partial fulfillment of the
requirements for the degree of

MASTER OF SCIENCE IN METEOROLOGY

from the

NAVAL POSTGRADUATE SCHOOL
March 1976

ABSTRACT

This is a final study of a radiational model for use in the FNWC prediction system. This model utilizes original FNWC data over oceanic gridpoints which were adapted to the FNWC five-layer initial data analysis in four mid-seasonal studies for the data year 16 January 1974, 16 April 1974, 16 July 1974 and 16 October 1973.

The radiational model parameterizes the large-scale cloud amounts in two layers. The primary objective was to tune model albedo values to those taken from satellite climatology by changing the cloud-reflectance coefficients used in previous studies. The albedo values were tuned for least squares deviation relative to satellite climatology albedos. The present model using tuned albedos better verified the radiational balance at the top of the atmosphere against satellite climatology than did pre-existing untuned models, both on a seasonal and annual basis.

TABLE OF CONTENTS

LIST OF SYMBOLS AND ABBREVIATIONS

Amn	solar insolation absorbed in the layer (m,n)
$\underline{a}$(m,n)	Manabe-Möller absorptivity function
ABA	absorptivity of the troposphere
ABG	fractional absorptivity of solar insolation by earth's surface
ALB	earth-atmosphere system albedo
ATRAN	transmissivity of the troposphere
B_k	Stefan-Boltzmann blackbody flux at T_k
BALB	24-hour averaged radiational balance at earth's surface
$BALk_1k_2$	24-hour averaged radiational balance for layer (k_1,k_2)
BALT	24-hour averaged radiational balance at tropopause
C	carbon dioxide layer absorber mass
cal cm^{-2} min^{-1}	calories per centimeter squared per minute
CL	total opaque cloud cover
CL_I	fractional cloud amount for layer: I = 1 in 600 to 400 mb; I = 2 in 900 to 800 mb
E	East longitude
e_x	vapor pressure at top of constant flux layer
F(A)	solar insolation subject to water vapor absorption only
F(2)	effective solar insolation at tropopause
FADJ	total incoming insolation at top of atmosphere
Fk_1k_2	net infrared flux divergence in layer (k_1,k_2)

F_k^*	net infrared flux at level k
FNWC	Fleet Numerical Weather Central
F(S)	solar insolation subject to Rayleigh scattering only
F_T	net IR flux to space
g	gravity = 9.8067 m sec^2
f	multiplicative factor for tuning cloud reflectances
h	hour angle
H	height of homogeneous atmosphere; 24-hour averaged hour angle
HL	population of gridpoints north of 25N
I	abscissa grid location
IA10(m,n)	solar insolation absorbed at surface with cloud condition (m,n)
IS10(m,n)	solar insolation at surface subject to Rayleigh scatter with cloud condition (m,n)
J	ordinate grid location
k	pressure level used in this study equal to 10σ
ly min^{-1}	langleys per minute
N	North latitude
P	pressure
P_k	pressure in millibars (mb) at level k
q_k	mixing ratio at level k
Qk_1k_2	24-hour averaged solar warming in layer (k_1,k_2)
QAVE	24-hour averaged insolation at the tropopause
Q_N	solar net insolation at level k = 0
r	Bowen ratio; actual earth-sun distance
r_m	mean earth-sun distance

R	net radiation balance at the surface
R_a	mean radiative cooling rate in troposphere
R_d	universal gas constant
REF	total insolation reflected back to space
REFA	F(A) insolation reflected back to space
REFS	F(S) insolation reflected back to space
RH	relative humidity
R_t	mean radiative energy gain (loss) rate at ocean-troposphere system
R_N	radiative net flux at level $k = 0$
S	South latitude; effective solar constant
S_o	heat storage in oceanic water mass
S_a	heat storage term for the troposphere
Study A	Spaeth's Thesis; using winter data (see references)
Study B	Meyers' Thesis; using spring data (see references)
Study C	Beahan's Thesis; using summer data (see references)
Study D	Warner's Thesis; using autumn data (see references)
T_k	temperature at level k
TR	population of gridpoints 20S-to-25N inclusive
TRAN	total insolation incident at the earth's surface
T_x	temperature at the top of constant flux layer
U	water-vapor layer absorber mass
W	West latitude
W(m,n)	cloud fractional weight for cloud condition (m,n)
Z	Zenith angle
$\alpha(G)$	surface albedo

$\alpha(R)$	Rayleigh clear sky albedo
δ	solar declination angle
Δ(ALB)	difference between ALBMOD and ALBRAS
ε_{wc}	emissivity due to water and carbon dioxide absorber mass at indicated layer
θ_k	potential temperature at level k
Λ	longitude
π	surface pressure; pi = 3.1416
ρ	density
σ	sigma pressure level used by FNWC, normalized to surface pressure
ϕ	latitude

ACKNOWLEDGEMENT

The author wishes to express his appreciation to his wife, Sheryn, for her patience, encouragement and support.

Appreciation is also expressed to the author's thesis advisor, Professor F. L. Martin, for his suggestions, advice, guidance and support in this research.

Further appreciation is expressed to Mr. Russell D. Schwanz for his programming assistance.

I. INTRODUCTION

This thesis is a refinement of previous radiational models described by (A) Spaeth (1975), (B) Meyers (1975), (C) Beahan (1975) and (D) Warner (1974) for use in the Fleet Numerical Weather Central (FNWC) prediction system. This study has as a primary objective, the comprehensive re-examination of the radiational physics in layers comprising the ocean-atmosphere system. FNWC atmospheric soundings defined at constant pressure levels for the four mid-seasonal dates of the "data year" 1973-74 as previously examined in studies (A,B,C,D) were utilized in this study.

The application of the FNWC radiative model may be made to any scale of analysis for which there is adequate resolution of the temperature and moisture data in the vertical. In the horizontal, the reliability of the data used here is consistent with that of the FNWC interpolation to gridpoints in the analysis procedure. Temperature and dew-point data in radiative soundings are typically reported to the nearest tenth of a degree. The radiative computations made here are applied to FNWC gridpoints and are designed to make a one-hour forward-time step at gridpoints in the FNWC primitive equation forecast model, with special adaptions to σ-levels.

The specification of cloud amounts in two designated layers, one at a mid-level and the other at a low-level, has an important influence on the radiative-model dispositions, both in the short- and long-wave spectral regions. Initially in (A,B,C,D), the specification of the fractional amounts of CL_1 and CL_2 had been based on large-scale formulations developed by Smagorinsky (1960), but during the course of these

studies it was found more realistic to modify initial CL-values to $CL' = 2/3\ CL$. This reduction in cloud amount was also used here as it had been chosen to prevent CL' from exceeding unity and to afford better agreement with satellite climatology, such as planetary albedo, for compatible data periods.

With the reduced cloud coverages CL_1' and CL_2' from the earlier studies (A,B,C,D), it was possible to obtain reasonably close agreement in the computed terrestrial net flux at the top of the atmosphere and that observed for comparable NIMBUS III subsatellite points and data periods (Raschke, Von der Haar, Bandeen and Pasternak, 1973). However even with the reduced cloud coverages CL_1' and CL_2' the computed planetary albedo remained generally excessive, particularly in tropical latitudes. Hence it became a major objective of this particular study to modify empirically the reflective capability of the cloud layers. This was done by defining a general factor f so that the initial choices (after Rodgers, 1967) of cloud reflectances R were modified to R' where

$$R' = fR .$$

Systematic substitution of the cloud reflectances R, wherever they entered the solar disposition equations, by R' then led to a relationship between the global albedo and f. Utilization of the least squares technique to minimize the differences between satellite and model albedos over a geographic sample of points led to best-fit value of the "tuning-factor" f. Separate values of f were deduced by least squares for each season, and subselections were deduced for the tropical and extratropical areas, respectively.

The modified solar cloud-reflectances improved the agreement between satellite and radiative model albedos in both geographic areas insofar as net incoming insolation was concerned. The terrestrial net flux at the top of the atmosphere was unaffected by the choice of f, while the use of CL_1' and CL_2' as specified gave good agreement with satellite terrestrial net flux data over the geographic range and the time-scales concerned.

II. DATA PREPARATION

A. DATA FIELDS

1. General Considerations

The initial temperature and humidity data used in this study were arranged in the form of soundings taken along four oceanic meridians (Fig. 1) of the Fleet Numerical Weather Central (FNWC) Northern Hemisphere mid-seasonal analyses for 16 October 1973, 16 January 1974, 16 April 1974 and 16 July 1974. Oceanic locations for these computations were chosen because:

(a) constant σ-surfaces (where $\sigma = \frac{P}{\pi}$) of the FNWC primitive equation system are nearly identical constant pressure levels.

(b) The maritime-area soundings are more likely to be systematically representative of the set of zonally-distributed gridpoints than over land.

The three meridians selected over the Pacific Ocean were located at 125W (25 soundings), 170W (25 soundings) and 145E (17 soundings). The Atlantic Ocean meridian was located at 35W (26 soundings). This method of selecting "soundings" along the indicated meridians of the FNWC polar stereographic map made it unnecessary to employ spatial interpolation between original data gridpoints along the meridians. Data along line 3 in the Pacific was not extended southward of gridpoint (9,55) because they fell over land masses (New Guinea and Northern Australia) where the surface temperatures and other sounding features were unrepresentative of the oceanic values.

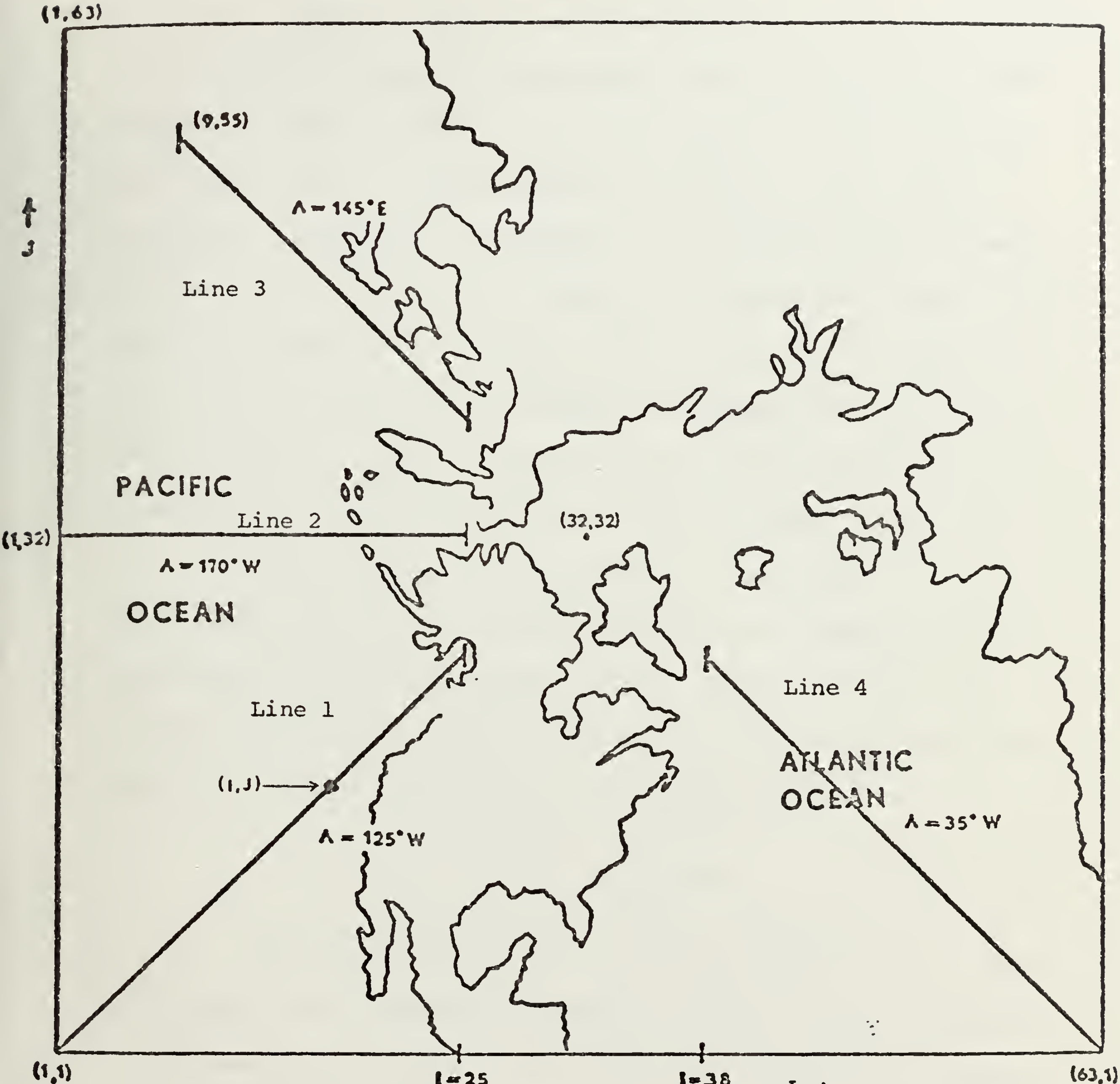

Figure 1. FNWC polar stereographic grid and meridians (lines 1, 2, 3, and 4) selected for study. The longitudes Λ are shown for each meridian as well as the extent considered of each meridian.

2. Data Treatment

a. Original Soundings and Modifications

The gridpoint soundings were taken from the original FNWC 63-by-63 Northern Hemisphere analyses of T(p) and of $T - T_D$ (the dew point depression) at standard pressure levels up to and including $p \approx 100$ mb. Examples of such original soundings were shown as Table I(a) in Meyers (1975, p. 24). Subsequently each original FNWC sounding was transformed --in previous studies (A, B, C, D) of this series --into what has been termed the radiative sounding having the format shown in Table I. The data levels of the radiative sounding contains essentially the five FNWC predictive σ-levels (dotted levels in Fig. 2).

At each gridpoint selected, the original FNWC humidity soundings were given in the form of five dew point depressions over the analyses levels from 925 mb to 400 mb. At the surface (level k = 10) the standard instrument level vapor pressure, e_{air}, was transformed into the surface mixing ratio, q_{10}, by means of

$$q_{10} \doteq 621.97 \, (e_{air}/1000) \ . \tag{2-1}$$

To obtain radiative soundings as in Table I, it is necessary to have water vapor and CO_2 absorber masses at certain required k-level boundaries (Fig. 2). All radiative soundings in this study start at sea level with the approximation of surface pressure $\pi \doteq 1000$ mb. Therefore, the eleven k-levels correspond closely to the FNWC levels P_k = 1000., 900., 800., ..., 200., 100., 0.0 mb and in turn to σ_k = 1.0, 0.9, ..., 0.1, 0.0.

TABLE I. Example of a radiative sounding at gridpoint (1,1) for 16 April 1974 with mixing ratio listed at odd k-levels (Fig. 2). Additionally, water-vapor and CO_2 absorber masses are also listed as these parameters have been modeled in the radiative theory presented in this study.

Pressure (mb)	Temp (°C)	Mixing Ratio (g/kg)	Absorber Masses Water Vapor (gm/cm^2)	CO_2 (cm/cm^2)
1000	25.60	17.10		
900	16.09	12.08		
800	11.21		2.26	45.53
700	5.00	6.21		
600	-2.10		3.23	83.53
500	-11.50	2.57		
400	-23.20	1.35	3.55	113.35
300	-38.00	0.65		
200	-56.60		3.61	133.99
100	-80.70	0.03	3.61	138.67
0	-80.70		3.61	143.35

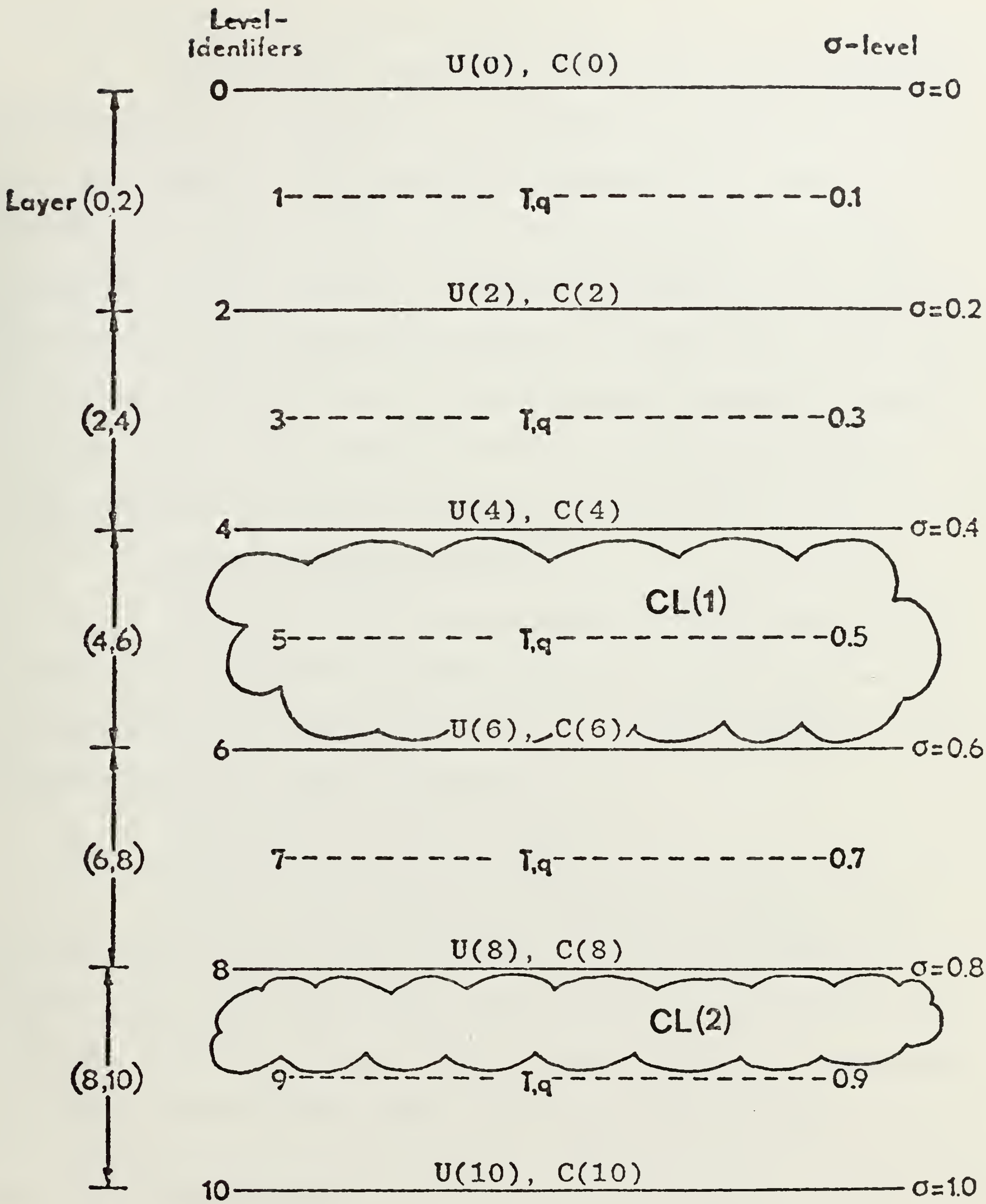

Figure 2. Five-layer radiative sounding used in this study. Levels are identified by their values on the k-scale, while layers are identified by their level boundary indices in parentheses, e.g. (8,10). Pressure-scaled water vapor and CO_2 mass increments ΔU and ΔC, respectively are integrated relative to the surface and the resulting U and C are carried at even levels. The temperature T is retained at all levels. Amounts of clouds CL_1 and CL_2 in the layers shown have been parameterized for consideration of their radiative effects.

b. Radiative Temperature Profiles

The gridpoint temperatures were listed at each mandatory level of Table I between 1000.,..., 100 mb (i.e., between k = 10,..., 1). The temperature was assumed to be isothermal from 100 mb to 0.0 mb. The temperature at level k = 10 was set equal to the FNWC listed sea-surface temperature. The radiative sounding temperatures for the remaining k-levels were obtained from either their corresponding listed temperature-level or by a three-point Lagrangian interpolation scheme [Eq. (2-1), Spaeth, 1975], to level k when the listed FNWC temperature profile did not include the value T_k.

c. Radiative Moisture Profiles

Similarly, the moisture profiles of Table I have been obtained by an interpolative procedure over the original-level FNWC mixing ratios to those required at k-levels in a manner analogous to that discussed by Spaeth (1975, pp. 29-31).

d. Pressure-Scaled Absorber Masses

The pressure-scaled water vapor and the carbon-dioxide scaled absorber masses were calculated for the six even numbered k-levels (Fig. 2) using Eqs. (2-8, 2-9, 2-10 and 2-11) respectively as outlined by Spaeth (1975, pp. 31-33). These equations use essentially the mixing ratios of water vapor and of CO_2 at odd k-levels.

B. CLOUD PARAMETERIZATION

The relative humidities (RH) at levels k = 5 and k = 9 are used in the calculations of the fractional cloud covers CL_1 and CL_2 in layers (4,6) and (8,9) respectively (Fig. 2). The equations for

parameterization of the two fractional cloud amounts are as follows:

$$CL_1 = 2/3\ [2.0\ (RH(5)) - 0.7] \tag{2-2a}$$

$$CL_2 = 2/3\ [3.33(RH(9)) - 2.0] \tag{2-2b}$$

The bracketed part of the equations (after Smagorinsky, 1960) were reduced by the 1/3 factor in an attempt to tune cloud amounts to obtain albedo values in closer agreement with the recent satellite radiational climatology of Raschke et al., (1973). The "2/3 CL" parameterization set forth in Eq. (2-2) is used here for estimating large scale radiational effects only. Thus small-scale convective activity and *a priori* climatological effects were not considered in specifying the form of Eq. (2-2). Tuning of the model-albedo values of this study by varying cloud reflectance coefficients with respect to season and latitude will be discussed in Section IV.

C. CLOUD-AREA COVERAGES

Fractional cloud amounts, CL_1 and CL_2, were computed at each gridpoint for levels k = 5 and k = 9 by Eqs. (2-2a,b). In addition the gridpoint area may be thought of as broken into random fractional segments of size

$$W(0,0) = (1-CL_1)\ (1-CL_2) \tag{2-3a}$$

wherein there is a combination of clear-over-clear segments in the layers. Similarly, the gridpoint area has the fractional area of cloud coverage

$$W(1,1) = CL_1 * CL_2 \tag{2-3b}$$

of an upper overcast amount overlying a lower overcast. Likewise the area-combinations of overcast over clear, and clear over overcast areas in two layers, may be visualized as occurring with the weights

$$W(1,0) = CL_1 *(1-CL_2) \tag{2-3c}$$

and

$$W(0,1) = (1-CL_1) *CL_2 \tag{2-3d}$$

respectively.

For radiational computations it was useful to carry the relative weights or fractions of the gridpoint area exposed to the specified cloud-layer combinations. Henceforth, the symbols denoted by W(0,0), W(1,1), W(1,0) or W(0,1) indicate the fractionally overcast (1) or clear (0) cloud-area combinations in the indicated layers (Fig. 2), with the first index 1 or 0 referring to layer CL_1, k = 5, and the second to CL_2, k = 9.

The usefulness of the cloud-area weighting device will be clarified in Sections III and IV, where the procedures for the terrestrial and solar radiational computations are discussed and the results are summarized over the set of soundings.

A measure of the effective cloud-cover area which has been found useful in previous radiational studies has been the <u>total opaque cloud cover</u>, CL, referring to the amount of thick cloud cover overhead regardless of the level. For the cloud model presented here CL may be expressed as

$$CL = CL_1 + CL_2 - CL_1 *CL_2 \ . \tag{2-4}$$

III. TERRESTRIAL RADIATION

A. THEORETICAL AND EMPIRICAL BASIS

Empirical formulas were developed by Sasamori (1968) for flux emissivities in the atmosphere associated with computations for the radiative balance requirements of the NCAR General Circulation Model. Sasamori derived the empirical emissivity formulas for water vapor and CO_2 by comparison with the theoretical values built into the Yamamoto Radiation Chart (1952). The Yamamoto chart has proved to be quite accurate for numerical checks of the Sasamori emissivities. This chart was also used in the previous studies (A, B, C, D) as a systematic guide for integration of the radiative transfer formulas developed by Martin (1972, 1975), who adapted the Sasamori emissivity formulas to the particular layers of interest in the gridpoint computations of the FNWC primitive equation model (Fig. 2).

The essential long-wave (IR) net-flux parameters required for use in this study are the following:

F_{10}^* = IR net flux at earth, k = 10

F_8^* = IR net flux at level k = 8

F_6^* = IR net flux at level k = 6

F_4^* = IR net flux at level k = 4

F_2^* = IR net flux at level k = 2

In addition the IR net-flux divergence coolings to be computed at each gridpoint are

F810 = IR net-flux divergence in the layer (8,10)

F68 = IR net-flux divergence in the layer (6,8)

F46 = IR net-flux divergence in the layer (4,6)

F24 = IR net-flux divergence in the layer (2,4).

In the Radiation Balance Studies in the series A, B, C, D only F610 and F26 were computed because time restraints in the present FNWC operational heating package have prevented the use of greater resolution in the vertical. Here, four flux divergences are computed in order to examine more closely the variability of the flux divergences over the layer thicknesses reduced to approximately 200 mb each. To compute these four flux divergences it was necessary to utilize additional formulas for F_8^* and F_4^* as developed by Martin (1975).

In order to make IR net-flux calculations along the path of integration, there must be a physically sound representation of the emissivity (ε_{wc}) as a function of both water vapor and CO_2 absorber masses in layers along the sounding. For a complete discussion of the emissivity formulas used in the quadrature scheme, refer to Spaeth's Appendix A (1975).

B. NET FLUX FORMULATIONS

The radiative sounding as depicted in Table I was computed as the combination of parameters U(k,10), C(k,10) and T_k for each required level, k = 10, 8, ... 1,0. Cloud parameters CL_1 and CL_2 were also computed by Eq. (2-2) at each gridpoint and in general are both non-zero. The grid area was then considered to be composed of areal fractions (weights) defined in Eqs. (2-3a,b,c,d) and denoted by the symbols W(0,0), W(1,1), W(1,0), W(0,1).

The composite net flux F_{10}^* (CL_1, CL_2) at level k = 10 at each gridpoint is then constructed by using the appropriate weight factors

to multiply the <u>reference net flux</u> F_{10}^{*} computations defined for the four special cloud-cover cases already defined in Section II.C:

$$F_{10}^{*}(0,0),\ F_{10}^{*}(1,0),\ F_{10}^{*}(0,1),\ F_{10}^{*}(1,1)$$

It therefore follows that

$$F_{10}^{*}(CL_1,\ CL_2) = W(0,0)F_{10}^{*}(0,0) + W(1,0)F_{10}^{*}(1,0) + W(0,1)F_{10}^{*}(0,1) + W(1,1)F_{10}^{*}(1,1). \qquad (3\text{-}1)$$

The reference net fluxes F_{10}^{*} of Eq. (3-1) are associated with (1) clear skies in both layers, (2) overcast in the upper layer only, (3) overcast in the lower layer only and (4) overcast in both layers respectively.

Spaeth (1975) has listed these reference net flux formulations in his Eqs. (3-6), (3-7) and (3-8). Using the definitions of W(0,0), W(1,0), W(0,1) and W(1,1), $F_{10}^{*}(CL_1,\ CL_2)$ can be shown to assume the form

$$\begin{aligned} F_{10}^{*}(CL_1,\ CL_2) = {} & [1-CL_2]\{(B_{10}-B_6)-.5[\varepsilon_{wc}(8,10)(B_{10}-B_8) \\ & + (\varepsilon_{wc}(8,10) + \varepsilon_{wc}(6,10))(B_8-B_6)]\} \\ & + (1-CL_2)(1-CL_1)\{B_6-.5[(\varepsilon_{wc}(6,10) \\ & + \varepsilon_{wc}(4,10))(B_6-B_4) + (\varepsilon_{wc}(4,10) \\ & + \varepsilon_{wc}(2,10))(B_4-B_2) + (\varepsilon_{wc}(2,10) \\ & + \varepsilon_{wc}(1,0))(B_2-B_1) + \tilde{\varepsilon}_{wc}((0,10),T_1)*B_1]\} \\ & + CL_2\ \{(B_{10}-B_9)[1.5\varepsilon_{wc}(9,10)]\}\ . \end{aligned} \qquad (3\text{-}2)$$

Here

$$B_k = 1.170403 \times 10^{-7}\ T_k^{\ 4} \qquad (3\text{-}3)$$

is the Stefan-Boltzmann blackbody flux in langlies per day.

Further, $\varepsilon_{wc}(U_k,C_k,10)$ is the combined water-vapor and CO_2 emissivity along the path from level 10 to level k. This emissivity is considered by Sasamori to be temperature independent for $T \geq 210K$, whereas $\tilde{\varepsilon}_{wc}$ represents the temperature dependent emissivity applicable for $T < 210K$. [See pp. 136-137, Spaeth (1975); Sasamori (1968)].

The formulas for $F_k^*(CL_1, CL_2)$, k = 2,4,6, and 8 have been developed by Martin (1975) in a manner analogous to the derivation of the weighted F_{10}^*. The results are reproduced as the following equations:

$$\begin{aligned}
F_8^* = {} & [1-CL_1]\ \{B_8-.5[\varepsilon_{wc}(6,8)(B_8-B_6) \\
& + (\varepsilon_{wc}(6,8) + \varepsilon_{wc}(4,8))(B_6-B_4) \\
& + (\varepsilon_{wc}(4,8) + \varepsilon_{wc}(2,8))(B_4-B_2) \\
& + (\varepsilon_{wc}(2,8) + \varepsilon_{wc}(1,8))(B_2-B_1) + \tilde{\varepsilon}_{wc}((0,8),T_1)*B_1]\} \\
& + CL_1\ [1-.5\varepsilon_{wc}(6,8)](B_8-B_6) + CL_1\ (1-CL_2)[1-.5\varepsilon_{wc}(8,10)](B_{10}-B_8) \\
& + (1-CL_1)(1-CL_2)[1-.5\varepsilon_{wc}(8,10)](B_{10}-B_8)
\end{aligned} \tag{3-4}$$

$$\begin{aligned}
F_6^* = {} & [1-CL_1]\ \{B_8-.5[\varepsilon_{wc}(6,8)(B_8-B_6) + \varepsilon_{wc}(4,6)(B_6-B_4) \\
& + (\varepsilon_{wc}(4,6) + \varepsilon_{wc}(2,6))(B_4-B_2) + (\varepsilon_{wc}(2,6) \\
& + \varepsilon_{wc}(1,6))(B_2-B_1) + \tilde{\varepsilon}_{wc}((0,6),T_1)*B_1]\} \\
& + (1-CL_1)(1-CL_2)\{(B_{10}-B_8)[1.-.5(\varepsilon_{wc}(6,8) \\
& + \varepsilon_{wc}(6,10))]\} + CL_1\ \{(B_8-B_6)* \\
& [1-.5\varepsilon_{wc}(6,8)]\} + CL_1\ (1-CL_2)\ \{(B_{10}-B_8)* \\
& [1-.5(\varepsilon_{wc}(6,8) + \varepsilon_{wc}(6,10))]\} .
\end{aligned} \tag{3-5}$$

$$
\begin{aligned}
F_4^* = {} & [1-CL_1]\ \{B_8-.5[\varepsilon_{wc}(4,6)(B_6-B_4) \\
& + (\varepsilon_{wc}(4,6) + \varepsilon_{wc}(4,8))(B_8-B_6) + \varepsilon_{wc}(2,4)(B_4-B_2) \\
& + (\varepsilon_{wc}(2,4) + \varepsilon_{wc}(1,4))(B_2-B_1) + \tilde{\varepsilon}_{wc}((0,4),T_1)*B_1]\} \\
& + CL_1\ \{B_4-.5[\varepsilon_{wc}(2,4)(B_4-B_2) \qquad (3\text{-}6) \\
& + (\varepsilon_{wc}(2,4) + \varepsilon_{wc}(1,4))(B_2-B_1) + \tilde{\varepsilon}_{wc}((0,4),T_1)*B_1]\} \\
& + (1-CL_1)(1-CL_2)\ \{(B_{10}-B_8)[1-.5(\varepsilon_{wc}(4,8) + \varepsilon_{wc}(4,10))]\}
\end{aligned}
$$

$$
\begin{aligned}
F_2^* = {} & [1-CL_1]\ \{B_8-.5[\varepsilon_{wc}(2,4)(B_4-B_2) + (\varepsilon_{wc}(2,4) \\
& + \varepsilon_{wc}(2,6))(B_6-B_4) + (\varepsilon_{wc}(2,6) + \varepsilon_{wc}(2,8))* \\
& (B_8-B_6) + \varepsilon_{wc}(1,2)(B_2-B_1) + \tilde{\varepsilon}_{wc}((0,2),T_1)*B_1]\} \qquad (3\text{-}7) \\
& + (1-CL_1)(1-CL_2)\ \{(B_{10}-B_8)[1-.5(\varepsilon_{wc}(2,8) \\
& + \varepsilon_{wc}(2,10))]\} + CL_1\ \ \{B_4-.5[\varepsilon_{wc}(2,4)(B_4-B_2) \\
& + \varepsilon_{wc}(1,2)(B_2-B_1) + \tilde{\varepsilon}_{wc}((0,2),T_1)*B_1]\}\ .
\end{aligned}
$$

As was described by Spaeth (1975, Section III.B.5.) concerning the use of the composite case, Eq. (3-2) can be reduced to give expressions for F_{10}^* for the various reference cloud-cover cases (0,0), (1,1), (1,0) and (0,1). The resulting schematics in the case of F_8^* and F_4^* are depicted as the unhatched area in Figs. 3(a,b,c,d) and 4(a,b,c,d), respectively below. Similar graphs for F_{10}^*, F_6^* and F_2^* can be found on pp. 41-43 of Spaeth (1975), and are not reproduced here.

A typical gridpoint listing of the IR net-flux computations, F_k^* ($k = 10,8,...2$), has been reproduced in Table II for gridpoint (1,1) based upon the radiative sounding of 16 April 1974 (see Table I). The printout procedure involves computation of the reference net-flux values

$$F_k^*(0,0),\ F_k^*(1,0),\ F_k^*(0,1),\ F_k^*(1,1)$$

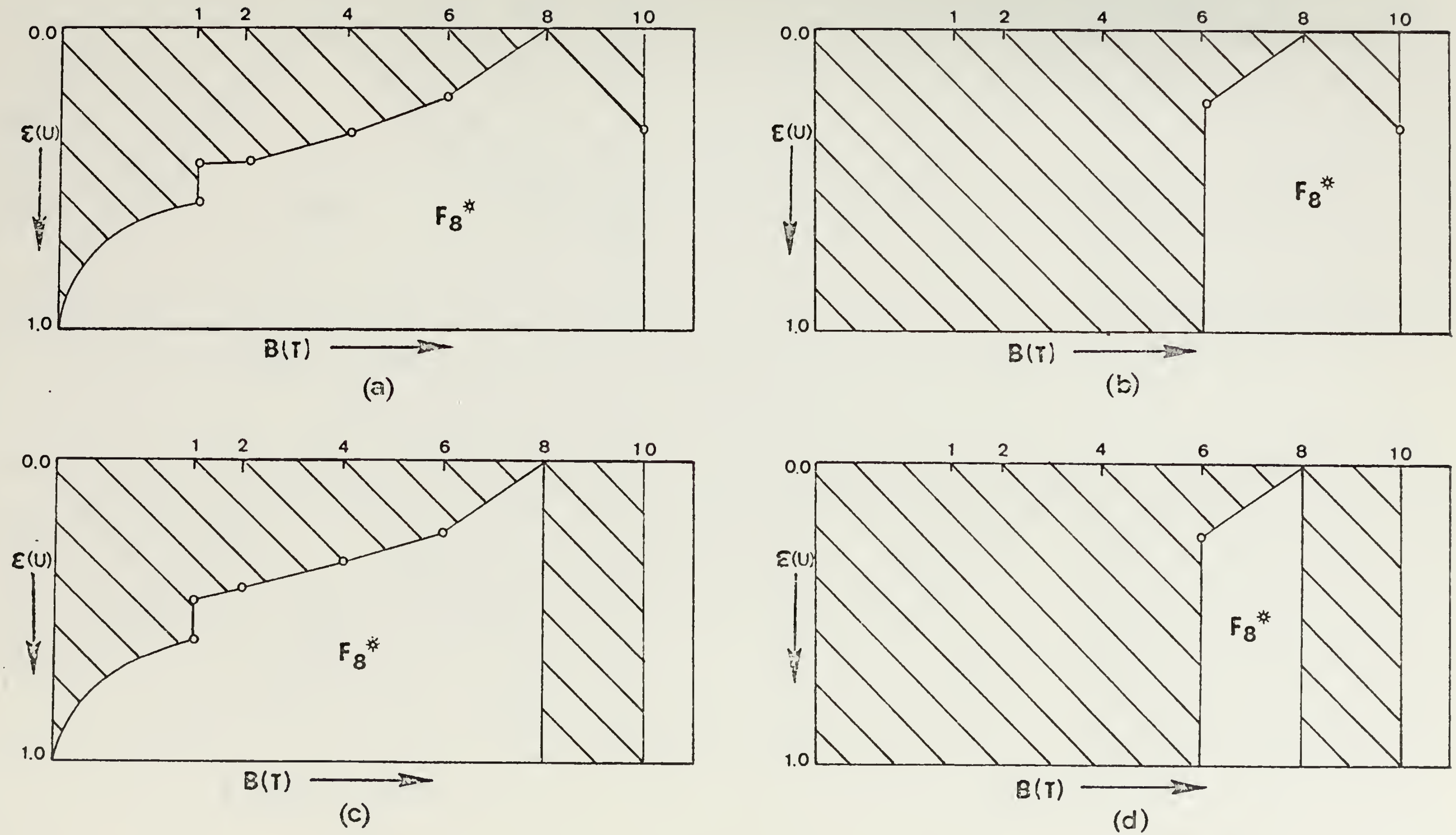

Figure 3. Terrestrial net flux F_8* with (a) clear skies (case (0,0)); (b) high overcast only case (1,0)); (c) low overcast only (case (0,1)); (d) both high and low overcast (case (1,1)). Unhatched area in each case depicts F_8*.

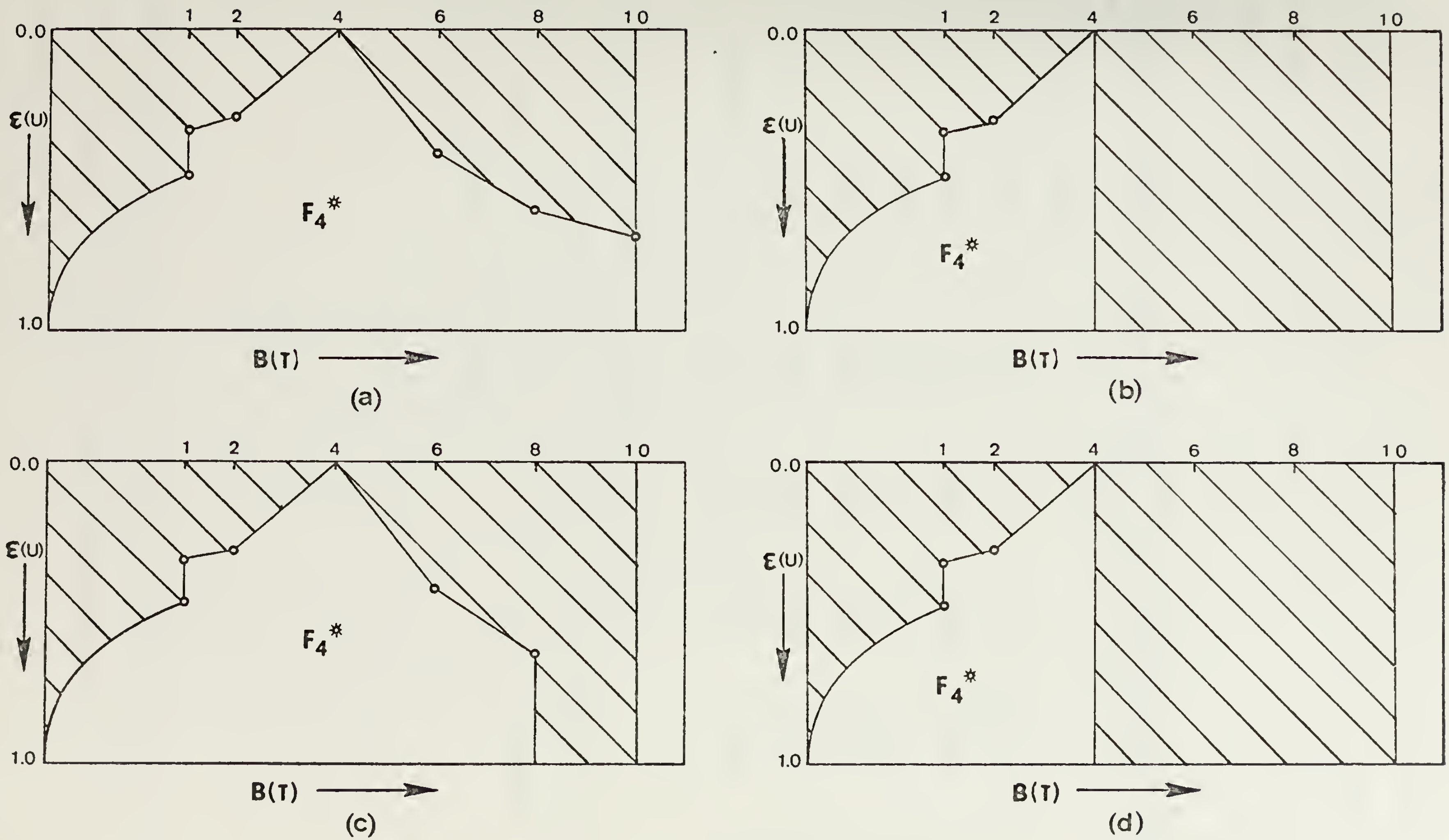

Figure 4. Terrestrial net flux F_4* with (a) clear skies (case),0); (b) high overcast only (case (1,0)); (c) low overcast only (case (0,1)); (d) both high and low overcast (case (1,1)). Unhatched area in each case depicts F_4*.

from each of Eqs. (3-2), (3-4), (3-5), (3-6) and (3-7) for level $k = 10, 8, \ldots 2$ respectively. Then Eq. (3-1) with the appropriate weight-factors of Eqs. (2-3a,b,c,d) has been utilized to derive the composite $F_k^*(CL_1, CL_2)$ values that are listed on the bottom line of Table II.

TABLE II. A sample listed of IR net-flux computations, weighting factors and composite values, $F_k^*(CL_1, CL_2)$, as computed for grid-point (1,1) for 16 April 1974. Net flux values in ly min^{-1}.

Cloud Case $(CL_1\ CL_2)$	Weight $W(CL_1, CL_2)$	F_{10}^*	F_8^*	F_6^*	F_4^*	F_2^*
(0,0)	.1002	.1664	.2288	.2649	.3160	.3487
(1,0)	.1497	.0943	.1331	.0915	.1706	.2338
(0,1)	.3007	.0512	.1563	.2341	.2871	.3202
(1,1)	.4494	.0512	.0586	.0607	.1706	.2338
F_k^*-composite values		.0692	.1171	.1379	.2202	.2713

C. TROPOSPHERIC COOLING BY LAYERS; F_{10}^* COOLING

For each mid-seasonal day listed and at each gridpoint, an IR net-flux computation in the format of Table II is easily converted into four sets of layer cooling effects.

$$
\begin{aligned}
F810 &= F_8^* - F_{10}^* \\
F68 &= F_6^* - F_8^* \\
F46 &= F_4^* - F_6^* \\
F24 &= F_2^* - F_4^*
\end{aligned}
\qquad (3\text{-}8)
$$

These layer cooling rates (ly min^{-1} have then been collected in meridional cross-section format for each longitude under study (see Section V) and by season.

The overall tropospheric cooling rate by IR net flux is then given simply by $F_2^* - F_{10}^*$ at each gridpoint for the date of the radiational sounding. The tropospheric cooling rates computed are then identical to

$$F_2^* - F_{10}^* = F24 + F46 + F68 + F810 . \qquad (3\text{-}9)$$

The values of $F_2^* - F_{10}^*$ so deduced are discussed on both a seasonal and a zonally-averaged basis in Section V.

It will suffice to discuss here the zonally-averaged values of F_{10}^* (CL_1, CL_2) as computed by the long-wave radiational model previously presented in this section. These results, listed simply as F_{10}^* in Table III, will be discussed as a function of seasons, latitudes and CL (total opaque cloud cover given by Eq. (2-4)). The listings of F_{10}^* in Table III are essentially as extracted from computations in the format of Table II followed by meridional-averaging of F_{10}^* across constant latitude lines. Finally the zonally-averaged annual values of both F_{10}^* and CL have been computed by arithmetic-averaging over the four mid-seasonal results at each five-degree increment of latitude from 20S to 65N (cf., Eq. (5-1)).

The model-annual values of F_{10}^* presented in Table III are presented with those derived from Budyko (1956), which in turn are listed in the final column of Table III. Corresponding values of total opaque cloud cover, CL, for the Budyko climatology were not available so that only a general comparison of the two annual F_{10}^* zonally-averaged distributions is possible.

LAT.	16 January		16 April		16 July		16 October		Annual Model Values		Budyko
	F_{10}^*	CL	F_{10}^*	CL	F_{10}^*	CL	F_{10}^*	CL	F_{10}^*	CL	F_{10}^*
20S	.0782	.766	.0738	.842	.1510	.267	.0927	.629	.0989	.626	.091
15S	.0789	.744	.0669	.827	.1330	.304	.0823	.629	.0903	.625	.092
10S	.0852	.639	.0712	.750	.1348	.256	.0807	.604	.0930	.563	.083
5S	.0748	.619	.0692	.727	.0937	.496	.0747	.707	.0781	.637	.085
0	.0867	.529	.0781	.629	.1016	.444	.0952	.489	.0904	.523	.084
5N	.0859	.518	.0804	.590	.0947	.533	.1011	.471	.0905	.528	.086
10N	.1071	.367	.0865	.567	.1024	.459	.1015	.459	.0994	.463	.086
15N	.1147	.337	.0921	.547	.1035	.428	.0988	.486	.1023	.450	.094
20N	.1198	.283	.0850	.534	.0943	.429	.1011	.437	.1000	.421	.102
25N	.1199	.318	.0941	.471	.0985	.373	.1056	.383	.1046	.386	.098
30N	.1116	.432	.0982	.445	.0920	.424	.1037	.448	.1014	.437	.099
35N	.1222	.397	.1116	.519	.0925	.381	.1087	.484	.1088	.445	.102
40N	.1080	.516	.1163	.466	.0863	.386	.1218	.325	.1081	.423	.109
45N	.0672	.781	.0996	.466	.0586	.564	.1188	.301	.0860	.531	.098
50N	.0688	.760	.0794	.674	.0634	.474	.1037	.381	.0789	.572	.099
55N	.0683	.723	.1083	.554	.0370	.818	.0921	.452	.0768	.637	.102
60N	.1058	.514	.0539	.814	.0853	.458	.0856	.451	.0827	.559	.104
65N	.0934	.000	.0817	.795	.0613	.591	.0346	.885	.0677	.558	.095
Wt. Avg.	.1004	.480	.0921	.547	.0881	.464	.1029	.435	.0959	.482	.0957

TABLE III. A listing of IR net-flux (F_{10}*) at level k = 10 and total opaque cloud cover (CL) by season and latitude and listed are the annually averaged model-values of F_{10}* and CL including Budyko-values of F_{10}*. Also listed are the Northern Hemisphere cosine-weighted means of the above parameters. All F_{10}* values in ly min^{-1}.

Table III depicts the zonally-distributed values of F_{10}^* and of CL at the earth's surface. In a seasonal comparison of the model-computed F_{10}^* values it is clearly shown that F_{10}^*(CL) is a decreasing function of cloud cover. There is a clear-cut tendency in each season for a maximum value of F_{10}^* to be located in the subtropics (latitudes 15N-25N). Also there is evidence of a high latitude (55N-60N) minimum F_{10}^* associated with a concentration of maximum cloud cover CL. An outstanding variation is the transition in the Southern Hemisphere latitudes (20S - 10S), which has small cloud cover in local winter and comparitively large cloud cover during the other three data periods. This cloud-cover variation corresponds in general to the ITCZ behavior in these latitudes across the indicated seasons; so that, F_{10}^* is a maximum in mid-July and a relative minimum in the period January-April.

The final entry in Table III, namely "Wt. Avg.", is the Northern Hemisphere mean, cosine-weighted with respect to latitude (cf., Eq. (6-1)). The cosine-weighted $\overline{F_{10}^*}$ values show a minimum in Northern Hemisphere summer with no clear-cut differences in $\overline{CL}$. This summer minimum is attributable to higher downward flux with increased summer vapor pressures.

D. OUTGOING IR NET FLUX TO SPACE

1. Parameterization Formula for Top-of-Atmosphere IR Net Flux

In the four previous radiation studies (A, B, C, D), an approximation to the IR net flux to space, designated as FF2, was computed from the radiative sounding at each gridpoint. FF2 was essentially an extrapolation of F_2^* to the top of the atmosphere obtained by deleting the downward IR flux due to stratospheric water-vapor and CO_2. A

more precise expression for the net IR flux to space was introduced here after Martin (1975). The development is analogous to the quadrature summations

$$F_T = \int_{B_{10}}^{B=0} \varepsilon_{wc} \, dB \qquad (3\text{-}10)$$

for the various reference-cloud combinations (0,0), (1,0), (0,1) and (1,1) of Fig. 5(a,b,c,d) respectively. The final quadrature-formula is then obtained as the weighted net-flux result as was also done in Eqs. (3-4), (3-5), (3-6), (3-7) and is listed below.

$$\begin{aligned} F_T = {} & [1-CL_1]\{B_8-.5[(\varepsilon_{wc}(0,1) + \varepsilon_{wc}(0,2))(B_2-B_1) \\ & + (\varepsilon_{wc}(0,2) + \varepsilon_{wc}(0,4))(B_4-B_2) \\ & + (\varepsilon_{wc}(0,4) + \varepsilon_{wc}(0,6))(B_6-B_4) + (\varepsilon_{wc}(0,6) + \varepsilon_{wc}(0,8))(B_8-B_6)]\} \\ & + CL_1 \{B_4-.5[(\varepsilon_{wc}(0,1) + \varepsilon_{wc}(0,2))(B_2-B_1) \qquad (3\text{-}11) \\ & + (\varepsilon_{wc}(0,2) + \varepsilon_{wc}(0,4))(B_4-B_2)]\} \\ & + (1-CL_1)(1-CL_2)\{[1-.5(\varepsilon_{wc}(0,8) + \varepsilon_{wc}(0,10))][B_{10}-B_8]\} \end{aligned}$$

where CL_1, CL_2 are given by Eq. (2-2). Note that F_T of Eq. (3-11) is representable by the unhatched areas of Figs. 5(a,b,c,d) for the various reference-cloud cases and that F_T has no downward IR flux corresponding to the level k = 0.

2. Comparisons of F_T with Mid-Seasonal Satellite Climatology

Comparison was made of computed-model values of F_T with satellite measurements of total long-wave flux to space (after Raschke et al., 1973) for the Nimbus III mid-seasonal periods most nearly comparable to that of the FNWC data. F_T for each mid-seasonal date was computed over the

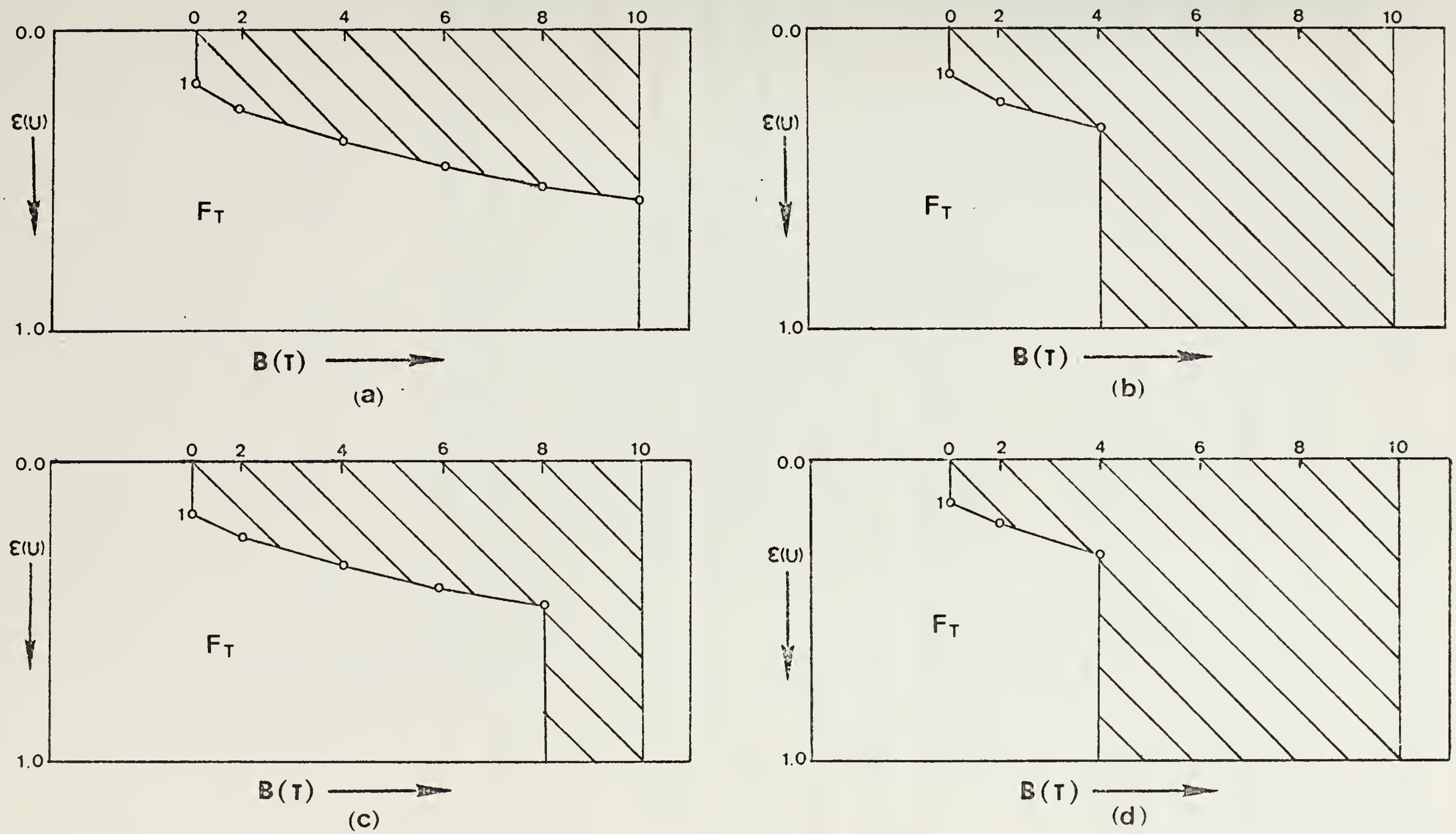

Figure 5. Outgoing terrestrial net flux to space F_T with (a) clear skies [case (0,0)]; (b) high overcast only [case (1,0)]; (c) low overcast only (0,1); (d) both high and low overcast [case (1,1)]. Unhatched area in each case depicts F_T.

four meridians considered. These F_T values were then averaged across the four meridians to get a mean zonal distribution of the type shown in Table IV.

Table IV shows the zonally-averaged model values compared with those extracted from Raschke. Raschke's results were obtained by averaging across the same oceanic meridians as those used in this study. Again, in the bottom line of each column in Table IV is listed the cosine-weighted mean of each set of column values for the Northern Hemisphere only.

The zonally-averaged values computed by the F_T-model are very close to those reported by Raschke, especially between 0-65N and in the Northern Hemispheric means. The limitations of the comparisons made here are obvious, when it is recalled that between latitudes 20S-5S and between 60N-65N there are fewer than four meridional lines available for computing the listed zonal values in Table IV. For all other zonally-averaged values, four meridional lines were used in the averaging.

The close comparison between model-values of F_T from (3-11) and those essentially derived from satellite climatology tend to support the cloud parameterization, Eq. (2-2), insofar as IR net flux is concerned.

LAT	16 January		16 April		16 July		16 October		Annual	
	MOD	RAS	MOD	RAS	MOD	RAS	MOD	RAS	MOD	RAS
20S	.3188	.3703	.2992	.4100	.3795	.4005	.3194	.3791	.3292	.3900
15	.3280	.3798	.3063	.4150	.3858	.4196	.3194	.4006	.3349	.4037
10	.3485	.3750	.3270	.4100	.3949	.4257	.3216	.4248	.3480	.4089
5	.3306	.3457	.3263	.3681	.3769	.3966	.3016	.4182	.3338	.3822
0	.3611	.3527	.3431	.3646	.3649	.3776	.3364	.4096	.3514	.3761
5N	.3712	.3685	.3609	.3414	.3547	.3538	.3473	.3687	.3585	.3581
10	.3799	.3892	.3750	.3616	.3666	.3360	.3537	.3409	.3688	.3569
15	.3843	.3952	.3755	.3899	.3754	.3500	.3574	.3535	.3722	.3727
20	.3870	.3943	.3779	.3956	.3841	.3743	.3649	.3893	.3785	.3884
25	.3645	.3724	.3794	.3867	.3872	.3947	.3762	.3974	.3768	.3878
30	.3345	.3418	.3621	.3613	.3768	.3922	.3673	.3879	.3602	.3708
35	.3491	.3163	.3514	.3542	.3849	.3769	.3519	.3666	.3593	.3535
40	.3291	.3026	.3404	.3400	.3745	.3630	.3621	.3459	.3515	.3379
45	.3042	.2891	.3268	.3300	.3564	.3560	.3564	.3238	.3360	.3247
50	.2999	.2727	.3121	.3221	.3306	.3497	.3398	.3005	.3206	.3112
55	.2643	.2701	.3125	.3151	.2857	.3274	.3106	.2951	.2933	.3019
60	.2720	.2696	.2889	.3103	.3294	.3304	.3020	.2896	.2981	.3000
65	.2681	.2700	.2651	.3000	.2937	.3300	.2543	.3101	.2703	.3025
Wt. Avg.	.3472	.3431	.3523	.3567	.3634	.3627	.3511	.3592	.3535	.3552

TABLE IV. Comparison of total outgoing IR radiation between computed-model values and satellite climatology from Raschke et al (1973) as zonally averaged over four oceanic meridians. The weighted averages are derived from cosine-weighting values from 0-65N latitude. All F_T-values in ly min^{-1}.

IV. SOLAR RADIATION

A. COMPOSITION OF SOLAR INSOLATION

At the top of the atmosphere (k=0) this study assumed a solar constant of 2.00 ly min^{-1} (Joseph, 1971). Furthermore, this constant was assumed subject to a four percent attenuation above the tropopause due to ozone and oxygen. Thus the effective solar constant at level k=2 in this study is 1.92 ly min^{-1}.

To compute the effective solar insolation at the tropopause the following formula was used

$$F(2) = S\left[\frac{r}{r_m}\right]^{-2} \text{Cos } Z \qquad (4\text{-}1)$$

where S is the effective solar constant at level k=2 and

r/r_m = ratio of the actual earth-sun distance to the mean earth-sun distance, a function of the Julian date

Cos Z= cosine of the zenith angle, a function of the Julian date determined by

$$\text{Cos } Z = \text{Sin } \phi \text{ Sin } \delta + \text{Cos } \phi \text{ Cos } \delta \text{ Cos } h \; . \qquad (4\text{-}2)$$

The symbols on the right side of Eq. (4-2) are defined as follows:

ϕ = latitude

δ = solar declination

h = hour angle

The Smithsonian Meteorological Tables (List, 1958) list the ratio of r/r_m and the solar declination, δ, for the mid-seasonal dates applicable to this study and reproduced in Table V.

TABLE V. Values of the ratio of the earth-sun radius vector, r/r_m, and of the solar declination angle, δ, used in this study for year 1973 - 1974.

Date	r/r_m	δ
16 January	0.98372	21.07917°S
16 April	1.00333	8.48333°N
16 July	1.01644	21.50000°N
16 October	0.99717	8.22500°S

The value of sin ϕ was calculated using one of two different formulas, depending on the data-line used for the computations, in terms of the FNWC map coordinates (I,J) as in Eq. (4-3a,b). Conversely for these lines one may solve for I in terms of sin ϕ as in (4-3c,d):

$$\text{Lines 1,3,4} \qquad \operatorname{Sin} \phi = \frac{973.752 - 2(32-I)^2}{973.752 + 2(32-I)^2} \tag{4-3a}$$

$$\text{Line 2} \qquad \operatorname{Sin} \phi = \frac{973.752 - (32-I)^2}{973.752 + (32-I)^2} \tag{4-3b}$$

$$\text{Lines 1,3,4} \qquad I = 32 - 22.065 \left[\frac{\operatorname{Cos} \phi}{1 + \operatorname{Sin} \phi}\right] \tag{4-3c}$$

$$\text{Line 2} \qquad I = 32 - 31.205 \left[\frac{\operatorname{Cos} \phi}{1 + \operatorname{Sin} \phi}\right] \tag{4-3d}$$

$$I = \begin{cases} 1,\ldots,25 & \text{for Lines 1,2} \\ 8,\ldots,25 & \text{for Line 3} \\ 63,\ldots,38 & \text{for Line 4} \end{cases}$$

Here I is the abscissa distance on the FNWC grid (Fig. 1) and varies by line as described in Section II. The soundings for lines 1, 2, and 3 were all taken at 0000GMT with the solar noon existing at the 180th meridian; therefore the hour angles for these three lines were 55°, 10°, and 35°, respectively. For line 4, the soundings were taken 12 hours earlier with solar noon at the Greenwich meridian, giving an hour angle for line 4 of 35°.

A very simple partition of solar insolation was utilized in this study after Joseph (1971). It consisted of dividing the insolation F(2) into two parts at level k=2. One part was considered to include all wavelengths $\lambda > .9$ µm where absorption by water vapor and carbon dioxide bands are the most prevalent attenuation processes in clear air. This part of the solar spectrum was termed the F(A) energy and considered subject to water-vapor absorption but not to Rayleigh scattering. For shorter wavelengths, $\lambda \leq .9$ µm, absorption of the solar insolation energy by water vapor was considered negligible. This part of the solar insolation was denoted F(S) suggestive of the fact that it was subject only to Rayleigh scattering attenuation in clear air. The two partitions are formulated after Joseph (1971) as follows:

$$F(A) = .349\ F(2) \qquad (4\text{-}4)$$

$$F(S) = .651\ F(2). \qquad (4\text{-}5)$$

In this study, the introduction of two cloud decks produced cloud-reflectivity effects upon both the F(A) and F(S) solar energy insolations. However, in the clear areas around any gridpoint only the absorption-attenuation applies to the F(A) insolation, while only Rayleigh scattering-attenuation applies to the F(S) insolation.

B. DISPOSITION OF F(S) INSOLATION

In the disposition of the F(S) insolation, Joseph (1971) determined that Rayleigh scattering reflectance to space by clear skies (after Coulson, 1959) could be effectively approximated by least squares in the following form

$$\alpha(R) = .085 + .25074 \, [\log (\frac{\pi}{P_o}) \text{ Sec } z)] \tag{4-6}$$

where P_o = 1013.25 mb. In Eq. (4-6), $\pi/P_o \doteq 1$ in view of the fact that mean sea level pressure π is close to 1000 mb. Also

$$\text{Sec } z = (\text{Cos } z)^{-1}$$

with Cos z given by Eq. (4-2).

The surface albedo $\alpha(G)$ is another reflective parameter utilized in this study. Over oceanic areas the following formula for $\alpha(G)$ after Gates et al (1971), was utilized:

$$\alpha(G) = \max \{.06, .06 + .54 \, (.7 - \text{Cos } z)\} . \tag{4-7}$$

As described in Section III, four combinations of reference-cloud cases are possible with a two-layer cloud model. The disposition of F(S) under each of these cases will be discussed in the remainder of this subsection.

1. Clear Sky Case

In the clear sky (0,0) case the F(S) insolation was subjected to both Rayleigh scattering reflectance $\alpha(R)$ and the surface reflectance $\alpha(G)$. Considering the likelihood of a succession of multiple reflections

between earth and atmosphere, the F(S) insolation actually penetrating the earth's surface after scattering is given by

$$IS10(0,0) = F(S)[1-\alpha(R)][1+\alpha(R)\alpha(G)+\ldots(\alpha(R)\alpha(G))^n + \ldots]*(1-\alpha(G)) \quad (4\text{-}8a)$$

that is, by

$$IS10(0,0) = F(S)[1-\alpha(R)][1-\alpha(G)]/[1-\alpha(R)\alpha(G)] \quad (4\text{-}8b)$$

2. Cloudy-Sky Cases

In the three cases in which clouds were present, F(S) insolation absorbed by the ground at each gridpoint was computed using the following equation (after Arakawa, 1972):

$$IS10(1,1) = F(S)(1-R(1))(1-R(2))(1-\alpha(G)) *\{1-[R(1)R(2) + R(2)\alpha(G) + R(1)\alpha(G) - 2R(1)R(2)\alpha(G)]\}^{-1} . \quad (4\text{-}9)$$

As indicated by the notation (1,1), denoted $CL_1 = CL_2 = 1.0$, Eq. (4-9) is the formula used in calculating F(S) insolation absorbed by the ground in the case where overcast clouds are present at both levels of Fig. 2. Also in Eq. (4-9), initial values of cloud-reflectance were chosen, namely R(1) = .54 for the mid-level clouds between k=4 and 6, and R(2) = .66 for the low-level clouds between k=8 and 9. Both cloud-reflectance values are as suggested by C. D. Rodgers (1967).

For all the other cloud cases, the following changes were applied to Eq. (4-9). In the (1,0) case ($CL_1 = 1.0$, $CL_2 = 0.0$), the

desired earth-absorbed insolation is obtained by setting R(2) = 0.0 in (4-9), from which it follows that

$$IS10(1,0) = F(S)(1-R(1))(1-\alpha(G))/[1-R(1)\alpha(G)]. \qquad (4\text{-}10)$$

In the case (0,1), one sets R(1) = 0.0 in (4-9) so that (4-9) simplifies to

$$IS10(0,1) = F(S)(1-R(2))(1-\alpha(G))/[1-R(2)\alpha(G)]. \qquad (4\text{-}11)$$

Note that with a cloud overcast present, the Rayleigh clear-sky scattering $\alpha(R)$ does not appear in Eqs. (4-9), (4-10) or (4-11), but is included empirically in the cloud reflectances R(1) and R(2).

3. Composite F(S) Insolation at Earth

Equations (4-8), (4-9), (4-10) and (4-11) were utilized in the computation of the cloud-weighted F(S) insolation penetrating the earth's surface considering the areal-weights of the cloud combinations denoted by (0,0), (1,1), (1,0) and (0,1) about a gridpoint. The resultant F(S) insolation penetrating the earth's surface denoted by IS10 is therefore expressible as

$$\begin{aligned} IS10(CL_1, CL_2) = {} & IS10(0,0)\ W(0,0) \\ & + IS10(1,1)\ W(1,1) \\ & + IS10(1,0)\ W(1,0) \\ & + IS10(0,1)\ W(0,1)\ . \end{aligned} \qquad (4\text{-}12)$$

Here the weighting factors W(0,0), W(1,1), W(1,0) and W(0,1) are computed in Eqs. (2-3a,b,c,d) respectively. Note finally that the part of F(S) insolation reflected to space is found by subtracting IS10 (CL_1, CL_2) from F(S).

Table VI lists the F(S)-disposition resulting from a particular radiative sounding at gridpoint (1,1) on 16 April 1974. The individual computations of IS10 as they apply for the possible overcast-clear layer cases are made under the heading "IS10." The difference

$$\text{REFS} = \text{F(S)} - \text{IS10} \tag{4-13}$$

in each case represents F(S)-insolation reflected to space while

$$\text{STRAN} = \frac{\text{IS10}}{1-\alpha(\text{G})} \tag{4-14}$$

has been computed as that portion of the F(S)-insolation incident at the sea surface just prior to transmission by the surface. Note that no absorption in air has been included in the computations of Table VI, and that the only absorption permitted is that implicit in IS10. Finally at the bottom of each column, e.g., IS10, the composite value has been computed by means of the weighting scheme of Eq. (4-12).

TABLE VI. A sample listing of values of F(S) insolation (ly min^{-1}) computed at gridpoint (1,1) for 16 April 1974 using Eqs. (4-6,..., 4-14).

Cloud-case (CL_1, CL_2)	Weight $W(CL_1, CL_2)$	IS10	REFS	STRAN
(0,0)	.0993	.4305	.1751	.5216
(1,0)	.1484	.2539	.3517	.3076
(0,1)	.3016	.1921	.4135	.2327
(1,1)	.4507	.1340	.4716	.1696
Composite-F(S) values		.2014	.4041	.2441

C. DISPOSITION OF F(A) INSOLATION

The fractional portion of the solar insolation subject to absorption by atmospheric water-vapor and carbon dioxide is covered in the following subsections.

1. Clear-sky Case (0,0)

The Manabe-Möller absorptivity function provided the necessary absorptivity values for the key layers in this case. The form of this absorptivity function is

$$\underline{a}(2,k) = .271[U(2,k) \text{ Sec } z]^{.303} . \tag{4-15}$$

Here $\underline{a}$ is the absorptivity applied to the pressure-scaled water vapor mass between levels 2 and k (Fig. 2) along the zenith slant-path angle z. The resultant <u>absorbed insolational energy</u> in the particular layer (2,4) is then given by the Manabe-Möller relation

$$A24 = 0.271F(A)[U(2,4) \text{ Sec } z]^{.303} . \tag{4-16}$$

In the same manner A26, A28 and A210 are found. Then the absorbed insolation in the layers (4,6), (6,8) and (8,10) are computed by

$$A46 = A26 - A24 \tag{4-17}$$

$$A68 = A28 - A26 \tag{4-18}$$

$$A810 = A210 - A28 . \tag{4-19}$$

Water-vapor mass above level 2 was assumed negligible in the F(A) disposition of the solar insolation.

By subtracting A210 from F(A), the direct transmission of F(A) insolation impinging at the earth's surface was determined. The transmission of F(A) insolation is then further reduced by the transmissivity

(1-α(G)) after surface-reflectance, which leads to the earth-absorbed insolation

$$IA10(0,0) = F(A)\{1-.271[U(2,10)\mathrm{Sec}\ z]^{.303}\}(1-\alpha(G)). \qquad (4\text{-}20)$$

The transmitted energy impinging upon the earth just prior to absorption is

$$TRANA(0,0) = IA10(0,0)/[1-\alpha(G)] \ . \qquad (4\text{-}21)$$

In the remainder of this subsection, which discusses the cloudy layer cases, representative cloud reflectivities and cloud absorptivities were initially adopted, after C. D. Rodgers (1967), for the two possible cloud layers. These initial cloud reflectivities were RA(1) = .46 and RA(2) = .50 while the cloud absorptivities were A(1) = .20 and A(2) = .30. Note that the reflectivities for the F(A) wavelengths are somewhat smaller than those adopted for the F(S) wavelengths. The procedure of considering the cloud conditions to be overcast whenever they appear and then applying the appropriate weighting factors in the composite summation will again be followed as in Sec. IV.B.

To simplify the discussion for the cloud-covered cases, the (1,1) case will be presented first as it contains representative type equations for the remaining two cases, (1,0) and (0,1).

2. Overcast in Both High- and Low-cloud Layers

The following set of formulas illustrate the model disposition of incoming solar insolation (F(A)) from level k=2 to the earth's surface and permits determination of the amount of insolation absorbed by the atmospheric layers and by the earth's surface. The dashed separation lines are introduced to subdivide the absorption and reflection

physics of the model into subsections which permit the analysis to proceed more or less within successive 200 mb layers. The equations relate to the parameters in Fig. 6 where the insolations, A24, A46, A68, A89 and A910, etc., represent the contributions to the insolation absorbed in the layers involved. Symbols F2, F4, F6, F8 and F9, etc., depict the streams of insolation passing through the indicated level. A vertical arrow implies the direction of insolation passage, i.e., $\downarrow$ denotes downward insolation, $\uparrow$ upward-reflected insolation, and $\downarrow\downarrow$ downward-reflected insolation. Terms involving the symbols "TD", as expressed by the functions of Eq. (4-22), indicate the Manabe-Möller transmissivities for diffuse insolation in the layer beneath an existing cloud. In the latter situation, the term Sec Z in Eq. (4-15) is effectively replaced by the mean slant-path, $\overline{\text{Sec Z}} \simeq 5/3$ (Katayama, 1966), e.g.,

$$\begin{aligned} TD68 &= 1-.271[U(6,8)\ 5/3]^{.303} \\ TD910 &= 1-.271[U(9,10)5/3]^{.303}\ . \end{aligned} \qquad (4\text{-}22)$$

In accordance with the above definitions and as described by Fig. 6, the formulas for the (1,1) case are listed:

$$\begin{aligned} F4\downarrow &= F(A)(1-.271[U(2,4)\ \text{Sec } z]^{.303}) \\ F4\uparrow &= F4\downarrow(RA(1)) \\ F2\uparrow &= F4\uparrow\ (1-.271[U(2,4)\ \text{Sec } z]^{.303}) \\ A24 &= F(A) - F4\downarrow + F4\uparrow - F2\uparrow \end{aligned} \qquad (4\text{-}23a)$$

- -

$$A46 = F4\downarrow(A(1)) \tag{4-23b}$$

- -

$$F6\downarrow = F4\downarrow - F4\uparrow - A46$$

$$F8\downarrow = F6\downarrow(TD68)$$

$$F8\uparrow = F8\downarrow(RA(2))$$

$$F6\uparrow = F8\uparrow(TD68)$$

$$F6\downarrow\downarrow = F6\uparrow(RA(1))$$

$$F8\downarrow\downarrow = F6\downarrow\downarrow(TD68)$$

$$A68 = F6\downarrow - F8\downarrow + F8\uparrow - F6\uparrow + F6\downarrow\downarrow - F8\downarrow\downarrow \tag{4-23c}$$

- -

$$A89 = (F8\downarrow + F8\downarrow\downarrow)(A(2))$$

$$F9\downarrow = F8\downarrow - F8\uparrow + F8\downarrow\downarrow - A89$$

$$F10\downarrow = F9\downarrow(TD910)$$

$$F10\uparrow = F10\downarrow(\alpha(G))$$

$$F9\uparrow = F10\uparrow(TD910)$$

$$F9\downarrow\downarrow = F9\uparrow(RA(2))$$

$$F10\downarrow\downarrow = F9\downarrow\downarrow(TD910)$$

$$A910 = F9\downarrow - F10\downarrow + F10\uparrow - F9\uparrow + F9\downarrow\downarrow - F10\downarrow\downarrow$$

$$A810 = A89 + A910 \tag{4-23d}$$

Note that the effect of multiple reflections between clouds or between the earth's surface and the lower cloud has been incorporated to include only the effect of two reflections, with the lowermost reflecting surface absorbing the remaining impinging insolation. Computations indicated that the insolation remaining after two reflections was

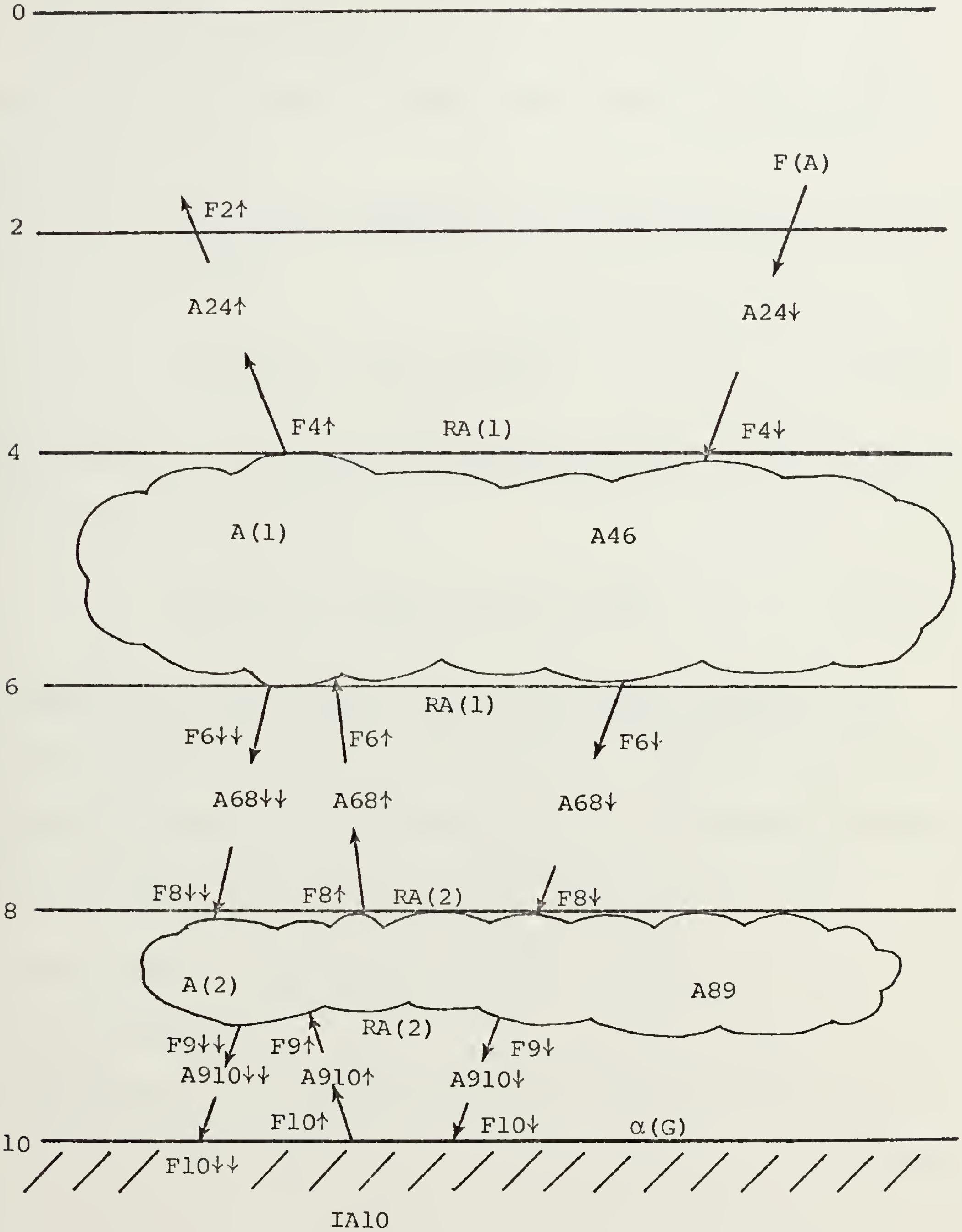

Figure 6. Schematic representation of F(A) insolation disposition in the case of two overcast layers.

too small to warrant the consideration of further reflections. Also insolation reflected upward from a lower interface (cloud or ground) to the base of an upper cloud deck has not been subjected to upper cloud absorption. This tends to reduce very slightly the secondary cloud-absorption.

From Eq. (4-23d), the impinging F(A) insolation at the earth's surface can be expressed

$$\mathrm{TRANA}(1,1) = \mathrm{F10}\downarrow + \mathrm{F10}\downarrow\downarrow \tag{4-24}$$

The F(A) insolation which is actually absorbed by the earth's surface (see Fig. 6) may be written as

$$\mathrm{IA10}(1,1) = \mathrm{F10}\downarrow(1-\alpha(G)) + \mathrm{F10}\downarrow\downarrow \tag{4-25}$$

3. <u>Disposition of F(A) Insolation with an Upper Overcast Only</u>

With a single cloud layer present only at the upper level (Fig. 7) the equations depicting the model-disposition of incoming insolation becomes a simplified subset of the previous case:

$$\mathrm{F4}\downarrow = \mathrm{F(A)}(1-.271[\mathrm{U}(2,4)\ \mathrm{Sec}\ z]^{.303})$$

$$\mathrm{F4}\uparrow = \mathrm{F4}\downarrow(\mathrm{RA}(1))$$

$$\mathrm{F2}\uparrow = \mathrm{F4}\uparrow(1-.271[\mathrm{U}(2,4)\ \mathrm{Sec}\ z]^{.303})$$

$$\mathrm{A24} = \mathrm{F(A)} - \mathrm{F4}\downarrow + \mathrm{F4}\uparrow - \mathrm{F2}\uparrow \tag{4-26a}$$

- -

$$\mathrm{A46} = \mathrm{F4}\downarrow(\mathrm{A1})) \tag{4-26b}$$

- -

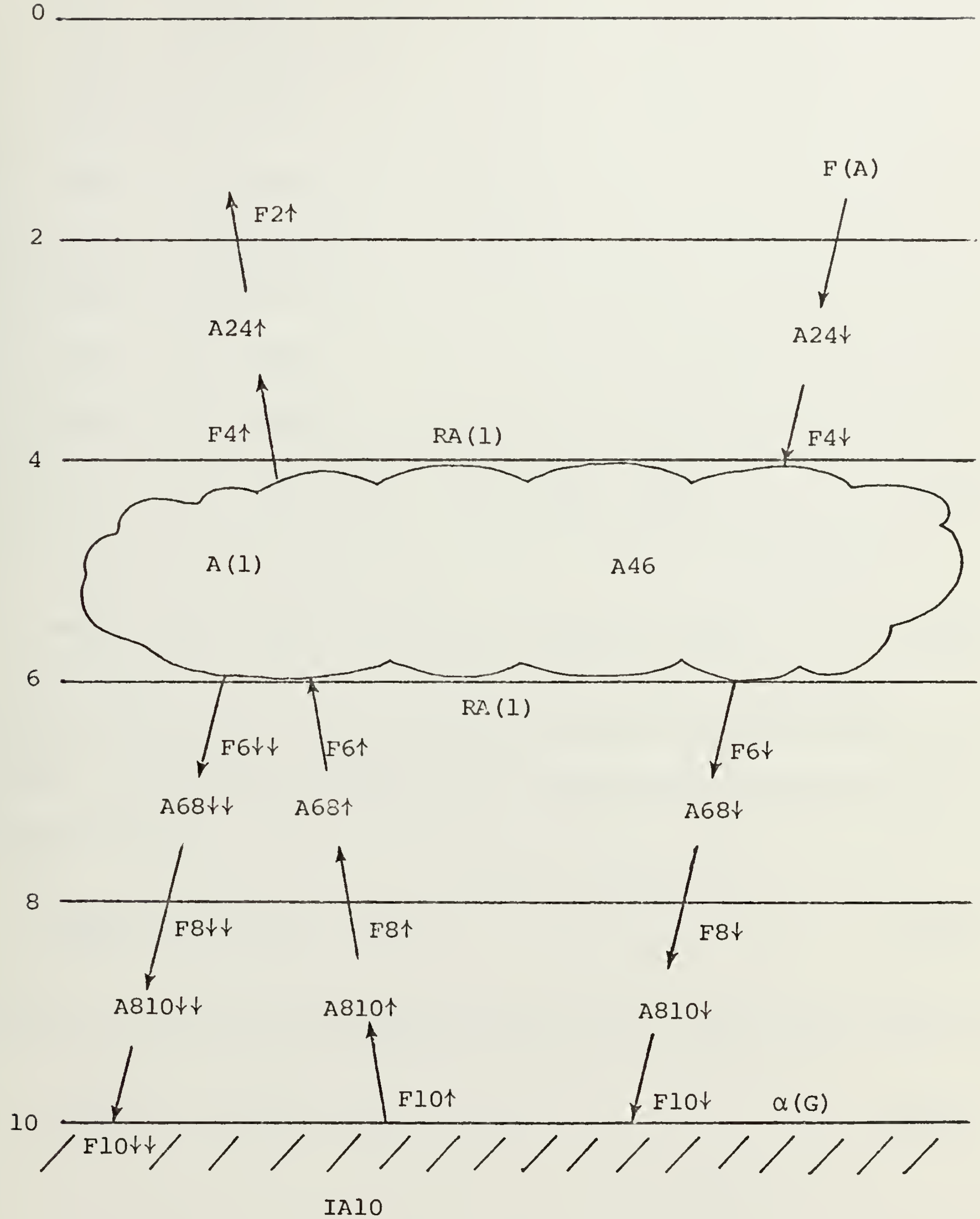

Figure 7. Schematic representation at F(A) insolation disposition with an upper overcast layer only.

$$F6\downarrow = F4\downarrow - F4\uparrow - A46$$

$$F8\downarrow = F6\downarrow(TD68)$$

$$F10\downarrow = F6\downarrow(TD610)$$

$$F10\uparrow = F10\downarrow(\alpha(G))$$

$$F8\uparrow = F10\uparrow(TD810)$$

$$F6\uparrow = F10\downarrow(TD610)$$

$$F6\downarrow\downarrow = F6\uparrow(RA(1))$$

$$F8\downarrow\downarrow = F6\downarrow\downarrow(TD68)$$

$$F10\downarrow\downarrow = F8\downarrow\downarrow(TD810)$$

$$A68 = F6\downarrow - F8\downarrow + F8\uparrow - F6\uparrow + F6\downarrow\downarrow - F8\downarrow\downarrow \tag{4-26c}$$

- -

$$A810 = F8\downarrow - F10\downarrow + F10\uparrow - F8\uparrow + F8\downarrow\downarrow - F10\downarrow\downarrow \tag{4-26d}$$

The variables used above are defined in a similar manner to those in the (1,1) case. The impinging insolation at the earth's surface may be formulated as follows

$$TRANA(1,0) = F10\downarrow + F10\downarrow\downarrow \tag{4-27}$$

while the F(A) insolation absorbed by the earth in this case is given by

$$IA10(1,0) = F10\downarrow(1-\alpha(G)) + F10\downarrow\downarrow \; . \tag{4-28}$$

4. Disposition of F(A) Insolation with a Low Overcast Only

With an overcast lower cloud layer the model-disposition symbols are as depicted in Fig. 8 and are physically related as follows:

$$F4\downarrow = F(A)(1-.271[U(2,4)\ \mathrm{Sec}\ z]^{.303})$$

$$F6\downarrow = F(A)(1-.271[U(2,6)\ \mathrm{Sec}\ z]^{.303})$$

$$F8\downarrow = F(A)(1-.271[U(2,8)\ \mathrm{Sec}\ z]^{.303})$$

$$F8\uparrow = F8\downarrow(RA(2))$$

$$F6\uparrow = F8\uparrow(1-.271[U(6,8)\ \mathrm{Sec}\ z]^{.303})$$

$$F4\uparrow = F8\uparrow(1-.271[U(4,8)\ \mathrm{Sec}\ z]^{.303})$$

$$F2\uparrow = F8\uparrow(1-.271[U(2,8)\ \mathrm{Sec}\ z]^{.303})$$

$$A24 = F(A) - F4\downarrow + F4\uparrow - F2\uparrow \qquad (4\text{-}29a)$$

- -

$$A46 = F4\downarrow - F6\downarrow + F6\uparrow - F4\uparrow \qquad (4\text{-}29b)$$

- -

$$A68 = F6\downarrow - F8\downarrow + F8\uparrow - F6\uparrow \qquad (4\text{-}29c)$$

- -

$$A89 = F8\downarrow\ (A(2))$$

$$F9\downarrow = F8\downarrow - F8\uparrow - A89$$

$$F10\downarrow = F9\downarrow(TD910)$$

$$F10\uparrow = F10\downarrow(\alpha(G))$$

$$F9\uparrow = F10\uparrow(TD910)$$

$$F9\downarrow\downarrow = F9\uparrow(RA(2))$$

$$F10\downarrow\downarrow = F9\downarrow\downarrow(TD910)$$

$$A910 = F9\downarrow - F10\downarrow + F10\uparrow - F9\uparrow + F9\downarrow\downarrow - F10\downarrow\downarrow$$

$$A810 = A89 + A910 \qquad (4\text{-}29d)$$

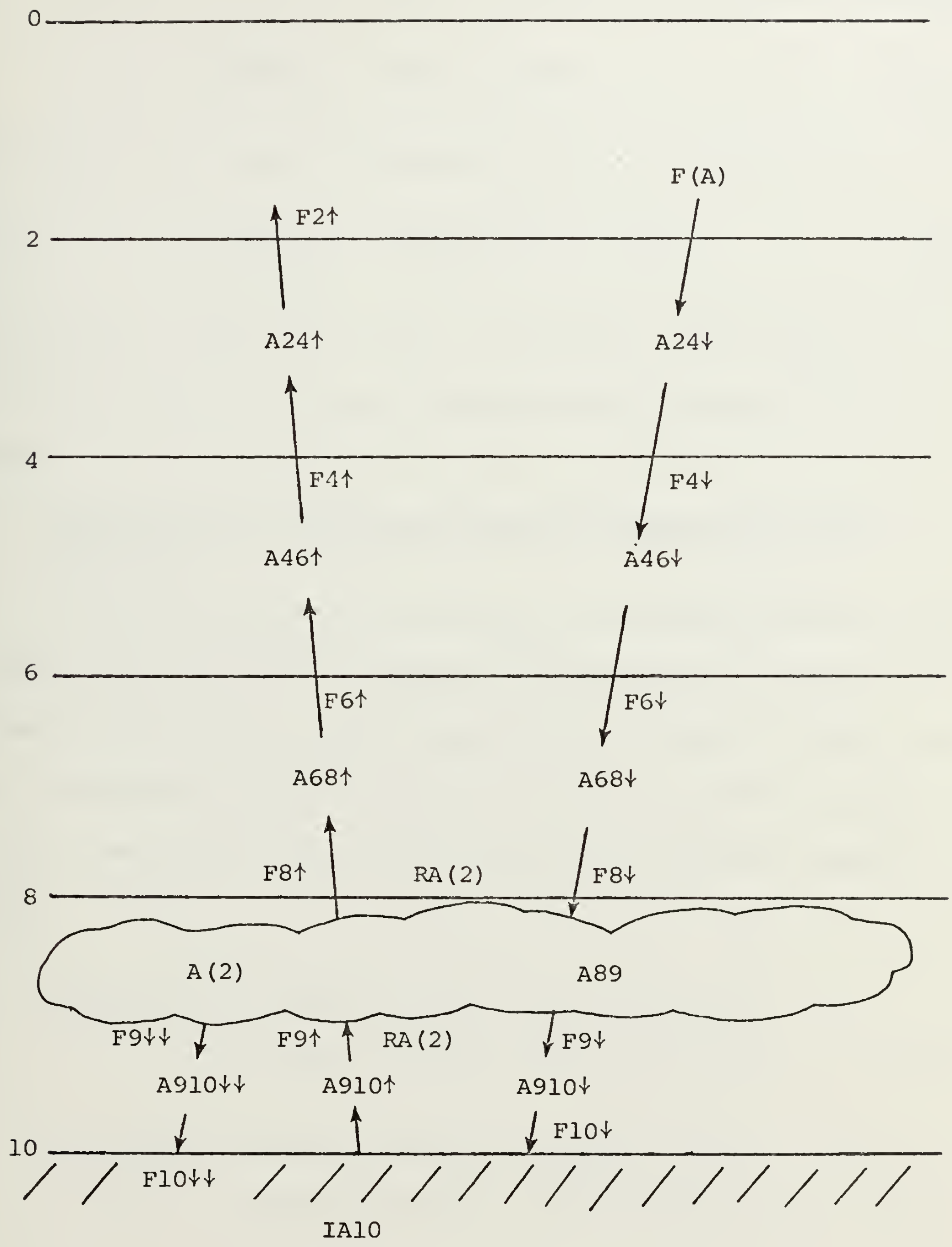

Figure 8. Schematic representation of F(A) insolation disposition with a lower overcast layer only.

Again the variables are defined as stated before in the (1,1) case. Likewise the incident flux is defined at the earth's surface as

$$\mathrm{TRANA}(0,1) = \mathrm{F10}\downarrow + \mathrm{F10}\downarrow\downarrow \tag{4-30}$$

while that portion which is absorbed by the earth (Fig. 8) is

$$\mathrm{IA10}(0,1) = \mathrm{F10}\downarrow(1-\alpha(G)) + \mathrm{F10}\downarrow\downarrow\ . \tag{4-31}$$

In Eqs. (4-25), (4-28), and (4-31), the quantity F10↓↓ is small enough in each case so that no further reflections from the earth were considered.

5. Composite F(A) Layer-Absorptions and Surface-Absorption Insolation

As has been previously discussed, the standard grid-area weighting scheme of this study was applied to obtain composite values of the absorbed F(A)-insolation in key layers and also within the earth's surface. The weighting factors applied to the corresponding overcast-combination absorption quantities provided the following composite results:

$$\begin{aligned}\mathrm{A24}(CL_1,CL_2) &= \mathrm{A24}(0,0)\ W(0,0) + \mathrm{A24}(1,0)\ W(1,0)\\ &\quad + \mathrm{A24}(0,1)\ W(0,1) + \mathrm{A24}(1,1)\ W(1,1)\end{aligned} \tag{4-32}$$

$$\begin{aligned}\mathrm{A46}(CL_1,CL_2) &= \mathrm{A46}(0,0)\ W(0,0) + \mathrm{A46}(1,0)\ W(1,0)\\ &\quad + \mathrm{A46}(0,1)\ W(0,1) + \mathrm{A46}(1,1)\ W(1,1)\end{aligned} \tag{4-33}$$

$$\begin{aligned}\mathrm{A46}(CL_1,CL_2) &= \mathrm{A68}(0,0)\ W(0,0) + \mathrm{A68}(1,0)\ W(1,0)\\ &\quad + \mathrm{A68}(0,1)\ W(0,1) + \mathrm{A68}(1,1)\ W(1,1)\end{aligned} \tag{4-34}$$

$$A810(CL_1,CL_2) = A810(0,0)\ W(0,0) + A810(1,0)\ W(1,0)$$
$$+ A810(0,1)\ W(0,1) + A810)1,1)\ W(1,1) \qquad (4\text{-}35)$$

$$IA10(CL_1,CL_2) = IA10(0,0)\ W(0,0) + IA10(1,0)\ W(1,0)$$
$$+ IA10(0,1)\ W(o,1) + IA10(1,1)\ W(1,1)\ . \qquad (4\text{-}36)$$

The weighting factors W(0,0),...,(W1,1) were listed in Eqs. (2-3a,b,c,d), and A24(0,0), A46(0,0), A68(0,0), A810(0,0) and IA10(0,0) are given in each clear sky case (0,0) about each gridpoint by Eqs.(4-15),(4-16),(4-17) (4-18), (4-19) and (4-20) respectively.

The results for the absorption in layers (2,4), (4,6), (6,8), (8,10) and at the surface, level k = 10, are shown in the following table:

TABLE VII. A sample listed of F(A) insolation values (ly min^{-1}) computed at gridpoint (1,1) for the 16 April case.

Cloud-Case CL_1, CL_2	Weight $W(CL_1,CL_2)$	A24	A46	A68	A810	IA10	REFA	TRANA
(0,0)	.0993	.0454	.0356	.0386	.0418	.1348	.0285	.1634
(1,0)	.1484	.0633	.0559	.0280	.0156	.0482	.1137	.0581
(0,1)	.3016	.0464	.0381	.0728	.0771	.0239	.0664	.0286
(1,1)	.4507	.0633	.0559	.0432	.0285	.0104	.1233	.0126
Composite-F(A) values		.0564	.0485	.0494	.0425	.0324	.0953	.0391

In the computational scheme indicated by the entries of Table VII, the reflected F(A) insolation to space has been depicted by the symbol REFA, and its values follow from

$$REFA = F(A) - A24 - A46 - A68 - A810 - IA10 \qquad (4\text{-}37)$$

whereas the TRANA dispositions are given by Eqs. (4-21), (4-24), (4-27) and (4-30) or by its weighted-mean value in the case of TRANA-composite.

6. Absorptivity (ABA) by Layers

Here the (fractional) absorptivity as well as the actual insolation values absorbed in the layers are considered. In the computation of absorptivity, which is fractional absorption, the total undepleted insolation at the top (k=0) is used as a base. The following equation was utilized in this calculation:

$$\mathrm{FADJ} = 2.00(r/r_m)^{-2}\ \mathrm{Cos}\ z\ . \tag{4-38}$$

The absorptivity of the troposphere ABA was computed from the ratio of the insolation absorbed in the troposphere to the insolation incident at the top of the atmosphere rather than at k=2:

$$\mathrm{ABA} = \frac{\mathrm{A24 + A46 + A68 + A810}}{\mathrm{FADJ}} \tag{4-39}$$

D. ALBEDO (ALB) OF THE EARTH-TROPOSPHERE SYSTEM

In considering the planetary albedo, the reflected insolations of the earth-troposphere systems in both the F(A) and F(S) insolational regions must be recalled by the program. Thus REF is computed at each gridpoint as the sum of the reflected insolation energy in F(A), denoted REFA in Eq. (4-37) and the reflected part of F(S) denoted REFS in Eq. (4-13):

$$\mathrm{REF} = \mathrm{REFS} + \mathrm{REFA} \tag{4-40}$$

Finally the planetary albedo is related to FADJ through

$$\mathrm{ALB} = \frac{\mathrm{REF}}{\mathrm{FADJ}}\ . \tag{4-41}$$

E. COMPOSITE ABSORPTIVITY (ABG) BY THE EARTH-SURFACE; COMPOSITE ATMOSPHERIC TRANSMISSIVITY (ATRAN)

1. Absorptivity (ABG) of Earth

By summing the weighted values of F(S) and F(A) portions of the incoming insolation entering the earth, the total insolation absorbed at the earth's surface was computed. This quantity when divided by the extraterrestrial insolation gave the fractional absorptivity (ABG) of the earth's surface. The equation for ABG was

$$ABG = \frac{IA10 + IS10}{FADJ} \tag{4-42}$$

where IA10, IS10, and FADJ were defined previously by Eqs. (4-36), (4-12) and (4-38) respectively.

2. Transmissivity (ATRAN) of the Troposphere

Also computed was the total insolational energy TRAN, incident at the earth's surface just before absorption by the surface. This calculation is given by

$$TRAN = TRANA + STRAN \ . \tag{4-43}$$

Here STRAN = [IS10/(1-α(G)] was previously defined in Eq. (4-14) and α(G) was given in Eq. (4-7). TRANA has also been defined as the weighted value of TRANA (0,0), TRANA (1,1), TRANA (1,0) and TRANA (0,1) given by Eqs. (4-21), (4-24), (4-27) and (4-30). Note also in justification of STRAN that the four cases for IS10 of (4-8), (4-9), (4-10), and (4-11) each have the common factor (1-α(G)) in the numerator and therefore each transmitted F(S) insolation component available at the earth just before absorption needs only be divided by (1-α(G)). TRAN may thus be viewed as the total insolational energy incident at a pyrheliometer located at

earth. The (fractional) transmissivity of the troposphere (ATRAN) is then computed from

$$ATRAN \equiv TRAN/FADJ \; . \qquad (4-44)$$

Note finally that the major dispositions of the total insolation at the indicated map times have now been identified by the fractional values, ALB, ABA or ABG, and ATRAN, representing the reflectivity (albedo), absorptivity of air or earth, or atmospheric transmissivity as the case may be.

F. ALBEDO TUNING BY COMPARISONS WITH SATELLITE CLIMATOLOGY

1. General Remarks Concerning a Need for Tuning Albedos

In the four previous radiational studies (A, B, C, D) comparisons were made between the solar-insolation albedo-model (ALBMOD) computations and the satellite-climatology albedo (ALBRAS) of Raschke et al. (1973). The results of these comparisons indicated excessively high values of ALBMOD especially in the tropical and subtropical oceanic areas. The question was raised by the previous investigators as to whether vertically-structured convective cloud elements in the tropics would have as high a reflective capability as attributed to the large-scale cloud masses existing primarily in horizontal layers as indicated by the parameterization of Eq. (2-2). It should be recalled that the initial cloud-reflectances used were as suggested by C. D. Rodgers (1967) and are listed in Secs. IV.B.2. and IV.C.1.

For the purpose of tuning the model solar dispositions, and in particular ALBMOD with ALBRAS, the initial values of Rodgers' cloud-reflectances were simply adjusted by a multiplicative factor (f) which

turns out by the least-squares fitting to be smaller than unity. This device allows a greater fraction of solar radiation to penetrate downward through the cloud-types in both the tropical and subtropical areas, and provides better agreement between ALBMOD and ALBRAS.

2. Method of Tuning ALBMOD to ALBRAS

The model-tuning process involved several steps. First, the new variable f was defined and allowed to range in value from 1.2 to 0.25 by 0.05 intervals. The f-values were then multiplied by the initially used cloud-reflectance values (after Rodgers, 1967) giving twenty sets of new cloud-reflectivity values. For each set of new values, ALBMOD and subsequently the difference Δ(ALB) between ALBMOD and ALBRAS; i.e.,

$$\Delta(\text{ALB}) = \text{ALBMOD} - \text{ALBRAS} \tag{4-45}$$

was recomputed at each gridpoint for the four midseasonal dates.

Because cloud-types differ in structure over tropical and extratropical oceanic areas the resulting Δ(ALB) data, from (4-45), were divided into two populations denoted TR and HL. The population TR included the set of gridpoints located south of and including 25N, while HL included the set of gridpoints located north of 25N over all four meridians.

Only those gridpoints where the value of at least one of CL_1 and CL_2 was greater than 0.1 were included in those populations. The gridpoints so excluded were considered climatologically unrepresentative for the purpose of cloud-tuning the albedo. The Δ(ALB) data was additionally divided by season giving a total of eight separate cases

further defined in sequence as WIN-TR, WIN-HL, SPR-TR, SPR-HL, SUM-TR, SUM-HL, AUT-TR and AUT-HL.

The Bimedical set of programs (Dixon, 1973) was utilized to compute the root-mean-square (RMS) of Δ(ALB) values corresponding to a wide range of f-values for each of the seasons and regions. Values of f leading to the minimum RMS of Δ(ALB) were isolated and appear in Table VIII, along with the RMS difference of Δ(ALB).

TABLE VIII. Values of f and corresponding minimum RMS values of Δ(ALB).

	f	Minimum RMS of Δ(ALB)
WIN-TR	.40	.069
WIN-HL	.80	.073
SPR-TR	.35	.067
SPR-HL	.65	.082
SUM-TR	.60	.079
SUM-HL	.70	.109
AUT-TR	.40	.052
AUT-HL	.60	.073

As can be seen from Table VIII, the listed values of f in winter indicates the largest difference between the tropical and extra-tropical cloud-types. The evenly layered cloud formations of the northern latitudes in mid-January seems more closely to approximate those considered by C. D. Rodgers (1967). On the other hand, the smallest difference in f-values occurs between SUM-TR and SUM-HL indicating a less significant difference in cloud types over the

complete latitude range during mid-July. As would be expected the Spring and Autumn f-ranges fall in between the Winter and Summer cases. A full listing of zonally-averaged ALBMOD values, after tuning at all gridpoints, and of zonally-averaged ALBRAS values, generated from identical gridpoints, can be found in Table IX.

Upon examination of Table IX it is apparent that the tuned model-albedo values compare closely with the satellite albedos derived from Raschke. Table IX includes the annual averages and the Northern Hemisphere cosine-weighted means as well as the mid-seasonal averages.

Further inspection of the weighted means shows that ALBMOD is somewhat smaller than ALBRAS for each of the four seasons and annual average. However most of this underestimate seems to occur in the HL-population where the result of minimizing Δ(ALB) led to values of f substantially less than unity (Table VIII). This result was unexpected and is probably due to a mismatch between the model clouds (Eq. (2-2)) and those averaged in the satellite climatology particularly in the higher latitudes.

The conclusion is that reflectance-tuning to satellite albedo appears valid in the tropics and subtropics where cloud-formations on a given day tend to be persistent. However tuning by this method in high latitudes is less conclusive because interdiurnal cloud variability is much greater.

In any case, all further computations of solar dispositions in this study will utilize the appropriate cloud-reflectance tuning factors as listed in Table VIII, depending upon season and latitude.

	WINTER		SPRING		SUMMER		AUTUMN		ANNUAL	
LAT.	ALBMOD	ALBRAS	ALBMOD	ALBRAS	ALBMOD	ALBRAS	ALBMOD	ALBRAS	ALBMOD	ALBRAS
20S	.224	.205	.238	.169	.252	.195	.208	.228	.229	.202
15S	.220	.195	.231	.170	.243	.175	.207	.176	.223	.180
10S	.203	.185	.212	.179	.221	.166	.204	.183	.209	.179
5S	.201	.151	.201	.191	.245	.183	.213	.201	.214	.181
0	.184	.229	.181	.210	.218	.236	.177	.175	.190	.212
5N	.185	.219	.174	.221	.232	.217	.178	.196	.192	.213
10N	.176	.205	.169	.202	.211	.247	.178	.233	.184	.222
15N	.188	.211	.169	.185	.203	.239	.185	.215	.186	.213
20N	.199	.237	.166	.182	.200	.215	.183	.207	.187	.208
25N	.249	.237	.217	.203	.202	.207	.209	.199	.216	.210
30N	.319	.268	.230	.247	.218	.213	.247	.204	.245	.230
35N	.327	.338	.247	.272	.208	.233	.271	.267	.251	.267
40N	.371	.384	.248	.279	.209	.256	.259	.280	.251	.285
45N	.441	.436	.253	.296	.260	.314	.274	.263	.281	.312
50N	.447	.511	.309	.322	.242	.345	.299	.348	.292	.357
55N	.456	.528	.299	.397	.352	.367	.330	.374	.338	.389
60N	.437	.473	.359	.421	.230	.395	.333	.416	.296	.410
65N	.429	.486	.363	.500	.250	.390	.393	.331	.309	.421
Wt. Avg.	.239	.260	.215	.243	.225	.256	.215	.228	.230	.247

TABLE IX. A comparison of zonally-averaged albedo values of Raschke et al. (1973) with model-albedo values as computed utilizing the appropriate reflectance tuning factors listed in Table VIII.

V. MERIDIONAL CROSS-SECTIONAL DEPICTION OF THE RADIATIVE-BALANCE COMPUTATIONS

A. GENERAL

The general design of this section is to utilize all of the computational concepts discussed in Sections III and IV in the computations for a single time-step in the radiative heating package developed for use in the FNWC prediction model. After testing ALBMOD with the corresponding values of Raschke et al. (1973), it was decided that only the computations by the appropriate cloud-reflectance tuning factors (Table VIII) would be displayed in the meridional cross-sections (Figs. 10... 17) and in the comparisons of the four-layer versus the two-layer cooling rates summarized in Table X.

The radiative calculations were performed at each gridpoint of the four meridians for each of the four mid-seasonal days considered; however, only the winter and summer cases, as illustrating the two extreme situations, are presented in this section.

B. GEOGRAPHICAL REPRESENTATION OF THE RADIATIVE-BALANCE DISTRIBUTION

The FNWC gridpoint processed analyses for 0000GMT were used at the three Pacific cross-sections, while that for 1200GMT were used for the single Atlantic meridian. This was done so that the set of gridpoints was considered to be subject to the actual radiative-transfer calculations involved for these specific times. Figure 9 depicts in symbolic language the key to the computational entries in Figs. 10, 11,...16, 17. This symbolic list presents the computations made at each radiative sounding gridpoint (I,J)having data in the form of Table I. The

computations proceed from the tropopause (approximately level k=2) to the ocean surface. For purposes of climatological data comparison, Figs. 10, 11,...16, 17 were developed by interpolating gridpoint results to integral multiples of 5-degree latitudinal increments. The interpolation routine to this gridpoint spacing made use of the Lagrangian cubic interpolation scheme (after Spaeth, 1975).

$$Q(I) = Q_1 \frac{(I-2)(I-3)(I-4)}{(I-2)(I-3)(I-4)} + Q_2 \frac{(I-1)(I-3)(I-4)}{(2-1)(2-3)(2-4)}$$
$$+ Q_3 \frac{(I-1)(I-2)(I-4)}{(3-1)(3-2)(3-4)} + Q_4 \frac{(I-1)(I-2)(I-3)}{(4-1)(4-2)(4-3)} \qquad (5-1)$$

Finally for ease in reconciling the magnitudes of all radiative-transfer rates, the time-dependent solar disposition rates have been averaged to 24-hourly rates.

C. EXPLANATION OF SYMBOLIC TERMS

1. Cross-Section at Level k=2

The discussion of all insolation parameters discussed previously in Section IV dealt with the specific time of day that corresponded to the hour angle h for the instantaneous time t under consideration. The incident solar insolation dealt with is then

$$F(2) = S\left(\frac{r}{r_m}\right)^{-2} \mathrm{Cos}\ z\ . \qquad (5-2)$$

In order to avoid reference to specific map times t, the instantaneous solar hour-angles were h = 35, 10, 55, and 35 degrees, respectively for cross-sections 1,2,3 and 4 as depicted in Figs. 10, 11, 12 and 13 for winter, and in Figs. 14, 15, 16, and 17 for summer.

QAVE represents the 24-hour average of F(2) and appears as the first input symbol in Fig. 9. Its value is considered to be more representative climatologically for the data day under consideration than F(2).

QAVE is derived by the formula

$$\mathrm{QAVE} = F(2)\ \frac{\overline{\overline{\mathrm{Cos}\ z}}}{\mathrm{Cos}\ z} \qquad (5\text{-}3)$$

where

$$\overline{\overline{\mathrm{Cos}\ z}} = [H\ \mathrm{Sin}\phi\mathrm{Sin}\delta + \mathrm{Cos}\phi\mathrm{Cos}\delta\mathrm{Sin}H]/\pi \qquad (5\text{-}4)$$

$$H = \mathrm{ArcCos}\ [-\mathrm{Tan}\phi\mathrm{Tan}\delta] \qquad (5\text{-}5)$$

Here δ is the appropriate solar declination angle as listed in Table V, and H is the appropriate hour angle at local sunset at latitude ϕ. The value of H also depends upon which mid-seasonal date is being considered. $\overline{\overline{\mathrm{Cos}\ z}}$ in Eq. (5-4) is equal to the 24-hour average cosine of the zenith angle, Eq. (4-2). The 24-hour time averaging period for QAVE gives heating results consistent in magnitude with the terrestrial flux divergences, which change only slightly with the time of day. The conversion to expected daily averaged solar disposition quantities is compatible with the determination of a hemispheric radiative balance for the given mid-seasonal dates (Sec. IV.A.).

Other parameters needed for level k=2 are

$$\mathrm{QREF} = \mathrm{REF}(t)\left(\frac{\overline{\overline{\mathrm{Cos}\ z}}}{\mathrm{Cos}\ z}\right) \qquad (5\text{-}6)$$

where

$$\mathrm{REF}(t) = F(2) - A24 - A46 - A68 - A810$$
$$- (IA10 + IS10) \qquad (5\text{-}7)$$

REF(t) is the instantaneous solar reflected insolation at a gridpoint and QREF is its 24-hour average, assuming that the instantaneous planetary albedo remains constant for the 24-hour period. This assumption requires that the cloud amounts computed at the indicated synoptic times are representative of the entire day.

The same principle will be used with regard to all other solar parameters in the conversion from time-dependent values at solar time t to 24-hour averaged values. Superior bars ($\overline{}$) are not used in the symbolism for the averaged values shown in the cross-sections key, Fig. 9, but are implied by the use of QAVE, etc. in the solar-disposition terms. The 24-hour average tropopause balance, BALT, is computed from

$$\mathrm{BALT} = \mathrm{QAVE} - (\mathrm{QREF} + F_2^*) \qquad (5\text{-}8)$$

for the level k=2 at the indicated latitude. Net terrestrial fluxes, such as F_2^*, were considered to be constant throughout the 24-hour period, a valid assumption if the cloud cover remains quasi-constant for the period.

2. Cross-Sections in Layers (2,4),(4,6),(6,8) and (8,10)

The following definitions apply for the four layers identified in the present section heading and are further identified in Fig. 9. All of the heat transfers shown in these layers are assumed to be of radiative character only. The daily-averaged radiative heating (cooling) rate in layer (2,4) is given by

$$\mathrm{BAL\ 24} = \mathrm{Q24} - \mathrm{F24} \qquad (5\text{-}9)$$

k		
	a) QAVE	24-hour averaged insolation at level k=2, positive for incoming radiation
	b) QREF	Reflected average insolation at level k=2
	c) F_2^*	Net outgoing long-wave flux at level k=2
	d) BALT	Averaged earth-tropospheric gain or loss (a-b-c)
2		
	e) Q24	Averaged solar insolation absorbed by layer (2,4), positive for heating
	f) F24	IR flux loss by layer (2,4)
	g) BAL24	Averaged radiative cooling in layer (2,4) (e-f)
4		
	CL_1	Upper layer (4,6) cloud amount
	h) Q46	Averaged solar insolation absorbed by layer (4,6), positive for heating
	i) F46	IR flux loss by layer (4,6)
	j) BAL46	Averaged radiative cooling in layer (4,6) (h-i)
6		
	k) Q68	Averaged solar insolation absorbed by layer (6,8)
	ℓ) F68	IR flux loss by layer (6,8)
	m) BAL68	Averaged radiative cooling in layer (6,8) (k-ℓ)
8		
	CL_2	Lower layer (8,9) cloud amounts
	n) Q810	Averaged solar insolation absorbed by layer (8,10)
	o) F810	IR flux loss by layer (8,10)
	p) BAL810	Averaged radiative cooling in layer (8,10) (n-o)
10		
	q) QABG	Averaged solar insolation absorbed by surface
	r) F_{10}^*	Net long-wave flux at earth's surface
	s) BALB	Averaged warming or cooling at earth's surface (q-r)

Figure 9. Key to radiative cross-sections for Figs. 10,...,17. All radiative values (ly min^{-1}) for the levels or layers considered are computed utilizing the appropriate reflectance tuning factor as listed in Table VIII for the 16 January and 16 July cases.

-20.0	-15.0	-10.0	-5.0	0.0	5.0	10.0	15.0	20.0	25.0
0.6812	0.6646	0.6437	0.6184	0.5893	0.5563	0.5197	0.4799	0.4372	0.3920
0.1793	0.1754	0.1604	0.1482	0.1414	0.1370	0.1277	0.1224	0.1167	0.1274
-.2943	-.2958	-.3111	-.3322	-.3531	-.3724	-.3847	-.3942	-.3918	-.3276
0.2075	0.1935	0.1721	0.1381	0.0949	0.0468	0.0073	-.0368	-.0712	-.0630
0.0314	0.0309	0.0293	0.0266	0.0230	0.0199	0.0177	0.0147	0.0145	0.0209
-.0465	-.0471	-.0453	-.0428	-.0412	-.0400	-.0386	-.0383	-.0369	-.0387
-.0153	-.0162	-.0161	-.0162	-.0180	-.0201	-.0210	-.0236	-.0224	-.0178
(.436)	(.434)	(.358)	(.246)	(.139)	(.054)	(.005)	(.0)	(.0)	(.224)
0.0321	0.0312	0.0292	0.0265	0.0240	0.0218	0.0196	0.0178	0.0164	0.0171
-.0777	-.0775	-.0746	-.0726	-.0713	-.0688	-.0674	-.0681	-.0654	-.0665
-.0459	-.0463	-.0454	-.0462	-.0474	-.0470	-.0478	-.0502	-.0490	-.0495
0.0388	0.0378	0.0359	0.0352	0.0370	0.0380	0.0350	0.0334	0.0292	0.0190
-.0359	-.0348	-.0385	-.0511	-.0687	-.0823	-.0839	-.0859	-.0829	-.0487
0.0027	0.0029	-.0026	-.0159	-.0317	-.0443	-.0489	-.0526	-.0536	-.0297
(.753)	(.722)	(.580)	(.494)	(.503)	(.555)	(.358)	(.204)	(.034)	(.0)
0.0531	0.0505	0.0457	0.0430	0.0429	0.0436	0.0345	0.0266	0.0182	0.0119
-.0655	-.0656	-.0740	-.0840	-.0935	-.0990	-.0879	-.0763	-.0620	-.0532
-.0127	-.0151	-.0283	-.0411	-.0505	-.0554	-.0534	-.0498	-.0438	-.0413
0.3469	0.3389	0.3433	0.3390	0.3210	0.2959	0.2853	0.2649	0.2421	0.1955
-.0683	-.0706	-.0787	-.0816	-.0785	-.0823	-.1068	-.1254	-.1446	-.1203
0.2785	0.2682	0.2645	0.2574	0.2425	0.2137	0.1784	0.1395	0.0975	0.0752

Figure 10(a). 125W Longitudinal cross-section, tropical section. Refer to Fig. 9 for key. Values computed from data for 16 January 1974.

30.0	35.0	40.0	45.0	50.0	55.0
0.3446	0.2957	0.2459	0.1958	0.1462	0.0984
0.1256	0.1239	0.1173	0.1000	0.0765	0.0471
-.2941	-.2645	-.2045	-.2398	-.2307	-.1804
-.0751	-.0927	-.0760	-.1441	-.1510	-.1292
0.0216	0.0219	0.0253	0.0155	0.0120	0.0149
-.0396	-.0385	-.0403	-.0491	-.0565	-.0524
-.0180	-.0166	-.0151	-.0336	-.0445	-.0375
(.357)	(.526)	(.388)	(.711)	(.662)	(.881)
0.0159	0.0142	0.0130	0.0106	0.0083	0.0048
-.0628	-.0743	-.0963	-.0872	-.0739	-.1057
-.0469	-.0601	-.0833	-.0766	-.0558	-.1009
0.0121	0.0083	0.0090	0.0107	0.0078	0.0029
-.0280	-.0178	0.0054	-.0134	-.0192	0.0055
-.0159	-.0095	0.0145	-.0028	-.0113	0.0084
(.0)	(.238)	(.327)	(.738)	(.852)	(.238)
0.0100	0.0124	0.0075	0.0086	0.0071	0.0013
-.0518	-.0570	-.0346	-.0601	-.0464	0.0122
-.0418	-.0445	-.0271	-.0514	-.0394	0.0135
0.1594	0.1148	0.0738	0.0504	0.0345	0.0273
-.1120	-.0768	-.0387	-.0302	-.0347	-.0400
0.0474	0.0380	0.0350	0.0203	-.0001	-.0127

Figure 10(b). 125W Longitudinal cross-section, higher latitude section. Refer to Fig. 9 for key. Values computed from data for 16 January 1974.

0.0	5.0	10.0	15.0	20.0	25.0
0.5892	0.5563	0.5198	0.4799	0.4372	0.3919
0.0964	0.0901	0.0767	0.0765	0.0754	0.0847
-.3502	-.3693	-.3992	-.4003	-.3933	-.3576
0.1426	0.0969	0.0437	0.0030	-.0315	-.0503
0.0242	0.0209	0.0167	0.0145	0.0137	0.0149
-.0407	-.0393	-.0375	-.0382	-.0404	-.0438
-.0167	-.0184	-.0208	-.0238	-.0267	-.0290
(.201)	(.111)	(.0)	(.0)	(.0)	(.124)
0.0228	0.0203	0.0169	0.0149	0.0148	0.0155
-.0715	-.0705	-.0688	-.0727	-.0740	-.0770
-.0486	-.0501	-.0519	-.0577	-.0593	-.0615
0.0279	0.0273	0.0238	0.0164	0.0241	0.0256
-.0530	-.0668	-.0810	-.0663	-.0869	-.0786
-.0250	-.0395	-.0572	-.0499	-.0628	-.0529
(.294)	(.351)	(.312)	(.372)	(.495)	(.599)
0.0349	0.0372	0.0365	0.0379	0.0347	0.0297
-.0859	-.0962	-.1041	-.1076	-.1033	-.1028
-.0510	-.0590	-.0677	-.0696	-.0686	-.0731
0.3830	0.3604	0.3491	0.3196	0.2746	0.2216
-.0991	-.0964	-.1079	-.1155	-.0887	-.0553
0.2839	0.2640	0.2413	0.2041	0.1858	0.1662

Figure 11(a). 170W longitudinal cross-section, tropical section. Refer to Fig. 9 for key. Values computed from data for 16 January 1974.

30.0	35.0	40.0	45.0	50.0	55.0	60.0	65.0
0.3446	0.2957	0.2459	0.1958	0.1462	0.0984	0.0542	0.0170
0.1372	0.1081	0.1038	0.0864	0.0658	0.0451	0.0237	0.0076
-.2783	-.3450	-.3478	-.3241	-.3280	-.2445	-.1673	-.2355
-.0708	-.1573	-.2057	-.2148	-.2477	-.1913	-.1368	-.2260
0.0190	0.0087	0.0025	0.0029	0.0023	0.0044	0.0039	0.0007
-.0506	-.0440	-.0163	-.0286	-.0270	-.0333	-.0159	-.0330
-.0317	-.0354	-.0138	-.0257	-.0247	-.0290	-.0121	-.0325
(.521)	(.066)	(.0)	(.0)	(.0)	(.293)	(.564)	(.0)
0.0169	0.0098	0.0055	0.0046	0.0035	0.0038	0.0023	0.0004
-.0827	-.0645	-.0609	-.0512	-.0478	-.0570	-.0527	-.0298
-.0659	-.0546	-.0554	-.0467	-.0443	-.0531	-.0505	-.0294
0.0192	0.0200	0.0210	0.0119	0.0109	0.0046	0.0015	0.0005
-.0297	-.0819	-.1219	-.0847	-.0979	-.0357	0.0055	-.0495
-.0104	-.0619	-.1009	-.0728	-.0870	-.0310	0.0069	-.0489
(.559)	(.661)	(.861)	(.851)	(.869)	(.574)	(.0)	(.0)
0.0165	0.0221	0.0223	0.0183	0.0130	0.0053	-.0000	0.0003
-.0701	-.0992	-.0925	-.0945	-.0876	-.0314	-.0065	-.0297
-.0536	-.0771	-.0702	-.0761	-.0747	-.0261	-.0064	-.0294
0.1358	0.1270	0.0907	0.0716	0.0506	0.0351	0.0229	0.0076
-.0451	-.0554	-.0562	-.0651	-.0678	-.0871	-.0976	-.0934
0.0907	0.0716	0.0346	0.0065	-.0171	-.0521	-.0748	-.0858

Figure 11(b). 170W longitudinal cross-section, higher latitude section. Refer to Fig. 9 for key. Values computed from data for 16 January 1974.

-5.0	0.0	5.0	10.0	15.0	20.0	25.0
0.6188	0.5893	0.5563	0.5197	0.4799	0.4372	0.3920
0.1334	0.1000	0.1036	0.0910	0.0966	0.0896	0.0922
-.2799	-.3939	-.4018	-.4070	-.3981	-.4062	-.4074
0.2054	0.0954	0.0509	0.0218	-.0147	-.0585	-.1077
0.0349	0.0202	0.0172	0.0158	0.0149	0.0112	0.0098
-.0525	-.0393	-.0419	-.0409	-.0410	-.0402	-.0462
-.0175	-.0190	-.0247	-.0251	-.0261	-.0290	-.0364
(.544)	(.021)	(.0)	(.0)	(.0)	(.0)	(.0)
0.0336	0.0215	0.0201	0.0182	0.0173	0.0143	0.0109
-.0872	-.0717	-.0767	-.0752	-.0739	-.0759	-.0792
-.0530	-.0504	-.0565	-.0570	-.0565	-.0616	-.0685
0.0380	0.0368	0.0380	0.0322	0.0295	0.0219	0.0081
-.0151	-.0877	-.1004	-.0911	-.0909	-.0797	-.0214
0.0229	-.0508	-.0624	-.0589	-.0614	-.0577	-.0133
(.445)	(.475)	(.641)	(.480)	(.599)	(.415)	(.140)
0.0317	0.0450	0.0497	0.0415	0.0428	0.0350	0.0243
-.0788	-.1030	-.1159	-.1031	-.1132	-.0991	-.0860
-.0472	-.0580	-.0662	-.0616	-.0704	-.0640	-.0617
0.3477	0.3658	0.3277	0.3210	0.2787	0.2652	0.2467
-.0464	-.0922	-.0668	-.0967	-.0791	-.1114	-.1746
0.3009	0.2735	0.2608	0.2243	0.1998	0.1538	0.0720

Figure 12(a). 145E Longitudinal cross-section, tropical section. Refer to Fig. 9 for key. Values computed from data for 16 January 1974.

30.0	35.0	40.0	45.0	50.0	55.0
0.3446	0.2957	0.2459	0.1958	0.1462	0.0984
0.0919	0.0877	0.0831	0.1026	0.0702	0.0498
-.3612	-.3612	-.3330	-.2206	-.2122	-.2011
-.1084	-.1531	-.1703	-.1275	-.1362	-.1526
0.0111	0.0057	0.0040	0.0066	0.0062	0.0053
-.0483	-.0408	-.0369	-.0586	-.0528	-.0476
-.0372	-.0351	-.0329	-.0520	-.0466	-.0422
(.0)	(.0)	(.0)	(.656)	(.612)	(.618)
0.0105	0.0030	0.0053	0.0098	0.0072	0.0051
-.0666	-.0533	-.0414	-.0509	-.0470	-.0500
-.0561	-.0459	-.0362	-.0409	-.0398	-.0449
0.0144	0.0162	0.0103	0.0086	0.0057	0.0041
-.0320	-.0510	-.0449	-.0189	-.0123	-.0177
-.0176	-.0348	-.0346	-.0102	-.0066	-.0135
(.166)	(.189)	(.220)	(.870)	(.403)	(.491)
0.0149	0.0115	0.0114	0.0110	0.0055	0.0041
-.0526	-.0359	-.0429	-.0533	-.0297	-.0302
-.0377	-.0244	-.0316	-.0423	-.0243	-.0262
0.2018	0.1667	0.1318	0.0570	0.0513	0.0299
-.1616	-.1797	-.1668	-.0391	-.0703	-.0557
0.0402	-.0130	-.0350	0.0181	-.0191	-.0257

Figure 12(b). 145E Longitudinal cross-section, higher latitude section. Refer to Fig. 9 for key. Values computed from data for 16 January 1974.

-20.0	-15.0	-10.0	-5.0	0.0	5.0	10.0	15.0	20.0	25.0
0.6812	0.6646	0.6437	0.6184	0.5893	0.5563	0.5197	0.4799	0.4372	0.3920
0.1380	0.1289	0.1124	0.1068	0.1146	0.0970	0.0858	0.0800	0.0809	0.1023
-.3246	-.3469	-.3819	-.3716	-.3520	-.3535	-.3497	-.3666	-.3811	-.3565
0.2186	0.1887	0.1494	0.1401	0.1227	0.1059	0.0843	0.0332	-.0248	-.0669
0.0288	0.0254	0.0209	0.0221	0.0233	0.0225	0.0215	0.0175	0.0137	0.0136
-.0434	-.0416	-.0381	-.0396	-.0425	-.0411	-.0410	-.0385	-.0375	-.0405
-.0149	-.0162	-.0172	-.0175	-.0192	-.0186	-.0195	-.0211	-.0239	-.0268
(.318)	(.205)	(.033)	(.095)	(.194)	(.183)	(.203)	(.101)	(.006)	(.105)
0.0293	0.0264	0.0222	0.0229	0.0241	0.0223	0.0210	0.0175	0.0144	0.0145
-.0749	-.0739	-.0702	-.0721	-.0761	-.0730	-.0712	-.0656	-.0624	-.0652
-.0458	-.0474	-.0480	-.0491	-.0520	-.0507	-.0501	-.0481	-.0480	-.0506
0.0366	0.0376	0.0430	0.0385	0.0378	0.0310	0.0261	0.0212	0.0201	0.0207
-.0409	-.0576	-.0876	-.0743	-.0652	-.0576	-.0475	-.0523	-.0668	-.0546
-.0043	-.0201	-.0445	-.0358	-.0273	-.0266	-.0214	-.0311	-.0467	-.0339
(.496)	(.525)	(.522)	(.438)	(.538)	(.343)	(.187)	(.104)	(.184)	(.186)
0.0457	0.0482	0.0483	0.0421	0.0422	0.0337	0.0257	0.0222	0.0241	0.0176
-.0771	-.0866	-.0942	-.0893	-.0913	-.0835	-.0728	-.0714	-.0801	-.0668
-.0313	-.0384	-.0459	-.0472	-.0491	-.0500	-.0471	-.0492	-.0560	-.0494
0.4032	0.3980	0.3968	0.3860	0.3473	0.3500	0.3397	0.3215	0.2840	0.2232
-.0882	-.0872	-.0917	-.0964	-.0769	-.0982	-.1172	-.1387	-.1343	-.1294
0.3152	0.3109	0.3051	0.2896	0.2704	0.2516	0.2225	0.1828	0.1497	0.0938

Figure 13(a). 35W Longitudinal cross-section, tropical section. Refer to Fig. 9 for key. Values computed from data for 16 January 1974.

30.0	35.0	40.0	45.0	50.0	55.0	60.0
0.3446	0.2957	0.2459	0.1958	0.1462	0.0984	0.0541
0.1039	0.0825	0.0762	0.0709	0.0595	0.0447	0.0256
-.3384	-.3729	-.3534	-.3489	-.3354	-.2813	-.2751
-.0977	-.1597	-.1837	-.2241	-.2486	-.2276	-.2465
0.0124	0.0079	0.0067	0.0047	0.0033	0.0036	0.0020
-.0421	-.0378	-.0383	-.0386	-.0319	-.0410	-.0357
-.0297	-.0299	-.0317	-.0339	-.0286	-.0374	-.0337
(.162)	(.032)	(.061)	(.012)	(.0)	(.254)	(.265)
0.0133	0.0088	0.0077	0.0061	0.0047	0.0043	0.0024
-.0637	-.0539	-.0532	-.0548	-.0531	-.0488	-.0411
-.0504	-.0451	-.0455	-.0486	-.0484	-.0445	-.0388
0.0171	0.0090	0.0093	0.0120	0.0109	0.0056	0.0027
-.0432	-.0363	-.0362	-.0645	-.0781	-.0394	-.0272
-.0260	-.0273	-.0270	-.0526	-.0572	-.0338	-.0245
(.207)	(.052)	(.054)	(.264)	(.454)	(.427)	(.341)
0.0151	0.0122	0.0087	0.0096	0.0092	0.0053	0.0032
-.0618	-.0681	-.0553	-.0569	-.0701	-.0615	-.0570
-.0466	-.0560	-.0466	-.0472	-.0510	-.0562	-.0538
0.1827	0.1755	0.1374	0.0924	0.0586	0.0349	0.0183
-.1277	-.1769	-.1704	-.1343	-.1023	-.0905	-.1139
0.0550	-.0015	-.0329	-.0419	-.0435	-.0556	-.0957

Figure 13(b). 35W Longitudinal cross-section, higher latitude section. Refer to Fig. 9 for key. Values computed from data for 16 January 1974.

-20.0	-15.0	-10.0	-5.0	0.0	5.0	10.0	15.0	20.0	25.0
0.4062	0.4465	0.4842	0.5189	0.5504	0.5783	0.6025	0.6227	0.6390	0.6512
0.1197	0.1209	0.1147	0.1131	0.1237	0.1459	0.1639	0.1619	0.1380	0.1224
-.3893	-.3917	-.3967	-.3837	-.3630	-.3451	-.3345	-.3402	-.3653	-.3958
-.1032	-.0661	-.0272	0.0171	0.0636	0.0873	0.1041	0.1207	0.1357	0.1330
0.0130	0.0151	0.0167	0.0193	0.0234	0.0267	0.0289	0.0284	0.0242	0.0182
-.0342	-.0362	-.0360	-.0356	-.0377	-.0409	-.0436	-.0429	-.0384	-.0393
-.0210	-.0210	-.0193	-.0163	-.0143	-.0142	-.0148	-.0146	-.0142	-.0211
(.0)	(.0)	(.0)	(.011)	(.121)	(.220)	(.288)	(.247)	(.077)	(.0)
0.0142	0.0158	0.0167	0.0183	0.0215	0.0245	0.0270	0.0272	0.0237	0.0210
-.0590	-.0609	-.0613	-.0616	-.0657	-.0709	-.0757	-.0757	-.0681	-.0596
-.0447	-.0451	-.0445	-.0433	-.0443	-.0463	-.0487	-.0485	-.0444	-.0487
0.0175	0.0192	0.0193	0.0209	0.0240	0.0297	0.0362	0.0384	0.0364	0.0352
-.0494	-.0542	-.0541	-.0568	-.0516	-.0460	-.0453	-.0536	-.0778	-.0963
-.0319	-.0350	-.0349	-.0360	-.0275	-.0163	-.0091	-.0151	-.0415	-.0611
(.195)	(.155)	(.023)	(.005)	(.062)	(.241)	(.374)	(.372)	(.283)	(.165)
0.0246	0.0265	0.0242	0.0242	0.0255	0.0304	0.0331	0.0346	0.0370	0.0358
-.0803	-.0830	-.0765	-.0729	-.0714	-.0759	-.0763	-.0810	-.0913	-.0901
-.0555	-.0564	-.0522	-.0486	-.0460	-.0455	-.0431	-.0464	-.0542	-.0544
0.2165	0.2488	0.2927	0.3232	0.3322	0.3210	0.3134	0.3323	0.3798	0.4186
-.1663	-.1575	-.1689	-.1617	-.1365	-.1114	-.0935	-.0870	-.0398	-.1004
0.0499	0.0913	0.1238	0.1614	0.1958	0.2097	0.2199	0.2453	0.2899	0.3182

Figure 14(a). 125W Longitudinal cross-section, tropical section. Refer to Fig. 9 for key. Values computed from data for 16 July 1974.

30.0	35.0	40.0	45.0	50.0	55.0
0.6593	0.6634	0.6638	0.6606	0.6544	0.6460
0.1095	0.0989	0.0931	0.2344	0.2128	0.2131
-.4020	-.4038	-.3791	-.3357	-.2947	-.2784
0.1478	0.1607	0.1915	0.0905	0.1469	0.1546
0.0158	0.0141	0.0184	0.0173	0.0193	0.0186
-.0396	-.0350	-.0323	-.0454	-.0515	-.0603
-.0238	-.0209	-.0139	-.0281	-.0422	-.0417
(.0)	(.0)	(.0)	(.002)	(.236)	(.400)
0.0198	0.0173	0.0164	0.0186	0.0256	0.0274
-.0694	-.0632	-.0638	-.0639	-.0527	-.0460
-.0496	-.0460	-.0475	-.0452	-.0271	-.0186
0.0317	0.0227	0.0198	0.0316	0.0307	0.0255
-.1000	-.0967	-.0785	-.0712	-.0391	-.0287
-.0682	-.0740	-.0587	-.0396	-.0084	-.0032
(.074)	(.0)	(.0)	(.841)	(.494)	(.388)
0.0333	0.0225	0.0087	0.0621	0.0381	0.0337
-.0859	-.0768	-.0476	-.0924	-.0526	-.0679
-.0526	-.0543	-.0389	-.0303	-.0245	-.0343
0.4492	0.4879	0.5073	0.2965	0.3278	0.3278
-.1071	-.1322	-.1569	-.0629	-.0788	-.0753
0.3422	0.3557	0.3504	0.2336	0.2491	0.2525

Figure 14(b). 125W Longitudinal cross-section, higher latitude section. Refer to Fig. 9 for key. Values computed from data for 16 July 1974.

0.0	5.0	10.0	15.0	20.0	25.0
0.5504	0.5783	0.6024	0.6228	0.6390	0.6511
0.0778	0.0823	0.0846	0.1117	0.1173	0.1100
-.3865	-.3900	-.4036	-.3934	-.4018	-.4065
0.0860	0.1059	0.1143	0.1177	0.1199	0.1347
0.0192	0.0195	0.0176	0.0175	0.0145	0.0133
-.0373	-.0368	-.0371	-.0393	-.0388	-.0363
-.0179	-.0172	-.0196	-.0218	-.0243	-.0230
(.053)	(.033)	(.0)	(.0)	(.0)	(.0)
0.0184	0.0187	0.0182	0.0183	0.0185	0.0183
-.0666	-.0661	-.0679	-.0740	-.0746	-.0735
-.0482	-.0473	-.0496	-.0557	-.0561	-.0552
0.0224	0.0243	0.0250	0.0268	0.0364	0.0414
-.0609	-.0654	-.0718	-.0669	-.0831	-.0918
-.0386	-.0411	-.0469	-.0401	-.0468	-.0503
(.115)	(.144)	(.166)	(.337)	(.363)	(.295)
0.0268	0.0294	0.0331	0.0402	0.0402	0.0356
-.0813	-.0840	-.0896	-.0837	-.0795	-.0746
-.0545	-.0546	-.0565	-.0435	-.0395	-.0390
0.3856	0.4040	0.4240	0.4083	0.4122	0.4326
-.1404	-.1378	-.1371	-.1295	-.1257	-.1302
0.2453	0.2663	0.2868	0.2788	0.2864	0.3023

Figure 15(a). 170W longitudinal cross-section, tropical section. Refer to Fig. 9 for key. Values computed from data for 16 July 1974.

30.0	35.0	40.0	45.0	50.0	55.0	60.0	65.0
0.6593	0.6634	0.6638	0.6606	0.6544	0.6460	0.6371	0.6308
0.1115	0.1176	0.1207	0.1026	0.1650	0.2848	0.1552	0.1642
-.4053	-.3901	-.3576	-.3706	-.3413	-.2304	-.3121	-.2194
0.1425	0.1557	0.1855	0.1874	0.1480	0.1309	0.1697	0.2471
0.0142	0.0173	0.0219	0.0172	0.0172	0.0293	0.0189	0.0328
-.0378	-.0396	-.0422	-.0437	-.0468	-.0560	-.0505	-.0387
-.0236	-.0221	-.0203	-.0265	-.0295	-.0267	-.0315	-.0058
(.0)	(.0)	(.069)	(.0)	(.022)	(.629)	(.189)	(.569)
0.0189	0.0197	0.0220	0.0188	0.0184	0.0322	0.0198	0.0299
-.0727	-.0702	-.0695	-.0695	-.0692	-.0792	-.0588	-.0672
-.0539	-.0505	-.0476	-.0507	-.0508	-.0470	-.0389	-.0372
0.0392	0.0380	0.0370	0.0360	0.0371	0.0349	0.0178	0.0251
-.0896	-.0883	-.0891	-.1083	-.0878	-.0245	-.0420	-.0258
-.0504	-.0503	-.0520	-.0724	-.0507	0.0105	-.0242	-.0006
(.245)	(.278)	(.234)	(.182)	(.512)	(.911)	(.373)	(.050)
0.0340	0.0363	0.0324	0.0310	0.0443	0.0405	0.0354	0.0094
-.0776	-.0856	-.0855	-.0821	-.0920	-.0559	-.0817	-.0264
-.0436	-.0493	-.0531	-.0510	-.0478	-.0154	-.0463	-.0170
0.4415	0.4344	0.4297	0.4550	0.3723	0.2243	0.3898	0.3693
-.1275	-.1066	-.0714	-.0670	-.0455	-.0149	-.0791	-.0613
0.3140	0.3279	0.3583	0.3880	0.3268	0.2094	0.3107	0.3080

Figure 15(b). 170W longitudinal cross-section, higher latitude section. Refer to Fig. 9 for key. Values computed from data for 16 July 1974.

-5.0	0.0	5.0	10.0	15.0	20.0	25.0
0.5193	0.5504	0.5783	0.6025	0.6227	0.6390	0.6512
0.1269	0.1524	0.1781	0.1513	0.1487	0.1570	0.1693
-.3531	-.3316	-.3178	-.3656	-.3935	-.3992	-.3856
0.0396	0.0663	0.0824	0.0855	0.0805	0.0828	0.0963
0.0223	0.0269	0.0296	0.0231	0.0188	0.0197	0.0234
-.0457	-.0469	-.0488	-.0422	-.0423	-.0426	-.0444
-.0234	-.0201	-.0192	-.0191	-.0235	-.0228	-.0211
(.232)	(.336)	(.406)	(.123)	(.0)	(.0)	(.019)
0.0229	0.0251	0.0273	0.0228	0.0210	0.0223	0.0233
-.0775	-.0812	-.0840	-.0777	-.0780	-.0762	-.0796
-.0551	-.0560	-.0568	-.0550	-.0570	-.0538	-.0562
0.0334	0.0358	0.0363	0.0349	0.0365	0.0404	0.0390
-.0605	-.0495	-.0419	-.0666	-.0831	-.0927	-.0793
-.0267	-.0137	-.0056	-.0319	-.0464	-.0525	-.0403
(.451)	(.551)	(.665)	(.577)	(.600)	(.652)	(.572)
0.0323	0.0340	0.0379	0.0450	0.0521	0.0561	0.0502
-.0942	-.0874	-.0845	-.0917	-.1027	-.1218	-.1057
-.0626	-.0533	-.0465	-.0466	-.0505	-.0657	-.0554
0.2807	0.2762	0.2691	0.3254	0.3456	0.3436	0.3460
-.0745	-.0667	-.0587	-.0872	-.0876	-.0660	-.0767
0.2061	0.2095	0.2104	0.2381	0.2580	0.2776	0.2693

Figure 16(a). 145E Longitudinal cross-section, tropical section. Refer to Fig. 9 for key. Values computed from data for 16 July 1974.

30.0	35.0	40.0	45.0	50.0	55.0
0.6593	0.6634	0.6638	0.6606	0.6544	0.6460
0.2274	0.2053	0.2209	0.2374	0.0938	0.2522
-.3177	-.3479	-.3156	-.3135	-.3197	-.1899
0.1142	0.1103	0.1273	0.1097	0.2410	0.2039
0.0355	0.0284	0.0258	0.0202	0.0198	0.0450
-.0507	-.0488	-.0505	-.0440	-.0447	-.0429
-.0152	-.0204	-.0247	-.0238	-.0249	0.0020
(.362)	(.155)	(.231)	(.113)	(.080)	(.914)
0.0302	0.0255	0.0262	0.0206	0.0190	0.0367
-.0911	-.0804	-.0704	-.0599	-.0573	-.0794
-.0610	-.0549	-.0442	-.0393	-.0383	-.0428
0.0395	0.0430	0.0377	0.0357	0.0262	0.0285
-.0431	-.0710	-.0630	-.0723	-.0768	0.0033
-.0037	-.0280	-.0254	-.0366	-.0506	0.0319
(.696)	(.681)	(.705)	(.855)	(.020)	(.375)
0.0428	0.0491	0.0482	0.0578	0.0167	0.0221
-.0869	-.1069	-.0991	-.0961	-.0510	-.0520
-.0442	-.0578	-.0508	-.0384	-.0343	-.0299
0.2839	0.3123	0.3051	0.2890	0.4790	0.2616
-.0458	-.0410	-.0326	-.0412	-.0899	-.0187
0.2381	0.2713	0.2724	0.2478	0.3891	0.2429

Figure 16(b). 145E Longitudinal cross-section, higher latitude section. Refer to Fig. 9 for key. Values computed from data for 16 July 1974.

-20.0	-15.0	-10.0	-5.0	0.0	5.0	10.0	15.0	20.0	25.0
0.4062	0.4465	0.4842	0.5189	0.5504	0.5783	0.6025	0.6227	0.6390	0.6512
0.0933	0.1047	0.1085	0.1566	0.1451	0.1517	0.1289	0.1041	0.1209	0.1475
-.3747	-.3889	-.4102	-.4105	-.3847	-.3621	-.3655	-.3795	-.3915	-.3852
-.0620	-.0471	-.0345	-.0481	0.0206	0.0644	0.1081	0.1392	0.1266	0.1183
0.0127	0.0127	0.0099	0.0103	0.0171	0.0208	0.0218	0.0207	0.0178	0.0185
-.0367	-.0379	-.0329	-.0352	-.0384	-.0411	-.0402	-.0381	-.0381	-.0386
-.0242	-.0251	-.0230	-.0249	-.0213	-.0204	-.0184	-.0175	-.0202	-.0202
(.030)	(.0)	(.0)	(.0)	(.005)	(.127)	(.116)	(.040)	(.0)	(.0)
0.0136	0.0146	0.0148	0.0161	0.0190	0.0223	0.0225	0.0209	0.0201	0.0210
-.0626	-.0657	-.0729	-.0754	-.0698	-.0740	-.0719	-.0675	-.0673	-.0679
-.0491	-.0510	-.0581	-.0594	-.0508	-.0516	-.0493	-.0466	-.0477	-.0470
0.0189	0.0232	0.0356	0.0423	0.0383	0.0369	0.0337	0.0309	0.0355	0.0406
-.0589	-.0762	-.1063	-.1234	-.0958	-.0742	-.0689	-.0759	-.0890	-.0907
-.0398	-.0530	-.0707	-.0810	-.0575	-.0372	-.0353	-.0450	-.0536	-.0502
(.317)	(.453)	(.489)	(.900)	(.720)	(.627)	(.390)	(.226)	(.374)	(.450)
0.0253	0.0338	0.0359	0.0532	0.0486	0.0444	0.0379	0.0342	0.0429	0.0443
-.0806	-.1007	-.0975	-.1315	-.1178	-.1019	-.0929	-.0881	-.1011	-.1014
-.0553	-.0669	-.0615	-.0782	-.0692	-.0575	-.0550	-.0539	-.0582	-.0571
0.2420	0.2574	0.2794	0.2403	0.2823	0.3021	0.3577	0.4120	0.4019	0.3793
-.1357	-.1085	-.1006	-.0450	-.0629	-.0710	-.0915	-.1098	-.0956	-.0865
0.1061	0.1489	0.1788	0.1955	0.2195	0.2311	0.2662	0.3022	0.3063	0.2928

Figure 17(a). 35W Longitudinal cross-section, tropical section. Refer to Fig. 9 for key. Values computed from data for 16 July 1974.

30.0	35.0	40.0	45.0	50.0	55.0	60.0
0.6593	0.6634	0.6638	0.6606	0.6544	0.6460	0.6370
0.1495	0.1540	0.1423	0.1420	0.1889	0.1976	0.1499
-.3874	-.3882	-.3901	-.3286	-.2347	-.2178	-.2591
0.1224	0.1213	0.1314	0.1899	0.2307	0.2306	0.2281
0.0180	0.0169	0.0164	0.0260	0.0397	0.0397	0.0264
-.0401	-.0393	-.0422	-.0432	-.0469	-.0500	-.0548
-.0221	-.0224	-.0258	-.0172	-.0071	-.0103	-.0284
(.0)	(.0)	(.0)	(.187)	(.670)	(.770)	(.449)
0.0211	0.0204	0.0199	0.0249	0.0327	0.0340	0.0271
-.0696	-.0695	-.0695	-.0719	-.0762	-.0759	-.0539
-.0485	-.0492	-.0495	-.0470	-.0434	-.0420	-.0267
0.0439	0.0453	0.0420	0.0337	0.0295	0.0267	0.0213
-.0932	-.0970	-.0989	-.0712	-.0240	-.0122	-.0174
-.0493	-.0518	-.0570	-.0375	0.0055	0.0145	0.0039
(.449)	(.466)	(.403)	(.237)	(.105)	(.071)	(.035)
0.0436	0.0440	0.0422	0.0305	0.0167	0.0140	0.0152
-.0969	-.0920	-.0951	-.0790	-.0484	-.0408	-.0415
-.0533	-.0479	-.0529	-.0486	-.0317	-.0267	-.0263
0.3832	0.3828	0.4010	0.4036	0.3468	0.3341	0.3973
-.0875	-.0903	-.0843	-.0633	-.0393	-.0389	-.0916
0.2956	0.2925	0.3166	0.3403	0.3076	0.2952	0.3058

Figure 17(b). 35W Longitudinal cross-section, higher latitude section. Refer to Fig. 9 for key. Values computed from data for 16 July 1974.

where

$$Q24 = \text{daily-averaged solar absorption in layer } (2,4)$$

and is defined relative to A24(t) by a cosine transformation similar to Eq. (5-3), and

$$F24 = \text{terrestrial cooling rate in } (2,4).$$

Similarly the daily-averaged radiative heating (cooling) rates in layers (4,6), (6,8) and (810) are given by

$$BAL46 = Q46 - F46 \tag{5-10}$$

$$BAL68 = Q68 - F68 \tag{5-11}$$

$$BAL810 = Q810 - F810 \tag{5-12}$$

respectively.

3. Cross-Section at Air-Sea Interface (k=10)

The radiative balance at the earth's surface (BALB) is as defined in the following equation:

$$BALB = QABG - F_{10}^{*} . \tag{5-13}$$

QABG is the 24-hour average solar insolation absorbed by the surface as follows:

$$QABG = QABG(t)\,(\overline{\overline{\text{Cos } z}}/\text{Cos } z) . \tag{5-14}$$

D. MERIDIONAL CROSS-SECTIONS OF THE VERTICAL RADIATION BALANCE

Figs. 10, 11,...16, 17 as previously explained represent the single time step of heating computations for each of the four meridians

used in this study. The eight figures have been divided into (a) tropical results and (b) mid-to-high-latitude results for the mid-winter and mid-summer cases respectively. While the results depicted in these cross-sections are exhibited as representing daily-averaged values, they are actually based upon radiation-computations at the specific map times of 0000GMT and 1200GMT on 16 January and 16 July 1974. Therefore, for these results to be meaningful as a stepwise part of the heat package subroutine of FNWC, the solar radiative absorption and reflectance terms would have to be recoverable as a function of GMT, i.e.,

$$F(2,t) = QAVE^* \ (\text{Cos } z/\overline{\overline{\text{Cos } z}}) \qquad (5\text{-}15)$$

$$REF(t) = QREF^* \ (\text{Cos } z/\overline{\overline{\text{Cos } z}}) \qquad (5\text{-}16)$$

etc. Thus solar disposition terms may then be utilized in connection with the one-hour stepwise application of the thermodynamic equation of the set of primitive equations used in the FNWC prediction process, assuming the "2/3-CL" parameterization of Eq. (2-2).

E. COMPARISON OF THE FOUR-LAYER WITH THE TWO-LAYER FLUX DIVERGENCE MODEL

In previous studies (A, B, C, D) which considered only the two-layer flux-divergence model [layers (2,6) and (6,10)] it was assumed that the radiative-cooling rate in layer (2,6), BAL26, was uniformly distributed over layers (2,4) and (4,6). A similar remark is applicable to BAL610 relative to the sublayers (6,8) and (8,10). In an effort to determine the vertical resolution of the atmospheric flux-divergences separately, the four values of BAL24, BAL46, BAL68 and BAL810 have been averaged over all gridpoints for the four computational dates.

The computed values of BAL24 and BAL68 were then compared with one-half of BAL26 and BAL610 respectively to determine the relative percentage of heating (cooling) in these layers, as depicted in Table X for the mid-seasonal winter and summer dates. It is noted that the values of BAL46 and BAL810 are identical in magnitude but of opposite algebraic sign to BAL24 and BAL68 respectively.

The results of these four-layer computations (Table X) indicates that in layer (2,4) there is approximately thirty percent less cooling than would have been deduced in the simpler two-layer model. This implies less radiationally induced instability in the upper troposphere than that originally estimated. In the layer (4,6) there is compensating increased radiative de-stabilization. This radiative difference in the layer (4,6) appears to be primarily a result of the placement of clouds in both models. For instance, the upper clouds have tops at k=4, and IR net flux acts as the chief source of increased de-stabilization in layer(4,6) (and of decreased de-stabilization in layer (2,4)). Likewise the lower clouds have tops at k=8; so, it follows that IR net flux acts as the chief source of increased de-stabilization in layer (8,10), and finally, of reduced de-stabilization in layer (6,8).

The tuning of solar reflectances has not introduced a significant radiative influence on the results of the de-stabilization differences just outlined. Rather it was the placement of clouds relative to layer boundaries that affected primarily the IR net-flux calculations. The results summarized in Table X are then to be considered valid if the cloud-parameterization model approaches climatological reality.

Layers		WINTER RESULTS 2-Layer model Mean cooling rate ($ly\ min^{-1}$)	WINTER RESULTS 4-Layer model Cooling rate deviations ($ly\ min^{-1}$)	SUMMER RESULTS 2-Layer model Mean cooling rate ($ly\ min^{-1}$)	SUMMER RESULTS 4-Layer model Cooling rate deviations ($ly\ min^{-1}$)
	(2,4)		+.0133		+.0143
(2,6)		-.0397		-.0567	
	(4,6)		-.0133		-.0143
	(6,8)		+.0070		+.0075
(6,10)		-.0442		-.0770	
	(8,10)		-.0070		-.0075

TABLE X. Average values of cooling rates as computed in 200 mb layers by the two-layer model (studies A, B, C, D) and the layer-cooling deviations from the two-layer means as computed by the four-layer model.

VI. THE ZONAL DISTRIBUTION OF RADIATIONAL BALANCE TERMS OF THE OCEAN-ATMOSPHERE SYSTEM

A. GENERAL INTRODUCTION: ZONAL CROSS-SECTIONS

The zonally distributed cross-sections of the radiation contributions over the ocean-troposphere system are presented in Figs. 18, 19, 20 and 21 for winter, spring, summer and autumn seasons, respectively. The cross-sections, show the results after averaging over the four meridians on the mid-seasonal dates considered in this study. The results are displayed in the format of Fig. 9.

In obtaining zonally distributed seasonal means of radiative heating rates, denoted $\overline{Q(\phi)}$, at each five-degree multiple of latitude ϕ in the range 20S,... 65N, values of each radiative parameter listed in Fig. 9 were arithmetically averaged over the four meridians. At ϕ = 65N there was only one contribution to the zonal average, while in the Southern Hemisphere latitudes 20S, 15S and 10S, only two values (on λ = 125W and λ = 35W) of each parameter contributed to the means. At 5S, there were three meridional sets of radiative parameters entering into $\overline{Q(\phi)}$. Otherwise, there were four seasonal values of each radiative parameter entering into the arithmetic mean $\overline{Q(\phi)}$ at each latitude ϕ of the cross-sections, Figs. 18,...,21.

Consequently, near the northern and southern boundaries of Figs. 18, ...,21, the listed seasonal values may not be as representative as in mid-latitudes. Nevertheless, the general equatorial-to-polar trend in the radiative-change terms appears reliable in both hemispheres.

-20.0	-15.0	-10.0	-5.0	0.0	5.0	10.0	15.0	20.0	25.0
0.6812	0.6646	0.6437	0.6185	0.5893	0.5563	0.5197	0.4799	0.4372	0.3919
0.1586	0.1522	0.1364	0.1295	0.1131	0.1069	0.0953	0.0939	0.0907	0.1016
-.3094	-.3213	-.3465	-.3279	-.3623	-.3743	-.3851	-.3898	-.3931	-.3623
0.2131	0.1911	0.1608	0.1612	0.1139	0.0751	0.0393	-.0038	-.0465	-.0720
0.0301	0.0281	0.0251	0.0279	0.0227	0.0201	0.0179	0.0154	0.0133	0.0148
-.0450	-.0443	-.0417	-.0449	-.0409	-.0406	-.0395	-.0390	-.0387	-.0423
-.0151	-.0162	-.0167	-.0171	-.0182	-.0204	-.0216	-.0236	-.0255	-.0275
(.377)	(.319)	(.196)	(.295)	(.139)	(.087)	(.052)	(.025)	(.001)	(.113)
0.0307	0.0288	0.0257	0.0277	0.0231	0.0211	0.0189	0.0169	0.0150	0.0145
-.0763	-.0757	-.0724	-.0773	-.0727	-.0722	-.0706	-.0701	-.0694	-.0720
-.0459	-.0469	-.0467	-.0494	-.0496	-.0511	-.0517	-.0531	-.0545	-.0575
0.0377	0.0377	0.0395	0.0372	0.0349	0.0336	0.0293	0.0251	0.0238	0.0184
-.0384	-.0462	-.0630	-.0468	-.0686	-.0768	-.0759	-.0739	-.0791	-.0508
-.0008	-.0086	-.0236	-.0096	-.0337	-.0432	-.0466	-.0487	-.0552	-.0324
(.625)	(.624)	(.551)	(.459)	(.453)	(.472)	(.334)	(.320)	(.282)	(.231)
0.0494	0.0494	0.0470	0.0389	0.0412	0.0411	0.0345	0.0324	0.0280	0.0209
-.0713	-.0761	-.0841	-.0841	-.0934	-.0987	-.0920	-.0921	-.0861	-.0772
-.0220	-.0267	-.0371	-.0452	-.0522	-.0576	-.0575	-.0598	-.0581	-.0564
0.3750	0.3685	0.3701	0.3576	0.3543	0.3335	0.3238	0.2962	0.2665	0.2217
-.0782	-.0789	-.0852	-.0748	-.0867	-.0859	-.1071	-.1147	-.1198	-.1199
0.2969	0.2896	0.2848	0.2826	0.2676	0.2475	0.2166	0.1815	0.1467	0.1018

Figure 18(a). Zonally-averaged radiational cross-section for tropical latitudes. Refer to Fig. 9 for key. All values listed are daily averages in ly min^{-1} and are computed from data for 16 January 1974.

30.0	35.0	40.0	45.0	50.0	55.0	60.0	65.0
0.3446	0.2957	0.2459	0.1958	0.1462	0.0984	0.0541	0.0170
0.1146	0.1006	0.0951	0.0900	0.0680	0.0467	0.0246	0.0076
-.3180	-.3359	-.3097	-.2834	-.2766	-.2268	-.2212	-.2355
-.0880	-.1407	-.1589	-.1776	-.1984	-.1752	-.1917	-.2260
0.0160	0.0111	0.0096	0.0074	0.0060	0.0071	0.0030	0.0007
-.0452	-.0403	-.0330	-.0437	-.0420	-.0436	-.0258	-.0330
-.0291	-.0292	-.0234	-.0363	-.0361	-.0365	-.0229	-.0325
(.260)	(.156)	(.237)	(.345)	(.319)	(.512)	(.414)	(.0)
0.0142	0.0102	0.0079	0.0078	0.0059	0.0045	0.0023	0.0004
-.0689	-.0616	-.0630	-.0610	-.0554	-.0654	-.0469	-.0298
-.0548	-.0514	-.0551	-.0532	-.0495	-.0609	-.0446	-.0294
0.0157	0.0134	0.0124	0.0108	0.0088	0.0043	0.0021	0.0005
-.0332	-.0467	-.0494	-.0454	-.0519	-.0218	-.0108	-.0495
-.0175	-.0334	-.0370	-.0346	-.0430	-.0175	-.0088	-.0489
(.233)	(.285)	(.366)	(.681)	(.647)	(.432)	(.170)	(.0)
0.0141	0.0145	0.0125	0.0119	0.0087	0.0040	0.0016	0.0003
-.0591	-.0650	-.0563	-.0661	-.0585	-.0277	-.0317	-.0297
-.0449	-.0505	-.0439	-.0543	-.0498	-.0237	-.0301	-.0294
0.1699	0.1460	0.1084	0.0679	0.0488	0.0318	0.0206	0.0076
-.1116	-.1222	-.1080	-.0672	-.0688	-.0683	-.1058	-.0934
0.0583	0.0238	0.0004	0.0007	-.0200	-.0365	-.0853	-.0858

Figure 18(b). Zonally-averaged radiational cross-section for higher latitudes. Refer to Fig. 9 for key. All values listed are daily averages in ly min^{-1} and are from data for 16 January 1974.

-20.0	-15.0	-10.0	-5.0	0.0	5.0	10.0	15.0	20.0	25.0
0.5169	0.5441	0.5671	0.5859	0.6005	0.6105	0.6160	0.6168	0.6132	0.6049
0.1283	0.1307	0.1254	0.1225	0.1135	0.1108	0.1087	0.1037	0.1063	0.1365
-.2854	-.2943	-.3203	-.3193	-.3401	-.3614	-.3802	-.3805	-.3815	-.3817
0.1033	0.1190	0.1214	0.1441	0.1469	0.1382	0.1272	0.1277	0.1254	0.0867
0.0264	0.0276	0.0264	0.0278	0.0256	0.0230	0.0193	0.0179	0.0169	0.0146
-.0499	-.0492	-.0461	-.0464	-.0440	-.0410	-.0386	-.0392	-.0382	-.0346
-.0235	-.0216	-.0198	-.0185	-.0184	-.0180	-.0193	-.0213	-.0212	-.0200
(.534)	(.497)	(.360)	(.367)	(.269)	(.138)	(.065)	(.054)	(.013)	(.018)
0.0257	0.0266	0.0258	0.0274	0.0254	0.0234	0.0210	0.0201	0.0169	0.0177
-.0809	-.0814	-.0788	-.0806	-.0766	-.0727	-.0726	-.0730	-.0684	-.0675
-.0552	-.0548	-.0531	-.0532	-.0512	-.0493	-.0517	-.0528	-.0494	-.0498
0.0308	0.0331	0.0355	0.0379	0.0359	0.0341	0.0345	0.0322	0.0290	0.0287
-.0241	-.0303	-.0473	-.0443	-.0556	-.0689	-.0827	-.0791	-.0820	-.0826
0.0065	0.0028	-.0118	-.0064	-.0197	-.0348	-.0482	-.0470	-.0530	-.0539
(.660)	(.656)	(.610)	(.568)	(.493)	(.524)	(.537)	(.521)	(.528)	(.461)
0.0359	0.0383	0.0407	0.0401	0.0413	0.0476	0.0507	0.0505	0.0526	0.0459
-.0564	-.0665	-.0769	-.0790	-.0857	-.0984	-.0997	-.0971	-.1080	-.1029
-.0206	-.0281	-.0361	-.0386	-.0444	-.0508	-.0490	-.0467	-.0554	-.0570
0.2698	0.2876	0.3133	0.3304	0.3588	0.3716	0.3819	0.3876	0.3894	0.3615
-.0738	-.0669	-.0712	-.0692	-.0781	-.0804	-.0865	-.0921	-.0850	-.0941
0.1960	0.2207	0.2421	0.2612	0.2806	0.2911	0.2954	0.2955	0.3044	0.2674

Figure 19(a). Zonally-averaged radiational cross-section for tropical latitudes. Refer to Fig. 9 for key. All values listed are daily averages in ly min^{-1} and are computed from data for 16 April 1974.

30.0	35.0	40.0	45.0	50.0	55.0	60.0	65.0
0.5923	0.5752	0.5540	0.5288	0.4999	0.4675	0.4321	0.3944
0.1420	0.1481	0.1406	0.1396	0.1608	0.1455	0.1618	0.1493
-.3540	-.3374	-.3206	-.3012	-.2894	-.2793	-.2531	-.2086
0.0963	0.0898	0.0927	0.0880	0.0496	0.0427	0.0172	0.0365
0.0174	0.0167	0.0144	0.0120	0.0114	0.0128	0.0129	0.0133
-.0384	-.0334	-.0311	-.0230	-.0419	-.0420	-.0472	-.0473
-.0210	-.0167	-.0168	-.0110	-.0304	-.0292	-.0343	-.0341
(.106)	(.179)	(.191)	(.207)	(.181)	(.259)	(.327)	(.531)
0.0187	0.0175	0.0162	0.0147	0.0151	0.0153	0.0151	0.0173
-.0666	-.0664	-.0627	-.0588	-.0528	-.0436	-.0484	-.0475
-.0479	-.0489	-.0465	-.0441	-.0378	-.0332	-.0333	-.0303
0.0243	0.0232	0.0195	0.0258	0.0196	0.0164	0.0180	0.0100
-.0614	-.0596	-.0498	-.0669	-.0472	-.0318	-.0402	-.0082
-.0370	-.0364	-.0303	-.0411	-.0275	-.0154	-.0222	0.0018
(.379)	(.414)	(.340)	(.327)	(.600)	(.398)	(.724)	(.563)
0.0366	0.0307	0.0279	0.0257	0.0346	0.0236	0.0314	0.0194
-.0893	-.0664	-.0607	-.0529	-.0679	-.0487	-.0633	-.0237
-.0527	-.0356	-.0327	-.0272	-.0332	-.0251	-.0320	-.0045
0.3532	0.3391	0.3354	0.3110	0.2584	0.2539	0.1930	0.1851
-.0982	-.1116	-.1163	-.0996	-.0796	-.1083	-.0539	-.0817
0.2550	0.2275	0.2191	0.2113	0.1787	0.1456	0.1391	0.1034

Figure 19(b). Zonally-averaged radiational cross-section for higher latitudes. Refer to Fig. 9 for key. All values listed are daily averages in ly min^{-1} and are from data for 16 April 1974.

-20.0	-15.0	-10.0	-5.0	0.0	5.0	10.0	15.0	20.0	25.0
0.4062	0.4465	0.4842	0.5191	0.5504	0.5783	0.6025	0.6227	0.6390	0.6512
0.1065	0.1128	0.1116	0.1322	0.1247	0.1395	0.1322	0.1316	0.1333	0.1373
-.3820	-.3903	-.4034	-.3841	-.3664	-.3537	-.3673	-.3766	-.3895	-.3933
-.0826	-.0566	-.0308	0.0029	0.0591	0.0850	0.1030	0.1146	0.1163	0.1206
0.0129	0.0139	0.0133	0.0173	0.0216	0.0242	0.0228	0.0214	0.0190	0.0184
-.0354	-.0370	-.0344	-.0388	-.0401	-.0419	-.0408	-.0407	-.0394	-.0396
-.0226	-.0230	-.0211	-.0215	-.0184	-.0177	-.0180	-.0194	-.0204	-.0213
(.015)	(.0)	(.0)	(.081)	(.128)	(.196)	(.131)	(.072)	(.019)	(.005)
0.0139	0.0152	0.0157	0.0191	0.0210	0.0232	0.0226	0.0213	0.0212	0.0209
-.0608	-.0633	-.0671	-.0715	-.0708	-.0737	-.0733	-.0738	-.0717	-.0726
-.0469	-.0481	-.0513	-.0526	-.0498	-.0505	-.0507	-.0520	-.0505	-.0518
0.0182	0.0212	0.0274	0.0322	0.0301	0.0318	0.0324	0.0332	0.0371	0.0390
-.0542	-.0652	-.0802	-.0802	-.0645	-.0569	-.0632	-.0699	-.0857	-.0895
-.0359	-.0440	-.0528	-.0479	-.0343	-.0251	-.0308	-.0366	-.0486	-.0505
(.256)	(.304)	(.256)	(.452)	(.362)	(.419)	(.377)	(.384)	(.418)	(.370)
0.0250	0.0302	0.0301	0.0366	0.0337	0.0355	0.0373	0.0403	0.0440	0.0414
-.0804	-.0919	-.0870	-.0995	-.0895	-.0865	-.0876	-.0888	-.0984	-.0929
-.0554	-.0616	-.0569	-.0631	-.0557	-.0510	-.0503	-.0486	-.0544	-.0515
0.2292	0.2531	0.2861	0.2814	0.3191	0.3241	0.3551	0.3745	0.3843	0.3941
-.1510	-.1330	-.1348	-.0937	-.1016	-.0947	-.1024	-.1035	-.0943	-.0985
0.0780	0.1201	0.1513	0.1877	0.2175	0.2294	0.2528	0.2711	0.2901	0.2956

Figure 20(a). Zonally-averaged radiational cross-section for tropical latitudes. Refer to Fig. 9 for key. All values listed are daily averages in ly min^{-1} and are computed from data for 16 July 1974.

30.0	35.0	40.0	45.0	50.0	55.0	60.0	65.0
0.6593	0.6634	0.6638	0.6606	0.6544	0.6460	0.6371	0.6308
0.1495	0.1440	0.1443	0.1791	0.1651	0.2369	0.1526	0.1642
-.3781	-.3825	-.3606	-.3371	-.2976	-.2291	-.2856	-.2194
0.1317	0.1370	0.1589	0.1444	0.1917	0.1800	0.1989	0.2471
0.0209	0.0192	0.0206	0.0202	0.0240	0.0332	0.0227	0.0328
-.0421	-.0407	-.0418	-.0441	-.0500	-.0523	-.0527	-.0387
-.0212	-.0215	-.0212	-.0239	-.0259	-.0192	-.0300	-.0058
(.091)	(.039)	(.075)	(.075)	(.267)	(.678)	(.319)	(.569)
0.0225	0.0207	0.0211	0.0207	0.0239	0.0326	0.0234	0.0299
-.0757	-.0708	-.0683	-.0663	-.0638	-.0701	-.0563	-.0672
-.0533	-.0501	-.0472	-.0456	-.0399	-.0376	-.0328	-.0372
0.0386	0.0372	0.0341	0.0343	0.0309	0.0289	0.0195	0.0251
-.0815	-.0883	-.0824	-.0807	-.0569	-.0155	-.0297	-.0258
-.0429	-.0510	-.0483	-.0465	-.0261	0.0134	-.0102	-.0006
(.366)	(.356)	(.336)	(.529)	(.283)	(.436)	(.204)	(.050)
0.0384	0.0380	0.0329	0.0453	0.0289	0.0276	0.0253	0.0094
-.0868	-.0903	-.0818	-.0874	-.0535	-.0541	-.0616	-.0264
-.0484	-.0523	-.0489	-.0421	-.0346	-.0266	-.0363	-.0170
0.3895	0.4044	0.4108	0.3610	0.3815	0.2870	0.3936	0.3693
-.0920	-.0925	-.0963	-.0586	-.0634	-.0370	-.0853	-.0613
0.2975	0.3119	0.3244	0.3024	0.3181	0.2500	0.3082	0.3080

Figure 20(b). Zonally-averaged radiational cross-section for higher latitudes. Refer to Fig. 9 for key. All values listed are daily averages in ly min^{-1} and are from data for 16 July 1974.

-20.0	-15.0	-10.0	-5.0	0.0	5.0	10.0	15.0	20.0	25.0
0.6197	0.6238	0.6232	0.6181	0.6083	0.5940	0.5753	0.5523	0.5252	0.4942
0.1344	0.1345	0.1324	0.1370	0.1124	0.1103	0.1067	0.1062	0.1001	0.1075
-.3071	-.3038	-.3128	-.2901	-.3298	-.3432	-.3504	-.3542	-.3627	-.3753
0.1781	0.1806	0.1781	0.1911	0.1661	0.1405	0.1183	0.0918	0.0624	0.0113
0.0285	0.0305	0.0315	0.0345	0.0290	0.0269	0.0251	0.0226	0.0204	0.0176
-.0449	-.0452	-.0454	-.0505	-.0432	-.0418	-.0414	-.0411	-.0390	-.0373
-.0164	-.0147	-.0140	-.0158	-.0142	-.0149	-.0163	-.0185	-.0186	-.0196
(.391)	(.402)	(.398)	(.551)	(.311)	(.251)	(.205)	(.176)	(.128)	(.040)
0.0279	0.0285	0.0286	0.0309	0.0259	0.0244	0.0231	0.0216	0.0197	0.0173
-.0729	-.0755	-.0767	-.0815	-.0742	-.0724	-.0729	-.0733	-.0703	-.0666
-.0452	-.0471	-.0481	-.0509	-.0482	-.0480	-.0498	-.0517	-.0505	-.0492
0.0318	0.0334	0.0337	0.0366	0.0300	0.0279	0.0279	0.0282	0.0250	0.0238
-.0292	-.0325	-.0340	-.0212	-.0401	-.0464	-.0510	-.0569	-.0619	-.0717
0.0025	0.0008	-.0003	0.0156	-.0102	-.0186	-.0231	-.0286	-.0369	-.0480
(.390)	(.380)	(.348)	(.347)	(.258)	(.294)	(.320)	(.376)	(.354)	(.357)
0.0358	0.0358	0.0351	0.0297	0.0328	0.0352	0.0359	0.0369	0.0361	0.0338
-.0674	-.0733	-.0759	-.0621	-.0771	-.0814	-.0835	-.0842	-.0904	-.0940
-.0317	-.0375	-.0409	-.0326	-.0443	-.0463	-.0477	-.0474	-.0542	-.0603
0.3613	0.3611	0.3621	0.3492	0.3782	0.3693	0.3567	0.3367	0.3238	0.2941
-.0927	-.0823	-.0807	-.0747	-.0952	-.1011	-.1015	-.0988	-.1011	-.1056
0.2686	0.2789	0.2814	0.2745	0.2830	0.2682	0.2551	0.2380	0.2227	0.1885

Figure 21(a). Zonally-averaged radiational cross-section for tropical latitudes. Refer to Fig. 9 for key. All values listed are daily averages in ly min^{-1} and are computed from data for 16 October 1973.

30.0	35.0	40.0	45.0	50.0	55.0	60.0	65.0
0.4596	0.4216	0.3807	0.3370	0.2910	0.2432	0.1941	0.1443
0.1184	0.1192	0.1026	0.0961	0.0905	0.0837	0.0674	0.0591
-.3640	-.3434	-.3501	-.3384	-.3193	-.2743	-.2671	-.1852
-.0228	-.0410	-.0720	-.0976	-.1188	-.1148	-.1405	-.0999
0.0165	0.0151	0.0118	0.0106	0.0091	0.0112	0.0104	0.0110
-.0399	-.0406	-.0331	-.0359	-.0341	-.0348	-.0338	-.0390
-.0234	-.0255	-.0212	-.0254	-.0250	-.0236	-.0234	-.0281
(.093)	(.195)	(.115)	(.079)	(.126)	(.256)	(.325)	(.816)
0.0166	0.0155	0.0118	0.0104	0.0093	0.0090	0.0077	0.0076
-.0685	-.0683	-.0610	-.0590	-.0607	-.0595	-.0685	-.0727
-.0516	-.0527	-.0492	-.0485	-.0514	-.0506	-.0608	-.0650
0.0225	0.0195	0.0133	0.0121	0.0133	0.0093	0.0086	0.0052
-.0651	-.0536	-.0525	-.0508	-.0594	-.0397	-.0378	-.0022
-.0426	-.0341	-.0392	-.0387	-.0461	-.0304	-.0293	0.0030
(.391)	(.359)	(.237)	(.241)	(.292)	(.263)	(.186)	(.377)
0.0298	0.0245	0.0210	0.0188	0.0153	0.0109	0.0068	0.0052
-.0870	-.0722	-.0817	-.0739	-.0615	-.0480	-.0415	-.0366
-.0572	-.0477	-.0607	-.0552	-.0461	-.0371	-.0347	-.0314
0.2558	0.2278	0.2200	0.1888	0.1535	0.1191	0.0933	0.0563
-.1037	-.1087	-.1218	-.1188	-.1037	-.0921	-.0856	-.0346
0.1521	0.1191	0.0983	0.0701	0.0498	0.0269	0.0077	0.0217

Figure 21(b). Zonally-averaged radiational cross-section for higher latitudes. Refer to Fig. 9 for key. All values listed are daily averages in ly min^{-1} and are from data for 16 October 1973.

A zonal cross-section depicting the mean annual radiative distribution has been constructed, Fig. 22, by arithmetic averaging over the four mid-seasonal sets of results (Figs. 18,...,21).

It has also been convenient in earlier sections (cf. Tables III, IV, VIII) to compute "weighted averages" with respect to latitudes in the Northern Hemisphere. Thus a definition of a weighted-average parameter which takes into account the number of observations k_i available at each latitude has been given (Meyers, 1975) as

$$\bar{Q} \equiv Q_{\text{wt. avg.}} = \frac{\sum_{i=1}^{14} \frac{k_i}{4} \left(\sum_{j=1}^{4} \frac{Q_{ji}}{k_i} \right) \text{Cos}\ \phi_i}{\sum_{i=1}^{14} \frac{k_i}{4} \text{Cos}\ \phi_i} \tag{6-1}$$

Here Q_{ji} is the Q-value on meridian j at latitude ϕ_i and $k_i = 1,\ldots,4$ is the number of meridional observations available for the arithmetic average $\overline{Q(\phi_i)}$. Note that $i = 1,\ldots,14$ corresponds to the 14 latitudes, $\phi_i = 0,\ldots,65N$.

B. ANNUAL RADIATIVE BALANCE FOR THE EARTH-TROPOSPHERE SYSTEM

For purposes of this summary, the term BALT (at k=2) in Fig. 9 has been redesignated for simplicity as $R_t(\phi)$, and annual values of R_t have been plotted in Fig. 23 as a function of latitude. R_t represents the <u>net radiative-transfer rate</u> across the tropopause, that is at the top of the troposphere-ocean system considered here. Similarly, the net flux at the surface previously denoted BALB in the key, Fig. 9, is

-20.0	-15.0	-10.0	-5.0	0.0	5.0	10.0	15.0	20.0	25.0
0.5560	0.5697	0.5796	0.5854	0.5871	0.5848	0.5784	0.5679	0.5536	0.5356
0.1320	0.1325	0.1264	0.1303	0.1159	0.1169	0.1107	0.1101	0.1076	0.1208
-.3210	-.3287	-.3458	-.3304	-.3497	-.3582	-.3707	-.3753	-.3817	-.3781
0.1030	0.1085	0.1074	0.1248	0.1215	0.1097	0.0969	0.0826	0.0644	0.0367
0.0245	0.0251	0.0240	0.0269	0.0247	0.0236	0.0213	0.0193	0.0174	0.0164
-.0438	-.0439	-.0419	-.0451	-.0421	-.0413	-.0401	-.0400	-.0389	-.0385
-.0194	-.0189	-.0179	-.0182	-.0173	-.0178	-.0188	-.0207	-.0214	-.0221
(.329)	(.305)	(.238)	(.324)	(.212)	(.168)	(.113)	(.082)	(.041)	(.044)
0.0245	0.0248	0.0239	0.0263	0.0238	0.0230	0.0214	0.0201	0.0187	0.0176
-.0727	-.0740	-.0737	-.0777	-.0736	-.0728	-.0724	-.0725	-.0699	-.0697
-.0483	-.0492	-.0498	-.0515	-.0497	-.0497	-.0510	-.0524	-.0512	-.0521
0.0296	0.0313	0.0340	0.0360	0.0327	0.0318	0.0310	0.0297	0.0287	0.0275
-.0365	-.0436	-.0561	-.0481	-.0572	-.0623	-.0682	-.0699	-.0772	-.0737
-.0069	-.0122	-.0221	-.0121	-.0245	-.0304	-.0372	-.0402	-.0484	-.0462
(.483)	(.491)	(.441)	(.457)	(.391)	(.427)	(.392)	(.400)	(.396)	(.355)
0.0365	0.0384	0.0382	0.0363	0.0373	0.0398	0.0396	0.0400	0.0402	0.0355
-.0689	-.0769	-.0810	-.0812	-.0864	-.0913	-.0907	-.0906	-.0957	-.0918
-.0324	-.0385	-.0427	-.0449	-.0491	-.0514	-.0511	-.0506	-.0555	-.0563
0.3088	0.3176	0.3329	0.3296	0.3526	0.3496	0.3544	0.3488	0.3410	0.3179
-.0989	-.0903	-.0930	-.0781	-.0904	-.0905	-.0994	-.1023	-.1000	-.1045
0.2099	0.2273	0.2399	0.2515	0.2622	0.2591	0.2550	0.2465	0.2410	0.2133

Figure 22(a). Zonal-annual radiational cross-section for tropical latitudes. Refer to Fig. 9 for key. All values listed are daily averages in ly min^{-1} and are computed by arithmetic averaging over the four midseasonal results (Figs. 18,...,21).

30.0	35.0	40.0	45.0	50.0	55.0	60.0	65.0
0.5140	0.4890	0.4611	0.4306	0.3979	0.3638	0.3294	0.2966
0.1311	0.1279	0.1206	0.1262	0.1211	0.1282	0.1016	0.0951
-.3535	-.3498	-.3352	-.3150	-.2957	-.2524	-.2567	-.2121
0.0293	0.0113	0.0052	-.0107	-.0190	-.0168	-.0290	-.0106
0.0177	0.0155	0.0141	0.0125	0.0126	0.0161	0.0122	0.0144
-.0414	-.0387	-.0348	-.0367	-.0420	-.0432	-.0399	-.0395
-.0237	-.0232	-.0206	-.0241	-.0294	-.0271	-.0276	-.0251
(.137)	(.142)	(.154)	(.176)	(.223)	(.426)	(.346)	(.479)
0.0180	0.0160	0.0142	0.0134	0.0136	0.0153	0.0121	0.0138
-.0699	-.0668	-.0638	-.0613	-.0582	-.0609	-.0550	-.0543
-.0519	-.0508	-.0495	-.0478	-.0447	-.0456	-.0429	-.0405
0.0253	0.0233	0.0198	0.0207	0.0182	0.0147	0.0121	0.0102
-.0603	-.0621	-.0585	-.0609	-.0538	-.0272	-.0296	-.0214
-.0350	-.0387	-.0387	-.0402	-.0357	-.0125	-.0176	-.0112
(.342)	(.353)	(.320)	(.444)	(.455)	(.382)	(.321)	(.247)
0.0298	0.0269	0.0236	0.0254	0.0219	0.0165	0.0163	0.0086
-.0806	-.0735	-.0701	-.0701	-.0628	-.0446	-.0495	-.0291
-.0508	-.0465	-.0465	-.0447	-.0409	-.0281	-.0333	-.0206
0.2921	0.2793	0.2687	0.2322	0.2105	0.1729	0.1751	0.1546
-.1014	-.1088	-.1081	-.0860	-.0789	-.0764	-.0827	-.0677
0.1907	0.1705	0.1606	0.1461	0.1317	0.0965	0.0924	0.0868

Figure 22(b). Zonal-annual radiational cross-section for higher latitudes. Refer to Fig. 9 for key. All values listed are daily averages in ly min^{-1} and are computed by arithmetic averaging over the four midseasonal results (Figs. 18,...,21).

redesignated here following Malkus (1962) as $R(\phi)$ and its annual distribution has been graphed against latitude in Fig. 23. Finally, the relationship between R_t and R in any column is given by

$$R_t = R + R_a \tag{6-2}$$

where R_a is the <u>overall</u> net cooling rate or flux-divergence of the tropospheric column, e.g.,

$$R_a = BAL24 + BAL46 + BAL68 + BAL810 \tag{6-3}$$

In Fig. 23, values of $R_a(\phi)$ have also been plotted against latitude; however, a simpler method of obtaining R_a from (6-2), namely,

$$R_a = R_t - R \tag{6-4}$$

has been employed. The resulting zonal annual distributions of each of the three parameters, R_t, R and R_a, are shown as functions of latitude in Fig. 23, where they are superimposed against similar functions drawn from Sellers (1965).

The comparison which follows focuses on the annual distribution in the Northern Hemisphere only. It should also be noted that Sellers' radiative parameters were taken from climatology at the top of the mean zonal atmosphere, whereas this radiative model gives corresponding results for level k = 2, based upon tropospheric soundings over an oceanic surface only.

Throughout the latitude range (0-65N), the radiative net flux R at the ocean surface is substantially greater than the climatological amount

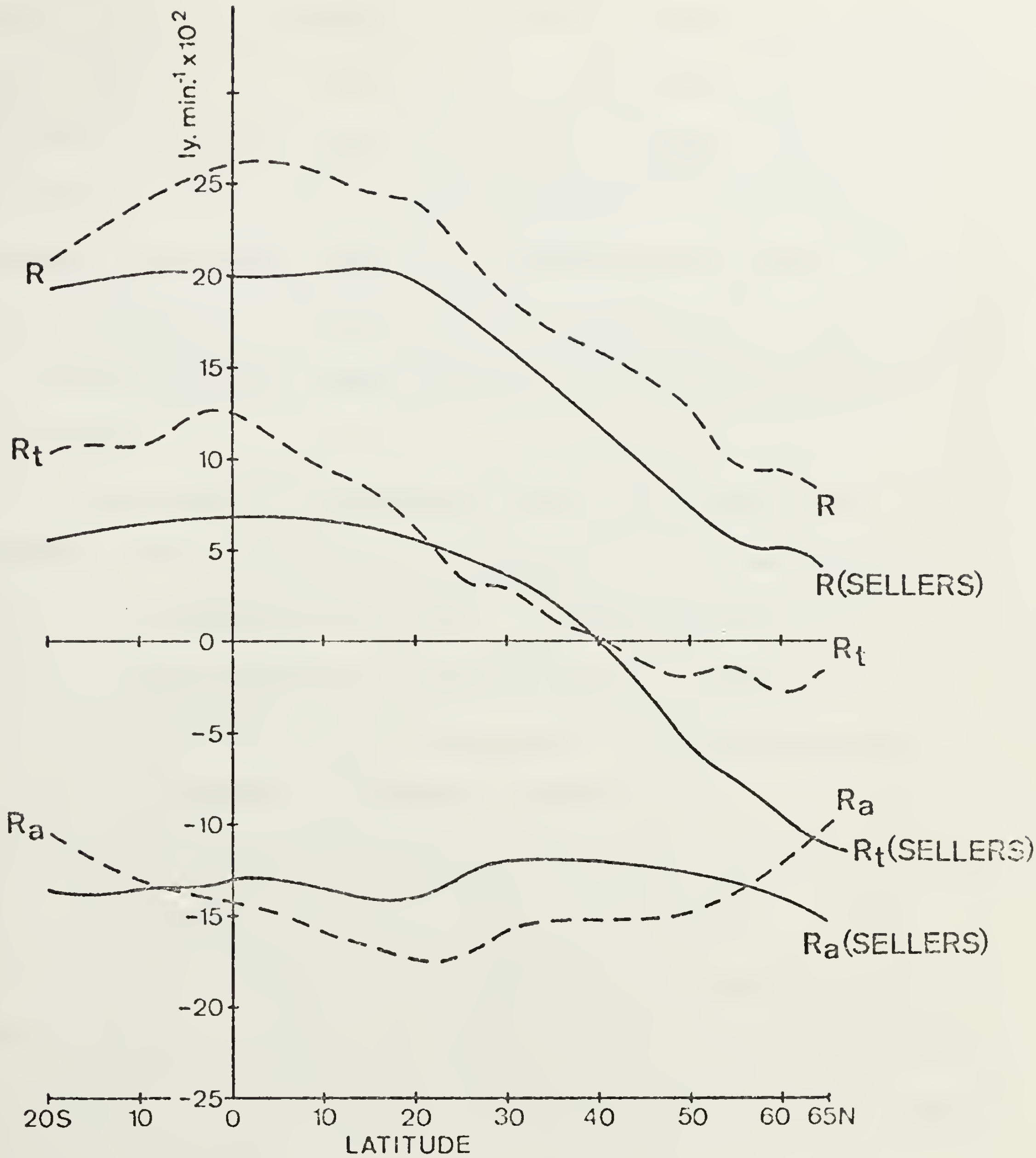

Figure 23. Radiative net fluxes at the tropopause (R_t) at the ocean surface (R); and net-flux divergence for the tropospheric column (R_a) from the zonal annual results (Fig. 22(a,b)). Solid lines indicate values of R_t, R and R_a after Sellers (1965).

of Sellers. This is attributable to the reduced model-albedo values of Sec. IV.F. This in turn allowed more insolational-absorption in the ocean thereby increasing R over all latitudes as compared to Sellers' values (Fig. 23). The term $R-R_t$ (which equals $-R_a$) may be regarded as an atmospheric "greenhouse effect" in contributing to warming of the surface both for the model and for Sellers' climatology. For each latitude, Fig. 23 indicates that the "model greenhouse" is in close agreement with that of Sellers.

The R_a-distributions of both Sellers and of the present model are in good agreement across the entire range of Fig. 23, both representing cooling rates in the troposphere for all ϕ. A minimum value of R_a at latitude 20N appears on both curves and is presumably due to a local maximum of IR net-flux divergence $F_2^* - F_{10}^*$ (resulting from the minimum opaque cloud cover) in subtropical latitudes. From 50N to 65N, an increase in the model values of R_a appears in Fig. 23 and seems to indicate a reduced IR net-flux loss associated with high CL-values (Table III) at these northerly latitudes. Sellers' results indicate the opposite trend, i.e., increasingly negative R_a-values from 50-60N, but his climatology may not include the kind of detail that would indicate reasonable oceanic cloudiness over these latitudes.

The radiative model gives R_t-values which are generally larger, both over tropical latitudes as well as over the northern latitudes, than the R_t-values of Sellers. As in the $R(\phi)$ comparison this is a result primarily of the reduced model-albedo. In the mid-latitude zone 25-40N of Fig. 23, close agreement occurs between the two R_t-curves presumably due to such similar climatological effects as for example, the mean polar

front. The positive-to-negative R_t crossover-point occurs very near to 40N for both R_t-distributions of Fig. 23. The model weighted-average is $\overline{R_t(\phi)} = 0.048$ ly min^{-1} if averaging is considered only to 65N. If negative R_t annual values exist in latitudes $\phi \geq 65N$, an ocean-troposphere radiative balance should very nearly be established over the Northern Hemisphere. However data for the model were not analyzed over ice-covered regions poleward of 65N, where presumably higher surface albedos and cooler drier soundings would enable R_t to assume larger negative values.

The radiative-model values of $R_t(\phi)$, $R(\phi)$ and $R_a(\phi)$ are in agreement with present albedo and IR net-flux observations from recent satellite climatology. It should be noted that Sellers' radiative results are based on climatology of London (1957), and include also data from the land areas of the Northern Hemisphere; on the other hand the radiative model values have been based only upon soundings over the ocean.

C. CROSS-SEASONAL EFFECTS IN THE NORTHERN HEMISPHERE

1. On the Net Flux Across the Tropopause, R_t

The seasonal distribution of the tropospheric net flux is presented as a function of latitude in Table XI(a) where the listed R_t-values correspond to the tropopause, level $k = 2$. One may discern two geographic regimes of annual waves in Table XI(a); a polar zone (25-65N) and a tropical-subtropical zone (0-25N).

The cross-seasonal variation of R_t in the northern regime has the following property: R_t-values are a minimum in winter increasing to a maximum in summer followed by a decrease in autumn. In the tropical zone (0-10N), R_t-values have positive peaks in spring and autumn. The summer minimum of R_t in 0-10N is presumably attributable to increased

Lat.	(a) R_t (ly min^{-1}) 16 Jan	16 Apr	16 Jul	16 Oct	(b) R (ly min^{-1}) 16 Jan	16 Apr	16 Jul	16 Oct
20S	.216	.103	-.083	.178	.297	.196	.078	.269
15	.191	.119	-.057	.181	.290	.221	.120	.279
10	.161	.121	-.031	.178	.285	.242	.151	.281
5	.161	.144	.003	.191	.283	.261	.188	.275
0	.114	.147	.059	.166	.268	.281	.218	.283
5N	.075	.138	.085	.141	.248	.291	.229	.268
10	.039	.127	.103	.118	.217	.295	.253	.255
15	-.004	.128	.115	.092	.182	.296	.271	.238
20	-.047	.125	.116	.062	.147	.304	.290	.223
25	-.072	.087	.121	.011	.102	.267	.296	.189
30	-.088	.096	.132	-.023	.058	.255	.298	.152
35	-.141	.090	.137	-.041	.024	.228	.312	.119
40	-.159	.092	.159	-.072	.000	.219	.324	.098
45	-.178	.088	.144	-.098	.001	.217	.302	.070
50	-.198	.050	.192	-.119	-.021	.178	.318	.050
55	-.175	.043	.180	-.115	-.037	.146	.250	.027
60	-.192	.017	.199	-.141	-.085	.139	.308	.008
65N	-.226	.037	.247	-.100	-.086	.103	.308	.022
Wt. Avg.	-.059	.103	.126	.020	.108	.251	.279	.173

TABLE XI. Seasonal and latitudinal distribution of (a) averaged earth-troposphere net radiative flux (R_t); (b) averaged radiative net flux at earth's surface (R).

cloudiness associated with the ITCZ in this latitude zone. The subtropical region 15-25N <u>does not</u> have a minimum in midsummer, and may be simply classified as intermediate in behavior between that exhibited by R_t in the polar and the tropical regimes. These geographic cross-sectional effects (Table XI(a)) tend to confirm the general validity of the radiative model.

2. <u>On the Sea-surface Model Balance, R</u>

The seasonal distribution of the net radiative flux R at the earth's surface is listed as a function of latitude in Table XI(b). Again a polar zone (25-65N) and a tropical-subtropical zone (0-25N) are defined for discussing cross-seasonal effects on R.

The model results for R are analogous to those just specified for R_t, namely:

(i) in the polar latitudes there is a single sine wave with annual periodicity and maximum in midsummer;

(ii) in tropical latitudes 0-10N, the double peaked character with maximum in spring and autumn appears;

(iii) there exists an intermediate subtropical zone of R-values which no longer exhibits a minimum in summer.

D. TOP OF THE ATMOSPHERE COMPARISON OF MODEL WITH SATELLITE DATA

1. <u>Net Radiative Transfer Rate at Top of the Atmosphere</u>

The three parameters that describe the radiative flux at level k = 0 are associated in the following way:

$$R_N = Q_N - F_T \qquad (6-5)$$

Q_N, the daily averaged incoming solar flux, can be related to QAVE and

QREF (Fig. 9) by the relationship

$$Q_N = \frac{2.00}{1.92} QAVE(1-ALB) = \frac{2.00}{1.92} QAVE - QREF \qquad (6-6)$$

where QAVE and QREF have already been evaluated according to Eqs. (5-3) and (5-6) respectively and the factor 2.00/1.92 has the effect of deriving the mean daily solar insolation at level k = 0 before ozone-oxygen absorption. F_T, the IR net flux to space, was previously discussed in Sec. III.D. [Eq. (3-11)], and R_N, the difference between Q_N and F_T, represents the daily-averaged radiative net flux at the top of the atmosphere. In order to more easily distinguish between model-values of R_N and the same parameter from satellite climatology of Raschke et al. (1973), R_N is further identified as R_NMOD or R_NRAS, respectively. QAVE is assumed identical both for the model and for the treatment of the Raschke data in this study.

2. Zonally-Averaged Computations of R_N

With the use of Eqs. (6-6) and (6-5), values of Q_N, F_T and R_N for each of the four mid-seasonal dates and by five-degree latitude intervals have been computed both for the model-parameters and the satellite-observed (RAS) parameters. The results of the computations both seasonally and for the annual mean case are presented in Table XII.

A comparison of R_NMOD with R_NRAS from the zonal-annual results at the bottom of Table XII shows that the crossover from positive-to-negative values of R_N occurs near 40N for both model- and Raschke-results.

A statistical accuracy check of R_NMOD as against R_NRAS data is conducted using the standard deviations of the difference parameter (R_NMOD - R_NRAS) over all Northern Hemisphere latitudes. A summary of

Lat.		-20.0	-15.0	-10.0	-5.0	0.0	5.0	10.0	15.0	20.0	25.0	30.0	35.0	40.0	45.0	50.0	55.0	60.0	65.0
(a)	MOD	0.5510	0.5401	0.5341	0.5147	0.5008	0.4726	0.4461	0.4060	0.3648	0.3066	0.2443	0.2075	0.1610	0.1140	0.0843	0.0557	0.0319	0.0101
		0.3188	0.3280	0.3485	0.3306	0.3611	0.3712	0.3799	0.3843	0.3870	0.3645	0.3345	0.3491	0.3291	0.3042	0.2999	0.2643	0.2720	0.2681
		0.2322	0.2121	0.1856	0.1841	0.1396	0.1013	0.0662	0.0217	-.0222	-.0579	-.0902	-.1416	-.1681	-.1902	-.2156	-.2086	-.2402	-.2579
	RAS	0.5639	0.5574	0.5467	0.5467	0.4727	0.4525	0.4306	0.3945	0.3475	0.3113	0.2629	0.2038	0.1577	0.1151	0.0743	0.0484	0.0297	0.0091
		0.3703	0.3798	0.3750	0.3457	0.3527	0.3685	0.3892	0.3952	0.3943	0.3724	0.3418	0.3163	0.3026	0.2891	0.2727	0.2701	0.2696	0.2700
		0.1936	0.1777	0.1717	0.2010	0.1201	0.0841	0.0414	-.0007	-.0468	-.0611	-.0789	-.1125	-.1449	-.1740	-.1984	-.2216	-.2399	-.2609
(b)	MOD	0.4103	0.4360	0.4653	0.4878	0.5120	0.5251	0.5330	0.5339	0.5324	0.4937	0.4750	0.4511	0.4365	0.4113	0.3598	0.3415	0.2884	0.2615
		0.2992	0.3063	0.3270	0.3263	0.3431	0.3609	0.3750	0.3755	0.3779	0.3794	0.3621	0.3514	0.3404	0.3268	0.3121	0.3125	0.2889	0.2651
		0.1111	0.1297	0.1383	0.1615	0.1689	0.1642	0.1580	0.1584	0.1545	0.1142	0.1129	0.0998	0.0960	0.0844	0.0477	0.0289	-.0006	-.0036
	RAS	0.4472	0.4703	0.4846	0.4939	0.4941	0.4953	0.5122	0.5237	0.5222	0.5022	0.4646	0.4364	0.4156	0.3878	0.3476	0.2934	0.2606	0.2053
		0.4100	0.4150	0.4100	0.3681	0.3646	0.3414	0.3616	0.3899	0.3956	0.3867	0.3613	0.3542	0.3400	0.3300	0.3221	0.3151	0.3103	0.3000
		0.0372	0.0553	0.0746	0.1258	0.1295	0.1539	0.1505	0.1339	0.1266	0.1155	0.1033	0.0822	0.0756	0.0578	0.0255	-.0218	-.0497	-.0947
(c)	MOD	0.3163	0.3523	0.3928	0.4085	0.4485	0.4629	0.4954	0.5171	0.5323	0.5410	0.5373	0.5471	0.5472	0.5090	0.5166	0.4361	0.5111	0.4927
		0.3795	0.3858	0.3949	0.3769	0.3649	0.3547	0.3666	0.3754	0.3841	0.3872	0.3768	0.3849	0.3745	0.3564	0.3306	0.2857	0.3294	0.2937
		-.0632	-.0335	-.0021	0.0316	0.0836	0.1082	0.1288	0.1417	0.1482	0.1538	0.1606	0.1622	0.1727	0.1526	0.1860	0.1504	0.1817	0.1990
	RAS	0.3404	0.3837	0.4207	0.4419	0.4378	0.4719	0.4726	0.4933	0.5223	0.5377	0.5401	0.5299	0.5145	0.4718	0.4460	0.4258	0.4015	0.4007
		0.4005	0.4196	0.4257	0.3966	0.3776	0.3538	0.3360	0.3500	0.3743	0.3947	0.3922	0.3769	0.3630	0.3560	0.3497	0.3274	0.3304	0.3300
		-.0601	-.0360	-.0050	0.0453	0.0602	0.1182	0.1365	0.1432	0.1480	0.1430	0.1479	0.1530	0.1515	0.1159	0.0964	0.0983	0.0711	0.0708
(d)	MOD	0.5110	0.5153	0.5168	0.5069	0.5213	0.5084	0.4926	0.4691	0.4470	0.4072	0.3604	0.3200	0.2939	0.2549	0.2126	0.1696	0.1347	0.0914
		0.3194	0.3194	0.3216	0.3016	0.3364	0.3473	0.3537	0.3574	0.3649	0.3762	0.3673	0.3519	0.3621	0.3564	0.3398	0.3106	0.3020	0.2543
		0.1916	0.1959	0.1953	0.2053	0.1849	0.1612	0.1389	0.1117	0.0821	0.0310	-.0069	-.0319	-.0683	-.1016	-.1271	-.1410	-.1673	-.1629
	RAS	0.4980	0.5353	0.5306	0.5143	0.5228	0.4973	0.4594	0.4516	0.4346	0.4124	0.3811	0.3220	0.2854	0.2589	0.1978	0.1587	0.1180	0.1006
		0.3791	0.4006	0.4248	0.4182	0.4096	0.3687	0.3409	0.3555	0.3893	0.3974	0.3879	0.3666	0.3459	0.3238	0.3005	0.2951	0.2896	0.3101
		0.1189	0.1348	0.1057	0.0960	0.1131	0.1286	0.1185	0.0961	0.0453	0.0150	-.0068	-.0446	-.0605	-.0649	-.1027	-.1364	-.1716	-.2094
(e)	MOD	0.4471	0.4609	0.4773	0.4794	0.4956	0.4923	0.4918	0.4815	0.4691	0.4371	0.4043	0.3814	0.3596	0.3223	0.2934	0.2507	0.2415	0.2139
		0.3292	0.3349	0.3480	0.3338	0.3514	0.3585	0.3688	0.3732	0.3785	0.3768	0.3602	0.3593	0.3515	0.3360	0.3206	0.2933	0.2981	0.2703
		0.1179	0.1260	0.1293	0.1456	0.1443	0.1337	0.1230	0.1084	0.0907	0.0603	0.0441	0.0221	0.0081	-.0137	-.0273	-.0426	-.0566	-.0563
	RAS	0.4624	0.4867	0.4956	0.4992	0.4818	0.4793	0.4687	0.4658	0.4567	0.4409	0.4122	0.3730	0.3433	0.3084	0.2664	0.2316	0.2024	0.1789
		0.3900	0.4037	0.4089	0.3822	0.3761	0.3581	0.3569	0.3727	0.3884	0.3878	0.3708	0.3535	0.3379	0.3247	0.3112	0.3019	0.3000	0.3025
		0.0724	0.0830	0.0868	0.1170	0.1057	0.1212	0.1117	0.0931	0.0683	0.0531	0.0414	0.0195	0.0054	-.0163	-.0448	-.0704	-.0975	-.1236

TABLE XII. Zonally averaged net-flux parameters at the top of the atmosphere. At each latitude the radiative parameters Q_N, F_T, R_N are listed (ly min^{-1}) for both the model- and Raschke-calculations. The letter code (a), (b), (c), (d) indicates the distribution over seasons while (e) denotes annual distribution of the same parameters as a function of latitude.

the mean and standard deviations of this parameter over the latitude range of these five cross-sections (Table XII) follows:

	16 Jan.	16 Apr.	16 Jul.	16 Oct.	Annual
$\overline{R_N MOD - R_N RAS}$	.004	.024	.019	.014	.015 ly min^{-1}
Std. Dev.	.028	.037	.053	.039	.039 ly min^{-1}

The zonally-averaged mean $(\overline{R_N MOD - R_N RAS})$ is positive for each season as well as for the annual distribution (whose mean is 0.015 ly min^{-1}). This small positive difference was anticipated from consideration of Sec. IV.F. (Table IX) where the middle-to-high latitude albedos were tuned slightly too small.

The overall standard deviation in $(R_N MOD - R_N RAS)$ of 0.039 ly min^{-1} is of the same order of magnitude as that of $Q_N MOD - Q_N RAS$. This comparatively small difference in the case of model versus satellite climatology was a considerable improvement over (A,B,C,D) where untuned albedos were used.

E. STRATOSPHERIC MODEL RADIATIVE BALANCE

It is clear that the flux-convergence in the stratosphere is given by

$$R_N - R_t$$

where R_N is given by Eq. (6-5). Note that R_t is identical to BALT of Fig. 9 which reduces to

$$R_t = QAVE - QREF - F_2^* \; . \qquad (6\text{-}7)$$

Forming the difference, $R_N - R_t$, leads to

$$R_N - R_t = .04\ \underset{\sim}{Q}AVE - (F_T - F_2^*) \ . \tag{6-8}$$

The stratospheric flux-convergence, $R_N - R_t$, is displayed in zonal-annual format in Table XIII. Based on the Northern Hemisphere weighted results (bottom line), it appears that a positive net-flux convergence exists between 0-65N. However the trend in $R_N - R_t$ at higher latitudes is towards increasingly negative radiative values in the stratosphere poleward of 65N such that an annual mean radiative balance may be inferred. For instance, assuming that in the latitude range 65-90N, an average zonal-annual value of $R_N - R_t = -0.0502$ ly min^{-1} exists at 77.5N, then, the cosine-weighted mean is -0.0126 ly min^{-1} in the region poleward of 65N. Thus the summed Northern Hemisphere weighted mean would be zero and a radiative balance would exist in the stratosphere.

F. ZONAL-ANNUAL NORTHERN HEMISPHERE HEAT BUDGET

1. <u>Tropospheric Radiation Budget</u>

The radiative heating rate of a tropospheric column may be expressed as a function of $R_a(\phi)$ by the right side of Eq. (6-9)

$$Q_{va} + S_a = R_a + (E + H_\Gamma) \tag{6-9}$$

S_a is the storage heating rate of the column and Q_{va} is the required flux-convergence of sensible and latent heat energies compatible with the heat balance at latitude ϕ. R_a is the tropospheric radiative net cooling rate and is depicted in Fig. 23. $(E + H_\Gamma)$ includes the latent and sensible heat parameters respectively, but these parameters are not part of this study and will be considered to be contained in Q_{va} of Eq. (6-9) for simplicity.

Lat.	R_N	R_t	$R_N - R_t$
20S	.1179	.1030	.0149
15	.1260	.1085	.0175
10	.1293	.1074	.0219
5	.1456	.1248	.0208
0	.1443	.1215	.0228
5	.1337	.1097	.0240
10	.1230	.0969	.0261
15	.1084	.0826	.0258
20	.0907	.0644	.0236
25	.0603	.0367	.0236
30	.0441	.0293	.0148
35	.0221	.0113	.0108
40	.0081	.0052	.0029
45	-.0137	-.0107	-.0030
50	-.0273	-.0190	-.0083
55	-.0426	-.0168	-.0258
60	-.0566	-.0290	-.0256
65N	-.0563	-.0106	-.0457
Wt. Avg.	.0602	.0476	.0126

TABLE XIII. Computed radiative net fluxes at the top of the atmosphere (R_N) at the tropopause (R_t); and the stratospheric absorption (R_N-R_t). All parameters are listed in the zonal-annual format in ly min^{-1}.

The Northern Hemisphere cosine-weighted R_a turns out to be

$$\overline{R_a} = - 0.1551 \text{ ly min}^{-1}$$

and if it is temporarily attributable to mean storage-cooling $\overline{S_a}$ of the troposphere alone, the mean storage rate corresponds to a temperature-change rate given by

$$(\frac{\delta T}{\delta t}) = 4.1 \frac{1440(\overline{R_a})}{\Delta P_{mb}} \text{ °C/day} \qquad (6-10)$$

with $\Delta P_{mb} \doteq 800$ mb in the troposphere. The resultant cooling rate (6-10) over the tropospheric depth, 800 mb, with zero lateral flux divergence, is approximately -1.14°C per day averaged over the mean cm^2 tropospheric column.

Thus the general circulation of the atmosphere would have to function to bring about the atmospheric heat balance. This process would require the proper flux-convergence Q_{va} to offset the annual radiative loss of the average cm^2 column of the troposphere.

2. Zonal-annual Heat Budget of the Ocean

An equation similar to (6-9) may be written for the zonal-annual heat budget for the ocean as a function of $R(\phi)$.

$$Q_{vo} + S_o = R - (E + H_\Gamma) \qquad (6-11)$$

Here, S_o is the storage rate of the ocean water mass and Q_{vo} is the required mean oceanic heat flux divergence for a balance at latitude ϕ. The primary ocean mass heating parameter is the net radiative heating flux at the ocean surface, R (Fig. 23), and $(E + H_\Gamma)$ is for convenience considered part of Q_{vo}.

The Northern Hemisphere annual weighted mean value of $\bar{R}$ is

$$\bar{R} = 0.2027 \text{ ly min}^{-1}$$

which corresponds (Table XI) to a mean radiative heating rate in the water-mass column. It should be noted that this mean heating rate is noticeably larger than $\bar{R}_a$ and of opposite sign to the corresponding tropospheric radiative cooling effect ($\bar{R}_a = -0.1551$ ly min^{-1}). However, if the three-dimensional oceanic flux divergence of both sensible and latent heat is considered, the oceanic heat balance should result.

VII. CONCLUSIONS

The major change in this radiative model from the model evolving from (A,B,C,D) was the introduction of tuned cloud reflectances. This innovation brought the resultant model-albedos into agreement with satellite climatology for comparable data dates.

Gridpoint comparisons at the top of the atmosphere of model net flux F_T and of the net incoming model insolation Q_N were made with similar parameters from Raschkes' satellite climatology (1973). Closer agreement was obtained between Q_NMOD and Q_NRAS than in any of the preceding studies (A,B,C,D). Similarly, close agreement in a least-squares sense was achieved here between F_TMOD and F_TRAS primarily because of an improved formulation for the F_T-computation than was used in earlier studies. Finally the ocean-atmosphere system net flux

$$R_N = Q_N - F_T$$

has only a small least-square error when model and satellite results are compared with properly stratified gridpoint and time cross-sections.

In this study, mid-latitude cloud reflectances were also tuned to obtain closer agreement between the global albedo and corresponding values from satellite climatology. The result was to systematically increase Q_N relative to Raschke's values. This result was undoubtedly due to a mismatch between the model clouds and those involved in the climatological average. The conclusion reached is that if tuning of cloud reflectances of this nature is to be attempted in mid-latitudes

using FNWC soundings, more accurate cloud-parameterization formulas should be established against observed cloud-cover amounts for identical experiment-periods similar to GATE. If then further cloud-reflectance tuning is necessary, it could proceed from a more certain knowledge of the "ground truth" provided by these experiments.

```
//FORT.SYSIN DD *
      COMMON BT(11),DATA(11,5),CL(2)
      COMMON/ABS/ FA2,ALPHAG,CZ,SECZ,FS,FADJ
      COMMON/TRIG/ ST,CT,SD,CD,ALAT
      COMMON/VP/ Q(11),QS(11)
      COMMON/ARM/ RM
      COMMON/RASKC/RASVAL
      COMMON/RASK/ ALBRAS(93),F2RAS(93),ISO
      COMMON/FACT/ K,ISEA
  502 FORMAT(4X,2(F8.4,2X))
  500 FORMAT (2X,F6.1,1X,F7.2,1X,5(F9.5,1X),6X,2I2)
      DO 68 ISEA=1,4
      IF(ISEA.EQ.1) DEC=-21.07917/57.29578
      IF(ISEA.EQ.2) DEC=  8.48333/ 57.29578
      IF(ISEA.EQ.3) DEC=  21.5000/57.29578
      IF(ISEA.EQ.4) DEC=   -8.225/57.29578
      IF(ISEA.EQ.1) RM=.983715**2
      IF(ISEA.EQ.2) RM=1.00333**2
      IF(ISEA.EQ.3) RM=1.01644**2
      IF(ISEA.EQ.4) RM=.997165**2
C
C   THE FOLLOWING READ STATEMENT APPLIES TO THE SATELLITE
C   CLIMATOLOGY DATA OF RASCHKE  ET AL. AS USED IN THE SUB-
C   ROUTINE REFT.
C
      DO 9 ISO=1,93
      READ(5,502) ALBRAS(ISO),F2RAS(ISO)
    9 CONTINUE
      DO 66 ISO=1,93
      DO 10 I=1,11
      READ(17,500,END=99) (DATA(I,K),K=1,2),Q(I),QS(I),
     1(DATA(I,KK),KK=3,5),LAB1,LAB2
   10 CONTINUE
      IF(ISEA.EQ.3.AND.ISO.EQ.25) LAB1=24
      CALL ANGLE(CZ,SECZ,ISO,LAB1,DEC)
      IF(ISEA.EQ.1.AND.ALAT.LE.25.) RASVAL =.4
      IF(ISEA.EQ.1.AND.ALAT.GT.25.) RASVAL =.8
      IF(ISEA.EQ.2.AND.ALAT.LE.25.) RASVAL =.35
      IF(ISEA.EQ.2.AND.ALAT.GT.25.) RASVAL =.65
      IF(ISEA.EQ.3.AND.ALAT.LE.25.) RASVAL =.6
      IF(ISEA.EQ.3.AND.ALAT.GT.25.) RASVAL =.7
      IF(ISEA.EQ.4.AND.ALAT.LE.25.) RASVAL =.4
      IF(ISEA.EQ.4.AND.ALAT.GT.25.) RASVAL =.6
      CALL BBB
      ALPHAG=(.54*(.7-CZ))+.06
      IF(ALPHAG.LT..06) ALPHAG=.06
      FS=.651*CZ*1.92/RM
      FADJ=(2.00*CZ)/RM
      FA2=(.349*1.92*CZ)/RM
      DO 20 I=1,4
      CL(1)=0.0
      CL(2)=0.0
      IF(I.EQ.2.OR.I.EQ.4) CL(1)=1.000
      IF(I.GE.3) CL(2)=1.000
      WT=(1.0-DATA(6,3))*(1.0-DATA(2,3))
      IF(I.EQ.2) WT=DATA(6,3)*(1.0-DATA(2,3))
      IF(I.EQ.3) WT=DATA(2,3)*(1.0-DATA(6,3))
      IF(I.EQ.4) WT=DATA(2,3)*DATA(6,3)
      CALL ABSORB(CL(1),CL(2),WT)
   20 CONTINUE
   66 CONTINUE
   68 CONTINUE
   99 STOP
      END
C
      SUBROUTINE ABSORB(C1,C2,WT)
      COMMON/ABS/ FA2,ALPHAG,CZ,SECZ,FS,FADJ
      COMMON/RASKC/RASVAL
      IF(C1.GT..5.OR.C2.GT..5) GO TO 20
      ALPHAR=(.085+(.25074*ALOG10(SECZ)))
      IF(ALPHAR.GT.1.000) ALPHAR=1.000
```

```
      A=((1.-ALPHAR)*(1.-ALPHAG))/(1.-(ALPHAR*ALPHAG))
      SOL=A*FS
      GO TO 21
   20 R1=.54*RASVAL
      R2=.66*RASVAL
      IF(C1.LT..5) R1=0.0
      IF(C2.LT..5) R2=0.0
      A=(1.-R1)*(1.-R2)*(1.-ALPHAG)
      D=1.0-((R1*R2)+(R2*ALPHAG)+(R1*ALPHAG))
      C=2.0*R1*R2*ALPHAG
      SOL=(A*FS)/(D+C)
   21 IF(C1.LT..1.AND.C2.LT..1) CALL AB00(WT,SOL)
      IF(C1.GT..9.AND.C2.LT..1) CALL AB10(WT,SOL)
      IF(C1.LT..1.AND.C2.GT..9) CALL AB01(WT,SOL)
      IF(C1.GT..9.AND.C2.GT..9) CALL AB11(WT,SOL)
      RETURN
      END
C
      SUBROUTINE TD(ANS,IND,N1,N2,SEC,C)
      COMMON BT(11),DATA(11,5),CL(2)
      U=DATA(N1,4)- DATA(N2,4)
      A=.303
      ANS=C*((U*SEC)**A)
      IF(IND.GT.10.) ANS=1.0-ANS
      RETURN
      END
C
      SUBROUTINE BBB
      COMMON BT(11),DATA(11,5),CL(2)
      SIGMA=1.170403
      E=1.E-7
      DO 10 I=1,11
      A=DATA(I,2)+273.16
      BT(I)=(A**4)*SIGMA*E
   10 CONTINUE
      DATA(2,4)=(DATA(1,4)+DATA(3,4))/2.00
      DATA(2,5)=(DATA(1,5)+DATA(3,5))/2.00
      RETURN
      END
C
      SUBROUTINE ANGLE(CZ,SECZ,IS,L2,D)
      COMMON/TRIG/ ST,CT,SD,CD,ALAT
      R=57.29578
      H=35.0/R
      IF(IS.LE.25) H=55.0/R
      IF(IS.GE.26.AND.IS.LE.50) H=10.0/R
      A=973.752
      S=2.0
      IF(IS.GE.26.AND.IS.LE.50) S=1.0
      AK=L2+1
      IF(IS.GE.68) AK=63-L2
      B=(S*((32.-AK)**2)   )
      ST=(A-B)/(A+B)
      CT=(1.-(ST**2))**.5
      SD=SIN(D)
      CD=COS(D)
      CH=COS(H)
      CZ=(ST*SD)+(CT*CD*CH)
      SECZ=1.00/CZ
      TANT=ST/CT
      ALAT=(ATAN(TANT))*57.29578
      RETURN
      END
C
      SUBROUTINE AB00(WT,SOL)
      COMMON/ABS/FA2,ALPHAG,CZ,SECZ,FS,FADJ
      CALL TD(U24,0,9,7,SECZ,.271)
      CALL TD(U26,0,9,5,SECZ,.271)
      CALL TD(U28,0,9,3,SECZ,.271)
      CALL TD(U210,0,9,1,SECZ,.271)
      CALL TD(U10,12,9,1,SECZ,.271)
      A24=FA2*U24
```

```
      A46=FA2*(U26-U24)
      A68=FA2*(U28-U26)
      A810=FA2*(U210-U28)
      TRANA=FA2*U10
      AI10=TRANA*(1.-ALPHAG)
      REFA=FA2-A24-A46-A68-A810-AI10
      CALL REFT(1,A24,A46,A68,A810,AI10,TRANA,REFA,SOL,WT)
      RETURN
      END
C
      SUBROUTINE AB10(WT,SOL)
      COMMON/ABS/FA2,ALPHAG,CZ,SECZ,FS,FADJ
      COMMON/RASKC/RASVAL
      R1=.46*RASVAL
      A1=.20
      CALL TD(TD24,12,9,7,SECZ,.271)
      CALL TD(TD68,12,5,3,1.6667,.271)
      CALL TD(TD610,12,5,1,1.66667,.271)
      CALL TD(TD810,12,3,1,1.6667,.271)
      F4D=FA2*TD24
      F4U=R1*F4D
      F2U=F4U*TD24
      A24=FA2-F4D+F4U-F2U
      A46=F4D*A1
      F6D=F4D*(1.-R1-A1)
      F8D=F6D*TD68
      F10D=F6D*TD610
      F10U=F10D*ALPHAG
      F8U=F10U*TD810
      F6U=F10U*TD610
      F6DD=F6U*R1
      F8DD=F6DD*TD68
      F10DD=F6DD*TD610
      A68=F6D-F8D+F8U-F6U+F6DD-F8DD
      A810=F8D-F10D+F10U-F8U+F8DD-F10DD
      AI10=(F10D*(1.-ALPHAG))+F10DD
      TRANA=F10D+F10DD
      REFA=FA2-A24-A46-A68-A810-AI10
      CALL REFT(2,A24,A46,A68,A810,AI10,TRANA,REFA,SOL,WT)
      RETURN
      END
C
      SUBROUTINE AB01(WT,SOL)
      COMMON/ABS/FA2,ALPHAG,CZ,SECZ,FS,FADJ
      COMMON/RASKC/RASVAL
      R2=.50*RASVAL
      A2=.30
      CALL TD(TD24,12,9,7,SECZ,.271)
      CALL TD(TD26,12,9,5,SECZ,.271)
      CALL TD(TD28,12,9,3,SECZ,.271)
      CALL TD(TD910,12,2,1,1.6667,.271)
      CALL TD(TD68,12,5,3,SECZ,.271)
      CALL TD(TD48,12,7,3,SECZ,.271)
      F4D=FA2*TD24
      F6D=FA2*TD26
      F8D=FA2*TD28
      F8U=F8D*R2
      F6U=F8U*TD68
      F4U=F8U*TD48
      F2U=F8U*TD28
      A24=FA2-F4D+F4U-F2U
      A46=F4D-F6D+F6U-F4U
      A68=F6D-F8D+F8U-F6U
      F9D=F8D*(1.-R2-A2)
      F10D=F9D*TD910
      F10U=F10D*ALPHAG
      F9U=F10U*TD910
      F9DD=F9U*R2
      F10DD=F9DD*TD910
      A810=(F8D*A2)+F9D-F10D+F10U-F9U+F9DD-F10DD
      TRANA=F10D+F10DD
      AI10=(F10D*(1.-ALPHAG))+F10DD
```

```
      REFA=FA2-A24-A46-A68-A810-AI10
      CALL REFT(3,A24,A46,A68,A810,AI10,TRANA,REFA,SOL,WT)
      RETURN
      END
C
      SUBROUTINE AB11(WT,SOL)
      COMMON/ABS/FA2,ALPHAG,CZ,SECZ,FS,FADJ
      COMMON/RASKC/RASVAL
      R1=.46*RASVAL
      R2=.50*RASVAL
      A1=.20
      A2=.30
      CALL TD(TD24,12,9,7,SECZ,.271)
      CALL TD(TD68,12,5,3,1.6667,.271)
      CALL TD(TD910,12,2,1,1.6667,.271)
      F4D=FA2*TD24
      F4U=R1*F4D
      F2U=F4U*TD24
      A24=FA2-F4D+F4U-F2U
      A46=F4D*A1
      F6D=F4D*(1.-R1-A1)
      F8D=F6D*TD68
      F8U=F8D*R2
      F6U=F8U*TD68
      F6DD=F6U*R1
      F8DD=F6DD*TD68
      A68=F6D-F8D+F8U-F6U+F6DD-F8DD
      F9D=F8D*(1.-R2-A2)+F8DD*(1.-A2)
      F10D=F9D*TD910
      F10U=F10D*ALPHAG
      F9U=F10U*TD910
      F9DD=F9U*R2
      F10DD=F9DD*TD910
      A810=((F8D+F8DD)*A2)+F9D-F10D+F10U-F9U+F9DD-F10DD
      AI10=(F10D*(1.-ALPHAG))+F10DD
      TRANA=F10D+F10DD
      REFA=FA2-A24-A46-A68-A810-AI10
      CALL REFT(4,A24,A46,A68,A810,AI10,TRANA,REFA,SOL,WT)
      RETURN
      END
C
      SUBROUTINE REFT(NSUB,A24,A46,A68,A810,AI10,TRANA,
     1REFA,SOL,WT)
C
      COMMON BT(11),DATA(11,5),CL(2)
      COMMON/ABS/ FA2,ALPHAG,CZ,SECZ,FS,FADJ
      COMMON/TRIG/ ST,CT,SD,CD,ALAT
      COMMON/ARM/ RM
      COMMON/RASK/ ALBRAS(93),F2RAS(93),ISO
      COMMON/RASKC/ RASVAL
      COMMON/FACT/ K,ISEA
      IF(NSUB.GT.1) GO TO 10
      CA24=0.0
      CA46=0.0
      CA68=0.0
      CA810=0.0
      CAI10=0.0
      CSI10=0.0
      CREF=0.0
   10 CA24=CA24+A24*WT
      CA46=CA46+A46*WT
      CA68=CA68+A68*WT
      CA810=CA810+A810*WT
      CAI10=CAI10+AI10*WT
      CSI10=CSI10+SOL*WT
      CREF=CREF+((FS-SOL)*WT)+REFA*WT
      CALL IR(NSUB,A10,A8,A6,A4,A2,F10,F8,F6,F4,F2,WT,FT)
      IF(NSUB.LT.4) RETURN
      ABG=(CAI10+CSI10)/FADJ
      TAND=SD/CD
      TANT=ST/CT
      TAN=-TAND*TANT
```

```
      H=ARCOS(TAN)
      SINH=SIN(H)
      BARCOS= ((ST*SD*H)+(CD*CT*SINH))/3.14159
      F200=1.92/RM
      QAVE=F200*BARCOS
      AF2=-F2
      QREF=(CREF*QAVE)/(FADJ*.9600)
      BALT= QAVE-QREF-F2
      Q24=(CA24*QAVE)/(FADJ*.9600)
      AF24=-(F2-F4)
      BAL24=Q24+AF24
      Q46=(CA46*QAVE)/(FADJ*.9600)
      AF46=-(F4-F6)
      BAL46=Q46+AF46
      Q68=(CA68*QAVE)/(FADJ*.9600)
      AF68=-(F6-F8)
      BAL68=Q68+AF68
      Q810=(CA810*QAVE)/(FADJ*.9600)
      AF810=-(F8-F10)
      BAL810=Q810+AF810
      QABG= (ABG*QAVE)/.9600
      BALB= QABG-F10
      AF10=-F10
      CA26=CA24+CA46
      Q26=(.5*CA26*QAVE)/(FADJ*.9600)
      AF26=-.5*(F2-F6)
      BAL26=Q26+AF26
      CA610=CA68+CA810
      Q610=(.5*CA610*QAVE)/(FADJ*.9600)
      AF610=-.5*(F6-F10)
      BAL610=Q610+AF610
      DIF24=BAL24-BAL26
      DIF46=BAL46-BAL26
      DIF68=BAL68-BAL610
      DIF810=BAL810-BAL610
      ALB=CREF/FADJ
      ALBDIF=ALB-ALBRAS(ISO)
      F2DIF=FT-F2RAS(ISO)
      RNRAS=(QAVE*1.041667*(1.-ALBRAS(ISO)))-F2RAS(ISO)
      RNMOD=(QAVE*1.041667*(1.-ALB))-FT
      DIFRN=RNMOD-RNRAS
      RETURN
      END
C
      SUBROUTINE IR(NSUB,F10,F8,F6,F4,F2,E10,E8,E6,E4,E2,
     1WT,ET)
C
      IF(NSUB.GT.1) GO TO 10
      OFF=1.0
      E10=0.0
      E8=0.0
      E6=0.0
      E4=0.0
      E2=0.0
      ET=0.0
   10 CALL FF10(F10,OFF)
      CALL FF8(F8,OFF)
      CALL FF6(F6,OFF)
      CALL FF4(F4,OFF)
      CALL FF2(F2,OFF)
      CALL FFTOP(FT,OFF)
      E10=E10+WT*F10
      E8=E8+WT*F8
      E6=E6+WT*F6
      E4=E4+WT*F4
      E2=E2+WT*F2
      ET=ET+WT*FT
      IF(NSUB.LT.4) RETURN
      E10=E10/1440.
      E8=E8/1440.
      E6=E6/1440.
      E4=E4/1440.
```

```
      E2=E2/1440.
      ET=ET/1440.
      RETURN
      END
C
      SUBROUTINE FF10(F10,OFF)
        COMMON BT(11),DATA(11,5),CL(2)
      IF(CL(1).GT..5.OR.CL(2).GT..5) GO TO 10
      CALL EWC(EW8,OFF,3,1)
      CALL EWC(EW6,OFF,5,1)
      CALL EWC(EW4,OFF,7,1)
      CALL EWC(EW2,OFF,9,1)
      CALL EWC(EW1,OFF,10,1)
      CALL EWC(EW9,OFF,2,1)
      CALL BOUND(WAVE,OFF,11,1)
      B1=(BT(3)-BT(5))*(EW8+EW6)
      B2=(BT(1)-BT(3))*EW8
      A1=((BT(1)-BT(5))-.5*(B1+B2))
      B1=BT(10)*WAVE
      B2=(BT(9)-BT(10))*(EW2+EW1)
      B3=(BT(7)-BT(9))*(EW4+EW2)
      B4=(BT(5)-BT(7))*(EW6 +EW4)
      A2=   (BT(5)-(.5*(B1+B2+B3+B4)))
      B1=(1.-(.5*EW9))
      A3=(BT(1)-BT(2))*B1
   10 F10=((1.-CL(2))*A1)+((1.-CL(2))*(1.-CL(1))*A2)+
     1(CL(2)*A3)
      RETURN
      END
C
      SUBROUTINE FF8(F8,OFF)
      COMMON BT(11),DATA(11,5),CL(2)
      IF(CL(1).GT..5.OR.CL(2).GT..5) GO TO 10
      CALL EWC(EW68,OFF,5,3)
      CALL EWC(EW48,OFF,7,3)
      CALL EWC(EW28,OFF,9,3)
      CALL EWC(EW18,OFF,10,3)
      CALL EWC(EW810,OFF,3,1)
      CALL BOUND(WAVE,OFF,11,3)
      B1=EW68*(BT(3)-BT(5))
      B2=(EW68+EW48)*(BT(5)-BT(7))
      B3=(EW48+EW28)*(BT(7)-BT(9))
      B4=(EW28+EW18)*(BT(9)-BT(10))
      B5=WAVE*BT(10)
      A1=BT(3)-(.5*(B1+B2+B3+B4+B5))
      A2=(BT(1)-BT(3))*(1.-(.5*EW810))
      A3=(BT(3)-BT(5))*(1.-(.5*EW68))
   10 F8=((1.-CL(1))*A1)+((1.-CL(1))*(1.-CL(2))*A2)+(CL(1)
     1*A3)+(CL(1)*(1.-CL(2))*A2)
      RETURN
      END
C
      SUBROUTINE FF6(F6,OFF)
      COMMON BT(11),DATA(11,5),CL(2)
      IF(CL(1).GT..5.OR.CL(2).GT..5) GO TO 10
      CALL EWC(EW68,OFF,5,3)
      CALL EWC(EW46,OFF,7,5)
      CALL EWC(EW26,OFF,9,5)
      CALL EWC(EW16,OFF,10,5)
      CALL EWC(EW610,OFF,5,1)
      CALL BOUND(WAVE,OFF,11,5)
      B1=WAVE*BT(10)
      B2=(BT(9)-BT(10))*(EW26+EW16)
      B3=(BT(7)-BT(9))*(EW46+EW26)
      B4=EW46*(BT(5)-BT(7))
      B5=EW68*(BT(3)-BT(5))
      A1=(BT(3)-(.5*(B1+B2+B3+B4+B5)))
      A2=(BT(1)-BT(3))*(1.-(.5*(EW68+EW610)))
      A3=(1.-(.5*EW68))*(BT(3)-BT(5))
   10 F6=((1.-CL(1))*A1)+((1.-CL(1))*(1.-CL(2))*A2)+(CL(1)
     1*A3)+(CL(1)*(1.-CL(2))*A2)
      RETURN
```

```
      END
C
      SUBROUTINE FF4 (F4,OFF)
      COMMON BT(11),DATA(11,5),CL(2)
      IF(CL(1).GT..5.OR.CL(2).GT..5) GO TO 10
      CALL EWC(EW46,OFF,7,5)
      CALL EWC(EW48,OFF,7,3)
      CALL EWC(EW24,OFF,9,7)
      CALL EWC(EW14,OFF,10,7)
      CALL EWC(EW410,OFF,7,1)
      CALL BOUND(WAVE,OFF,11,7)
      WAVE=WAVE*BT(10)
      B1=(BT(5)-BT(7))*EW46
      B2=(BT(3)-BT(5))*(EW46+EW48)
      B3=(BT(7)-BT(9))*EW24
      B4=(BT(9)-BT(10))*(EW14+EW24)
      A1=BT(3)-(.5*(B1+B2+B3+B4+WAVE))
      A2=BT(7)-(.5*(B3+B4+WAVE))
      A3=(BT(1)-BT(3))*(1.-(.5*(EW48+EW410)))
   10 F4=((1.-CL(1))*A1)+(CL(1)*A2)+((1.-CL(1))*(1.-CL(2))
     1*A3)
      RETURN
      END
C
      SUBROUTINE FF2(F2,OFF)
      COMMON BT(11),DATA(11,5),CL(2)
      IF(CL(1).GT..5.OR.CL(2).GT..5) GO TO 10
      CALL EWC(EW24,OFF,9,7)
      CALL EWC (EW26,OFF,9,5)
      CALL EWC(EW28, OFF,9,3)
      CALL EWC(EW12,OFF,10,9)
      CALL EWC(EW210,OFF,9,1)
      CALL BOUND(WAVE,OFF,11,9)
      C1=(BT(1)-BT(3))
      C2=(1.-((EW28+EW210)/2.0))
      A3=C1*C2
      B1=WAVE*BT(10)
      B2=EW12*(BT(9)-BT(10))
      B3=(EW26+EW28)*(BT(3)-BT(5))
      B4=(EW24+EW26)*(BT(5)-BT(7))
      B5=(EW24)*(BT(7)-BT(9))
      B=B1+B2+B3+B4+B5
      A1=(BT(3)-(.5*B))
      B3=EW24*(BT(7)-BT(9))
      A2=(BT(7)-(.5*(B1+B2+B3)))
   10 F2=(A3*(1.-CL(2))*(1.-CL(1)))+(A1*(1.-CL(1)))+(A2*
     1CL(1))
      RETURN
      END
C
      SUBROUTINE FFTOP(FT,OFF)
      COMMON BT(11),DATA(11,5),CL(2)
      IF(CL(1).GT..5.OR.CL(2).GT..5) GO TO 10
      CALL EWC(EW01,OFF,11,10)
      CALL EWC(EW02,OFF,11,9)
      CALL EWC(EW04,OFF,11,7)
      CALL EWC(EW06,OFF,11,5)
      CALL EWC(EW08,OFF,11,3)
      CALL EWC(EW010,OFF,11,1)
      B1=(EW01+EW02)*(BT(9)-BT(10))
      B2=(EW02+EW04)*(BT(7)-BT(9))
      B3=(EW04+EW06)*(BT(5)-BT(7))
      B4=(EW06+EW08)*(BT(3)-BT(5))
      A1=(BT(3)-(.5*(B1+B2+B3+B4)))
      B3=(1.-(.5*(EW08+EW010)))
      A2=B3*(BT(1)-BT(3))
      A3=(BT(7)-(.5*(B1+B2)))
   10 FT=(A1*(1.-CL(1)))+(A2*(1.-CL(1))*(1.-CL(2)))+(A3*
     1CL(1))
      RETURN
      END
C
```

```
      SUBROUTINE BOUND(WAVE,OFF,N1,N2)
      COMMON BT(11),DATA(11,5),CL(2)
      T=DATA(10,2)+273.16
      U=DATA(N1,4)-DATA(N2,4)
      IF(U.LT..00001) U=.000005
      AL=ALOG10(U)
      D=.353*AL-.44
      A1=8.34*T**D
      D=-.03455*AL-.705
      A2=U**D
      A3=(8.00/(.353*AL+3.56))
      WAVE=A1*A2*A3
      IF(OFF.GT.10.) RETURN
      C=DATA(N1,5)-DATA(N2,5)
      D=( U+.0286)**.26
      B1=.07262*(1.-(.62556*D))
      B2= ALOG10(C)+(1.064)
      WAVE=WAVE+B1*B2
      RETURN
      END
C
      SUBROUTINE EWC(EW,OFF,M1,M2)
       COMMON BT(11),DATA(11,5),CL(2)
      U=DATA(M1,4)-DATA(M2,4)
      D=ALOG10(U+.010)
      A1=(.240*D)+.622
      EW=A1
      IF(OFF.GT.10.) RETURN
      C=DATA(M1,5)-DATA(M2,5)
      B1=1.-(.62556*((U+.0286)**.26))
      B2=ALOG10(C)+1.064
      EW=A1+(.07262*B1*B2)
      RETURN
      END
C
C
C   CONTROL CARD FORMAT FOR 2/3 CLOUD DATA AND "RADIATIVE
C   SOUNDING" DATA ON NPS-304

//GO.FT17F001 DD UNIT=3400-4,VOL=SER=NPS304,DISP=(OLD,KEEP),
// DCB=(DEN=2,RECFM=FB,LRECL=77,BLKSIZE=847),LABEL=(1,SL),
// DSN=WOOSET
```

LIST OF REFERENCES

1. Arakawa, A., 1972: Design of the UCLA General Circulation Model, Numerical Simulation of Weather and Climate Tech. Rpt. No. 7, Department of Meteorology, University of California.

2. Beahan, T. W., 1975: Radiational Parameterization for the FNWC Primitive Equation Model Using Data over the Oceans for 16 July 1974, M. S. Thesis, Department of Meteorology, Naval Postgraduate School, Monterey, California.

3. Budyko, M. I., 1956: The Heat Balance of the Earth's Surface, Leningrad, pp. 255 (Translated by N. A. Slepanova; translation distributed by U. S. Weather Bureau, Washington, D. C.)

4. Coulson, K. L., 1959: Radiative Flux from the Top of Rayleigh Atmosphere, Ph.D. Dissertation, Department of Meteorology, University of California, pp. 60.

5. Dixon, W. J., 1973: Biomedical Computer Programs, University of California Press, pp. 773.

6. Joseph, J. H., 1971: "On the Calculation of Solar Radiation Fluxes in the Troposphere," Solar Energy, Vol. 13, Pergamon Press, London, pp. 251-161.

7. Malkus, J. S., 1962: "Large Scale Interactions," The Sea, Vol. 1, Interscience Publishers.

8. Martin, F. L., 1972: Description of a Radiation Package for the Naval Postgraduate School General Circulation Model, Department of Meteorology, Naval Postgraduate School, Monterey, California.

9. Martin, F. L., 1975: Unpublished manuscript, Department of Meteorology, Naval Postgraduate School, Monterey, California.

10. Meyers, W. T., 1975: Radiational Parameterization for the FNWC Primitive Equation Model Using Data over the Oceans for 16 April 1974, M. S. Thesis, Department of Meteorology, Naval Postgraduate School, Monterey, California.

11. Raschke, E., Vonder Haar, T., Bandeen, W., Pasternak, M., 1973: "The Annual Radiation Balance of the Earth-Atmosphere System during 1969-1970 from NIMBUS III Measurements," Journal of the Atmospheric Sciences, Vol. 30, No. 3, pp. 341-364.

12. Rodgers, C. D., 1967: "The Radiative Heat Budget of the Troposphere and Lower Stratosphere," Planetary Circulation Project Report N.A2, Department of Meteorology, Massachusetts Institute of Technology, pp. 99.

13. Sasamori, T., 1968: "The Radiative Cooling Calculation for Application to General Circulation Experiments," Journal of Applied Meteorology, Vol. 7, No. 5, pp. 721-729.

14. Sellers, W. D., 1965: Physical Climatology, University of Chicago Press, pp. 272.

15. Smagorinsky, J., 1960: "On the Dynamical Prediction of Large Scale Condensation by Numerical Methods," Geophysical Monograph, No. 5, American Geophysical Union, Washington, D. C., pp. 71-78.

16. Spaeth, W. T., Jr., 1974: Heat Budget Parameterization for the FNWC Primitive Equation Model Using Data for 16 January 1974, M. S. Thesis, Department of Meteorology, Naval Postgraduate School, Monterey, California.

17. Vonder Haar, T. H., Oort, A. H., 1973: "New Estimate of Annual Poleward Energy Transport by Northern Hemisphere Oceans," Journal of Physical Oceanography, Vol. 3, No. 2, pp. 169-172.

18. Warner, D. W., 1974: Heat Budget Parameterization for the FNWC Primitive Equation Model Using Data for 16 October 1973, M. S. Thesis, Department of Meteorology, Naval Postgraduate School, Monterey, California.

19. Yamamoto, G., 1952: "On a Radiation Chart," Science Reports of the Tohoku University, Series No. 5, pp. 9-23.

INITIAL DISTRIBUTION LIST

		No. Copies
1.	Defense Documentation Center Cameron Station Alexandria, Virginia 22314	2
2.	Library, Code 0212 Naval Postgraduate School Monterey, California 93940	2
3.	Professor F. L. Martin, Code 51Mr Department of Meteorology Naval Postgraduate School Monterey, California 93940	2
4.	CDR. Robert D. Woods 55289 N. Berry Avenue South Bend, Indiana	1
5.	Department Chairman, Code 51 Department of Meteorology Naval Postgraduate School Monterey, California 93940	1
6.	Director, Naval Oceanography and Meteorology Building 200 Washington Navy Yard Washington, D. C. 20374	1
7.	Fleet Numerical Weather Centra l Attn: Mr. Leo Clarke Monterey, California 93940	1

165137
Thesis
W84352 Woods
c.1
Satellite-tuned fleet numerical weather central radiational model applied to the 1973-1974 data year over oceanic gridpoints.